ANGÉLICA SOUSA DA MATA

EPIDEMIC PROCESSES AND DIFFUSION ON NETWORKS: ANALYTICAL AND COMPUTATIONAL APPROACHES

Thesis presented at the Universidade Federal de Viçosa in partial fulfillment of the requirements of the Programa de Pós-Graduação em Física for the degree of *Doctor Scientiae*.

VIÇOSA
MINAS GERAIS - BRAZIL
2015

Ficha catalográfica preparada pela Biblioteca Central da Universidade Federal de Viçosa - Câmpus Viçosa

T

M425e
2015

Mata, Angélica Sousa da, 1987-
Epidemic processes and diffusion on networks : analytical and computational approaches / Angélica Sousa da Mata. - Viçosa, MG, 2015.
xviii, 120f : il. ; 29 cm.

Orientador : Silvio da Costa Ferreira Junior.
Tese (doutorado) - Universidade Federal de Viçosa.
Referências bibliográficas: f.109-120.

1. Física estatística. 2. Epidemias. 3. Transformação de fase (Física estatística). 4. Teoria de campos (Física) .
I. Universidade Federal de Viçosa. Departamento de Física. Programa de Pós-graduação em Física. II. Título.

CDD 22. ed. 513

ANGÉLICA SOUSA DA MATA

Epidemic Processes and Diffusion on Networks:
analytical and computational approaches

Thesis presented at the Universidade Federal de Viçosa in partial fulfillment of the requirements of the Programa de Pós-Graduação em Física for the degree of *Doctor Scientiae*.

APPROVED: February 25th, 2015.

Romualdo Pastor-Satorras
(Co-adviser)

Marcelo Lobato Martins
(Co-adviser)

Ronald Dickman

José Soares Andrade Jr.

Silvio da Costa Ferreira Jr.
(Adviser)

For my beloved family.
You represent everything to me.

"- Do you know who first explained the true
origin of the rainbow? I asked.
- He was Descartes, he said. After a moment he looked me in the eye.
- And what do you think was the salient feature of the rainbow that inspired Descartes'
mathematical analysis? He asked.
- I supposed his inspiration was the realization that the problem could be analyzed by
considering a single drop, and the geometry of the situation.
-You're overlooking a key feature of the phenomenon, he said.
- Okay, I give up. What would you say inspired his theory?
- I would say his inspiration was that he thought rainbows were beautiful. "
Feynman's Rainbow: A Search for Beauty in Physics and in Life
(Leonard Mlodinow)

ACKNOWLEDGEMENTS

First and above all, I thank God for providing me the capability to conclude this stage.

My warmest thanks to my parents, Sebastião and Mara, and my lovely sisters, Carol and Jacque, for being always present. It is wonderful to share in these accomplishment with you.

Special thanks go to Ana Paula, my adorable roommate, for her best company during many years in Viçosa. I extend this thanks to Marcela, Gabi and Poli.

Thanks also to the friends from the Universidade Federal de Viçosa (UFV) for providing a good atmosphere in our department. Particularly, to Saulo, Renan, Aline, Mari, Thiago, Pri, Tati, Mirela, Ronan, Aline Viol, Eduardo, Fábio, Jader and Herman.

I also would like to thank my friends from Barcelona. Specially Juan, Sebastian, Oriol, Jorge and Michele. We enjoyed good time together.

There are not enough words to express my deepest gratitude to my advisor, Prof. Silvio, for his guidance, support, helpfulness and encouragement.

I also thank Prof. Romualdo Pastor-Satorras. I really appreciated his excellent assistance during my PhD internship. It has been an honor to work with him.

I am also indebted to Marian Boguñá, Claudio Castellano, Ronan Ferreira and Wesley Cota, the coauthors of part of the papers that are the basis of this thesis.

I acknowledge all professors and staff of the Departamento de Física at UFV.

I also acknowledge the funding agencies CNPq, FAPEMIG and CAPES for the grants that partially supported the research activities of the thesis. I specially acknowledge CAPES for the scholarships during both my doctorate at UFV - Viçosa, and the internship at UPC.

My gratitude also goes to the GISC (Grupo de Investigaçãoo de Sistemas Complexos) and to the Departament de Física i Enginyeria Nuclear of the Universitat Politècnica de Catalunya for their computer support.

Finally, I would like to thank the UFV, where I have spent great moments of my life.

Contents

LIST OF PUBLICATIONS

The scientific literature produced by the studies related to this thesis is listed below.

- A. S. Mata, S. C. Ferreira, *Pair quenched mean-field theory for the susceptible-infected-susceptible model on complex networks*, EPL **103**, 48003 (2013).
- A. S. Mata, R. S. Ferreira, S.C. Ferreira, *Heterogeneous pair-approximation for the contact process on complex networks*, New J. Phys. **16**, 053006 (2014).
- A. S. Mata, S. C. Ferreira, *Multiple transitions of the susceptible-infected-susceptible epidemic model on complex networks*, Phys. Rev. E **91**, 012816 (2015).
- A. S. Mata, R. Pastor-Satorras, *Slow relaxation dynamics and aging in random walks on activity driven temporal networks*, Eur. Phys. J. B **88**, 38 (2015).
- A. S. Mata, M. Boguñá, C. Castellano, R. Pastor-Satorras, *The lifespan method as a tool to study criticality in absorbing-state phase transitions*, Phys. Rev. E **91**, 052117 (2015).
- W. F. C. Cota, A. S. Mata, S. C. Ferreira, *Numerical recipes for efficient simulations of the Markovian epidemic models on large complex networks*, in preparation.

LIST OF ABBREVIATIONS

BCPS: Boguñá, Castellano and Pastor-Satorras theory

CP: Contact Process

DRRN: Double Random Regular Network

FSS: Finite-Size Scaling

HMF: Heterogeneous Mean-Field

HPA: Homogeneous Pair Approximation

HTA: Homogeneous Triplet Approximation

GP: Griffiths Phase

LS: Lifespan

MFPT: Mean First Passage Time

NN: Nearest Neighbors

PHMF: Pair Heterogeneous Mean-Field

PQMF: Pair Quenched Mean-Field

PR: Participation Ratio

QMF: Quenched Mean-Field

QS: Quasistationary

RRN: Random Regular Network

SF: Scale-free

SIS: Susceptible-Infected-Susceptible

SIR: Susceptible-Infected-Removed

UCM : Uncorrelated Configuration Model

List of Figures

List of Tables

RESUMO

MATA, Angélica Sousa da, M. Sc., Universidade Federal de Viçosa, Fevereiro de 2015. **PROCESSOS EPIDÊMICOS E DIFUSÃO EM REDES: ABORDAGENS ANALÍTICA E COMPUTACIONAL**. Orientador: Silvio da Costa Ferreira Junior. Co-Orientadores: Marcelo Lobato Martins e Romualdo Pastor-Satorras.

Uma área de crescente interesse na Física Estatística é o estudo de processos dinâmicos em redes complexas. Neste contexto, o objetivo principal dessa tese é investigar o comportamento de processos epidêmicos em redes heterogêneas. Com esse intuito, aprimoramos as teorias de campo médio *quenched* e heterogênea através de aproximações de pares nas quais a correlação dinâmica entre vértices vizinhos é explicitamente levada em considerção. Essas abordagens nos permitem determinar, com maior precisão, os limiares epidêmicos do modelo suscetível-infectado-suscetível (SIS), e também as relações de escala dos expoentes críticos associados à transição de fase para o estado absorvente no processo de contato (CP). Também investigamos a dinâmica do modelo SIS em redes aleatórias com distribuição de conectividade em lei de potência ($P(k) \sim k^{-\gamma}$), com expoente $\gamma > 3$, uma vez que a existência ou ausência de um limiar finito envolvendo uma transição para a fase endêmica tem sido alvo de muitos estudos recentemente. Encontramos que o modelo pode exibir múltiplas transições envolvendo epidemias localizadas. Nossa análise numérica também indica que a transição para uma fase endêmica pode ocorrer num limiar finito. Nossos resultados mostram que teorias de campo médio a princípio contraditórias, na verdade são complementares porque elas descrevem diferentes limiares epidêmicos que podem aparecer concomitantemente em uma única rede. Finalmente, nós também investigamos processos de difusão em redes temporais através do modelo de caminhada aleatória. Além de ser estudada numericamente via simulações, tal dinâmica também foi estudada teoricamente através do seu mapeamento no modelo de armadilhas de Bouchaud. Nesse estudo foram encontradas evidências do comportamento de *aging* na relaxação de tal processo dinâmico.

ABSTRACT

MATA, Angélica Sousa da, M. Sc., Universidade Federal de Viçosa, February, 2015. **EPIDEMIC PROCESSES AND DIFFUSION ON NETWORKS: ANALYTICAL AND COMPUTATIONAL APPROACHES**. Adviser: Silvio da Costa Ferreira Junior. Co-Advisers: Marcelo Lobato Martins and Romualdo Pastor-Satorras.

A field of outstanding interest in Statistical Physics is the investigation of dynamical processes on complex networks. This thesis is devoted to explore the behavior of epidemic dynamics running on heterogeneous networks. We improved analytical approaches - quenched and heterogeneous mean-field theories - by means of pair approximations, which explicitly take into account dynamical correlations between connected vertices. These approaches yield more accurate predictions of the epidemic thresholds in the susceptible-infected-susceptible (SIS) model and the critical exponents associated to the absorbing state phase transition of the contact process (CP) obtained through finite-size scaling. These approaches can be applied to dynamical processes on networks in general providing a profitable strategy to analytically assess and fine-tune theoretical corrections. We also investigated the SIS dynamics on random networks having a power law degree distribution ($P(k) \sim k^{-\gamma}$), with exponent $\gamma > 3$, since the existence or absence of a finite threshold involving an endemic phase has been target of a recent and intense investigation. We found that this model on a single network can exhibit multiple transitions involving localized epidemics and our numerical analysis indicates that the transition to the endemic state occurs at a finite threshold. Our analysis points out that competing mean-field theories are, in fact, complementary since they describe different epidemic thresholds which can concomitantly emerge in a single network. Finally, we also investigated the diffusion processes on temporal networks by means of a random walk. We analyzed this dynamic theoretically by means of a mapping to Bouchaud's trap model and using numerical simulations. We found evidence of aging behavior in the random walk relaxation.

Part I

Preliminaries

Chapter 1

Introduction

There are many systems composed by a large number of elements connected according to a defined type of interactions. Examples can be found in different places present in our daily lives. The Internet is a collection of computers linked by data connections, the society consists of people linked by social relations, an ecosystem can be seen as a web of species connected by prey-predator relationships, our brain is constituted by a set of neurons connected by synapses, etc [1,2].

These examples have a common characteristic: they can be modeled as a network. The components of the system are the network vertices and the interactions among them are the edges [3]. These systems are often the scenario of interesting phenomena which can affect our routine. For instance, the Internet affects the way we access and produce information, the connections in a social network affect how people form opinions, interact sexually, or make working partnerships, etc. Beyond that, there are some disasters that can happen if some failure occurs in these systems: breakdown of the power grid can leave cities without electricity for many hours, a failure of a global financial system can lead a national economy to collapse, the fast spreading disease due to a dense air transport network can cause an epidemic outbreak [4].

The empirical studies of real-world systems were motivated by such phenomena and gave rise a important area of Science: the theory of complex networks. This area has a highly multidisciplinary nature, being the object of study in many fields including mathematics, computer science, sociology and physics. Particularly, in statistical physics, it is useful to reduce a complex system to a network representation. Even though this approach cannot capture all details of the system, one can use a set of statistical tools for the analysis, modeling and characterization of networks and to make predictions about dynamical processes taking place on it [1,5–8].

Indeed, the understanding of dynamical systems running on the top of complex networks rates among the hottest issues in complex network theory. Many studies have been conducted with

the aim of answering several questions [9–24]. *How can we describe the network topology with a small set of descriptors? How can different system as technological and social networks have similar connectivity patterns? How can the topology of the substrate affect the dynamics of the process taking place on it? What happens to the system behavior if the network has an intrinsic temporal dynamics?*

Our current research, supported by many previous works, try to shed light on some of these questions. We review, in the first part of this thesis (chapter 2), the fundamental concepts that are used during all the text. A brief review to describe complex systems using a toolset of complex networks theory is presented. We show that graphs representing different systems can have common features like heterogeneous topology, scale-free (SF) structure (their connectivity distribution follows power-law behavior), small-world property (vertices can be reached from every other with a small number of steps), etc [3,4,25,26] (section 2.1). We also present some static network models emphasizing the *uncorrelated configuration model* (UCM) [27] (section 2.2.1) that is useful to check the accuracy of analytical solutions of dynamical processes on networks. We also discuss the role of the intrinsic time-varying network on the dynamics running on top of it. Special attention is devoted to the *activity driven networks* [28] (section 2.2.2) since many studies about epidemic spreading and diffusion have been reported in this class of temporal networks [24,29–32].

We divided the thesis in two other parts beyond this introductory one. The part II is devoted to the study of epidemic spreading on static networks, and the part III refers to diffusion processes on temporal networks.

In the part II, we firstly review the theory and modeling of non-equilibrium dynamical systems on networks (chapter 3). Particularly relevant in this context are processes that exhibit absorbing-state phase transitions [33,34]. In the epidemic scenario, individuals can be in both infected or susceptible states. A phase transition between a disease-free (absorbing) state and an active stationary phase where a fraction of the population is infected are separated by an epidemic threshold λ_c [5]. The susceptible-infected-susceptible (SIS) model and the contact process (CP) [35] represent the simplest epidemic models possessing an absorbing-state phase transition (section 3.1). For the SIS model, the central issue of many recent works is to determine an epidemic threshold separating an absorbing, completely healthy state, from an active phase on heterogeneous networks [11,13–16,36–39] (section 3.6). In turn, for the CP model, most of the interest relies on the relation between critical exponents and statistical properties of the network, in particular the degree distribution [21,22,40–43] (section 3.5).

Many studies have been dedicated to investigate the criticality of the absorbing state phase transition observed in the CP [20–22,40,41] and SIS [11,13–16,19] models, mainly based on linear stability analysis around the transition point [11,13,14,18,21]. The heterogeneous mean-field

(HMF) approach [44] (section 3.4) for dynamical processes on complex networks has become widespread in the last decade. This theory, formerly conceived to investigate dynamical processes on complex networks, assumes that the number of connections of a vertex (the vertex degree) is the single quantity relevant to determine the state of the vertex, neglecting all dynamical correlations as well as the actual structure of the network. On the other hand, the quenched mean-field (QMF) theory [13,45] (section 3.3) still neglects dynamical correlations but the actual quenched structure of the network is explicitly taken into account by means of the adjacency matrix that contains the complete information of the connections among vertices [3].

However, neglecting dynamical correlations is an important drawback to ascertain the accuracy of the analytical results. The simplest way to explicitly consider dynamical correlations is by means of a pair-approximation [34]. In chapters 4 and 5, we present our original contribution to this topic by means pair QMF and HMF approximations for the CP [46] and SIS [39] models on heterogeneous networks.

In order to check the predictions of these theories, numerical investigations of the SIS and CP models on several networks have been recently reported [13,36,42,43,47–49]. Also in chapter 3 we present simulations techniques used to analyzed both models numerically. Numerical recipes for the simulation of Markovian epidemic models on complex networks can be found with more details in the Ref. [50], in which we present distinct algorithms and compare their computational efficiency (section 3.7.1).

To overcome the difficulties intrinsic to the stationary simulations of finite systems with absorbing states we use a robust approach called quasi-stationary (QS) method [51] (section 3.8.1). All simulations performed in chapters 4 and 5 we are done using this technique. However, recently, Boguñá *et al.* [16] proposed a new strategy, called lifespan (LS) method, in which the simulation starting from a single infected vertex and a diverging epidemic lifespan was used as a criterion to determine the thresholds (section 3.8.2). In Ref. [52], we check the feasibility of this method and conclude that it is an alternative way to numerically study systems with absorbing states.

Particularly, the existence or absence of finite epidemic thresholds involving an endemic phase of the SIS model on scale-free networks with a degree distribution $P(k) \sim k^{-\gamma}$, where γ is the degree exponent, has been target of a recent and intense investigation [11,13,15,16,36,38,53] (section 3.6). Distinct theoretical approaches for the SIS model were devised to determine an epidemic threshold produced different outcomes. The HMF theory predicts a vanishing threshold for the SIS model for the range $2 < \gamma \leq 3$ while a finite threshold is expected for $\gamma > 3$. Conversely, the QMF theory states a threshold inversely proportional to the largest eigenvalue of the adjacency matrix, implying that the threshold vanishes for any value of γ [13].

Motivated by controversial discussions [11,15,16,54,55], in chapter 6, we performed extensive simulations for the SIS dynamics on SF networks with exponent $\gamma > 3$. We found that a much more complex behavior with multiple transitions can arise from this dynamic. In individual networks with large gaps in the degree distribution we can observe multiple epidemic thresholds that are well described by different mean-field theories.

Finally, in the part III of this thesis, we advance in the study of networks considering now its temporal property. In the part II, we shown that the heterogeneous topology of a complex network [3] can have a relevant impact on the properties of dynamical systems running on top of it [1,26]. However, many dynamical effects can take a different, more complex turn when one considers the intrinsic time-varying, *temporal* nature of many real networks [56]. Indeed, networked systems are often not static, but show connections which appear and disappear during some characteristic time scales that can be of the same order of magnitude as those ruling a dynamical process on networks. Social networks [7] represent the prototypical example of this behavior, being defined in terms of a sequence of social contacts that are continuously established and broken. This mixing of time scales can induce new phenomenology on the dynamics of temporal networks, in stark contrast with what is observed in static networks [24,29,32].

Even considering a simple case, as a diffusion process represented by a random walk, a time-varying substrate can induce very noticeable differences with respect to the behavior expected in static networks [29–32] as reported in Ref. [24] and reviewed in chapter 7. Motivated by this evidence that the dynamics of temporal networks significantly alters the scenario for dynamical processes in static networks, we investigate in chapter 8 the relaxation dynamic of random walks on temporal networks by focusing in the activity driven model [28]. For realistic activity distributions with a power-law form, we observe the presence of a very slow relaxation dynamics compatible with aging effects. A theoretical description of this processes is achieved by means of a mapping to Bouchaud's trap model [57].

Chapter 2

Fundamentals of Network Theory

The study of complex networks is inspired by empirical analysis of real networks. Indeed, complex networks allow us to understand various real systems, ranging from communication networks to ecological webs [25]. In general terms, a network is a system that can be represented as a graph, composed by elements called nodes or vertices and a set of connecting links (edges) that represent the interactions among these elements [2] (Figure 2.1).

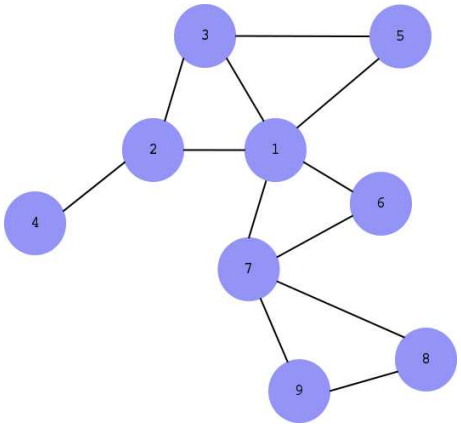

Figure 2.1: An example of a simple graph.

The advantage of modeling a system as a graph is that networks provide a theoretical framework that allows a suitable representation of interactions in complex systems. For instance, our brain is made up of a set of neurons connected by synapses, the Internet is formed by routers and computers cables and optical fibers, the society consists of people connected by social relationships as scientific collaboration, friendship, etc. [1,25,58].

On the one hand, the language for the description of networks is found in mathematical graph

theory. On the other hand, the study of very large systems requires a statistical characterization. In this chapter, we provide a brief introduction to the basic notions and notations of network theory which are used throughout this thesis. To conclude this short review, we will describe, in last section, network models that can be used to study dynamical processes in the context of computational approaches. Particular emphasis will be devoted to uncorrelated configuration model (UCM) and activity driven network, since the first one was used in this thesis to study epidemic spreading on static networks (Part II) and the latter was used to investigate slow dynamics on temporal networks (Part III).

2.1 Basic Concepts and Statistical Characterization of Networks

From a mathematical point of view, we can represent a network by means of an adjacency matrix $\mathbf{A}$. A graph of N vertices has a $N \times N$ adjacency matrix. The edges can be represented by the elements A_{ij} of this matrix such that [2]

$$A_{ij} = \begin{cases} 1, & \text{if the vertices } i \text{ and } j \text{ are connected} \\ 0, & \text{otherwise} \end{cases} \tag{2.1}$$

The concept of adjacency matrix is very useful in quenched mean-field theory that explicitly takes into account the actual connectivity of the network [13,45]. This issue is discussed with more details in section 3.3 of Part II.

A relevant information that can be obtained from the adjacency matrix is the degree k_i of a vertex i defined as the number of edges attached to the vertex i, *i.e.*, the number of nearest neighbors of the vertex i. The degree of the vertices can be written by means of the adjacency matrix as [2]

$$k_i = \sum_{j=1}^{N} A_{ij}. \tag{2.2}$$

A central issue in the structure of a graph is the reachability of its vertices, *i.e.*, the possibility that any information goes from one node to another through a path formed by the edges in the network [1]. For instance, we have a gossip spreading in a social network or a nerve impulse propagating in a neural network [2].

A path $\mathcal{P}_{ij}$ is defined as an ordered collection of $n+1$ vertices connected by n edges in a such a way that connect the vertices i and j. The concept of path leads us to define the distance between any pair of vertices in the network. The distance between the nodes i and j is defined as the number

of edges in the shortest connecting path denoted as ℓ_{ij} (see figure 2.2). The average shortest path length is defined as the value of ℓ_{ij} averaged over all the possible pairs of vertices in the network such that [59]

$$\langle l \rangle = \frac{1}{N(N-1)} \sum_{i \neq j} l_{ij}. \tag{2.3}$$

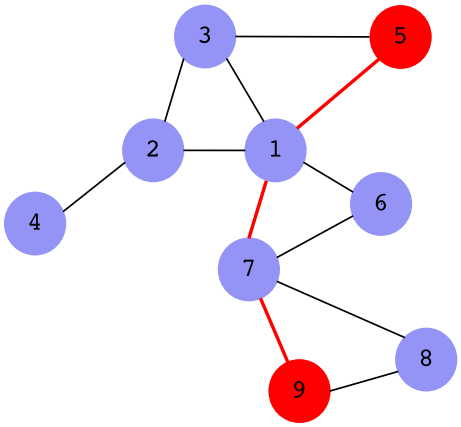

Figure 2.2: A network where the shortest path connecting two different vertices (5 and 9) is highlighted.

Typically, the number of neighbors in a complex network at a distance ℓ can be approximated by $\langle k \rangle^{\ell}$, considering that each vertex has degree equal to the average degree of the network $\langle k \rangle$ [see definition below - Eq. (2.7)] and there is no loop[1]. Since the quantity $\langle k \rangle^{\ell}$ rapidly grows with ℓ, we can thus roughly estimate $\langle \ell \rangle$ by the condition $\langle k \rangle^{\ell} \sim N$, then [1,59]

$$\langle \ell \rangle \simeq \frac{\ln N}{\ln \langle k \rangle}. \tag{2.4}$$

For a $d-$dimensional lattice, the number of neighbors at a distance ℓ scales as ℓ^d, implies that $\langle \ell \rangle \sim N^{1/d}$. So, the growth of $\langle \ell \rangle$ slower than any positive power of N characterizes the network with the small-world property[2] [1]. This scaling behavior is observed in many real-world phenomena, including websites, food chains, metabolite processing networks, etc [2,25,58].

Beyond the small-world characteristic, a network can be also described by the structure of the neighborhood of a vertex. The tendency to form cliques (fully connected sub-graphs) in the

[1] A loop or a cycle is a closed path $\mathcal{P}_{ij}(i = j)$ in which all nodes and all edges are distinct [2].
[2] Many authors refers to small-world effect to simultaneous small $\langle \ell \rangle$ and high clustering $\langle C \rangle$, Eqs. (2.4) and (2.5).

neighborhood of a given vertex is observed in many natural networks; for example, a group of friends who know each other. This property is called clustering and implies that if the vertex i is connected to the node j, and this one is connected to l, there is a high probability that i is also connected to l. The clustering $C(i)$ can be measured as the relative number of connections among the neighbors of i [59]:

$$C(i) = \frac{n_i}{k_i(k_i - 1)/2}. \tag{2.5}$$

Here k_i is the degree of the node i and n_i is the total number of edges among its nearest neighbors. The mean clustering coefficient is given by:

$$\langle C \rangle = \frac{1}{N} \sum_i C(i). \tag{2.6}$$

Apart from small-world and clustering properties, looking at very large systems as a protein network or the World Wide Web, an appropriate description can be done by means of statistical measures as the degree distribution $P(k)$. The degree distribution provides the probability that a vertex chosen at random has k edges [25,60].

The average degree is given by the average value of k over the network,

$$\langle k \rangle = \frac{1}{N} \sum_{i=1}^{N} k_i = \sum_k kP(k). \tag{2.7}$$

Similarly, it is useful to analyze the *n-th* moment of the degree distribution [1]

$$\langle k^n \rangle = \sum_k k^n P(k). \tag{2.8}$$

We can classify networks according to their degree distribution. The basic classes are homogeneous and heterogeneous networks. The first ones exhibit a fast decaying tail, as for example, a Poisson distribution. Here the average degree value corresponds to the typical value in the system. On the other hand, heterogeneous networks exhibit heavy tail that can be approximated by a power-law decay, $P(k) \sim k^{-\gamma}$. In this second case, the vertices will often have a small degree, but there is a non-negligible probability of finding nodes with very large degree values thus, depending on γ, the average degree does not represent any characteristic value of the distribution [1]. The contrast between these types of distributions is illustrated in Figure 2.3, where both Poisson and power-law degree distributions with the same average degree value are compared.

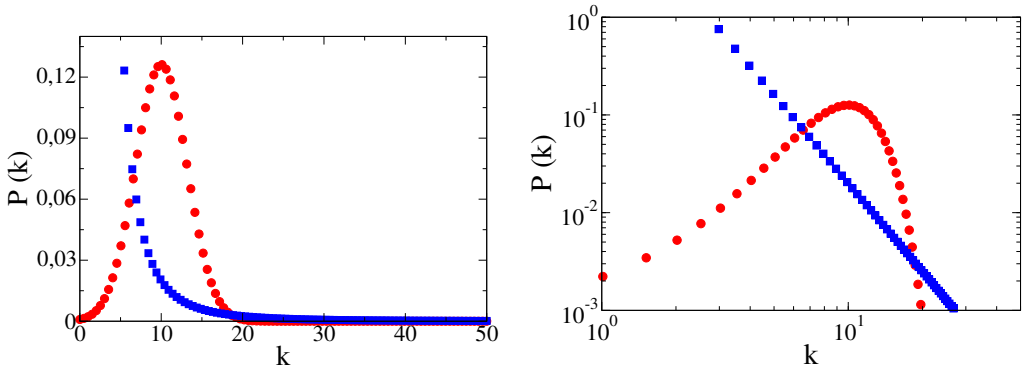

Figure 2.3: Comparison of a Poisson (circles) and a power law with $\gamma = 3$ (squares) degree distributions on a linear (left) and a double logarithmic plot (right). Both distributions have the same average degree $\langle k \rangle = 10$.

The role of the heterogeneity can be understood by looking at the first two moments of a power law distribution $P(k) \sim k^{-\gamma}$. We can compute the average degree value as[3]:

$$\langle k \rangle = \int_{k_0}^{k_{max}} kP(k)dk, \tag{2.9}$$

where $k_0 \geq 1$ is the lowest possible degree in the network and k_{max} is the maximal degree observed (upper cut-off of the distribution). Computing the integral one has [1],

$$\langle k \rangle = \int_{k_0}^{k_{max}} kAk^{-\gamma}dk = \frac{Ak^{2-\gamma}}{2-\gamma}\Bigg|_{k_0}^{k_{max}} \approx \frac{(\gamma-1)}{(\gamma-2)}k_0 \tag{2.10}$$

for $k_{max} \to \infty$ and for $\gamma > 2$. The normalization constant is given by $A \simeq (\gamma-1)k_0^{\gamma-1}$. We observe that the average degree is well defined and finite. The statistical fluctuations present in the system can be expressed by the normalized variance of the distribution $\sigma^2/\langle k \rangle^2$ whose main contribution is given by the second moment,

$$\langle k^2 \rangle = \int_{k_0}^{k_{max}} k^2 Ak^{-\gamma}dk \sim \begin{cases} k_{\text{max}}^{3-\gamma}, & \text{if } \ 2 < \gamma < 3 \\ \text{const.}, & \text{if } \ \gamma > 3. \end{cases} \tag{2.11}$$

In the thermodynamic limit, $\langle k^2 \rangle \to \infty$, for $2 < \gamma \leq 3$. This means that the fluctuations around the average degree are unbounded. We observe a scale free network since the absence of any intrinsic scale for the fluctuations implies that the average degree is not a characteristic scale for the system [25,59]. However, for $\gamma \geq 3$, the second moment remains finite. Indeed, besides the

[3]For simplicity, it is usual consider k a continuous variable. However when the integral is replaced by a discrete sum, the continuous results hold in the discrete case in the limit when $k_{max} \to \infty$.

shape of the power law degree distribution, we shall see further that the exponent γ has profound implications on dynamical processes running on top of heterogeneous substrates.

Other typical feature of networks is the tendency of nodes with a given degree connect with nodes with similar or dissimilar degree. When high or low degree vertices connect to other vertices with similar degree with higher probability, one says the correlations presented in the network are assortative. Conversely, if nodes of different degree are more likely to attach, the correlations are called disassortative [61].

One way to quantify the degree correlations is in terms of the conditional probability $P(k'|k)$ that a node with degree k is connected with a vertex with degree k' [1]. Since to determine $P(k'|k)$ can be a rather complicated task, a simple approach is given by the average degree of the nearest neighbors (NN) of a vertex i with degree k_i [62],

$$k_{nn,i} = \frac{1}{k_i} \sum_{j \in \mathcal{N}(i)} k_j, \tag{2.12}$$

where the sum runs over by the nearest neighbors vertices of i. Then, the behavior of the degree correlations is obtained by the average degree of the nearest neighbors, $k_{nn}(k)$, for vertices of degree k [63]:

$$k_{nn}(k) = \frac{1}{N_k} \sum_{i/k_i=k} k_{nn,i}, \tag{2.13}$$

where N_k is the number of nodes of degree k and the sum runs over all vertices with the same degree k. This quantity is related to the correlations between the degrees of connected nodes because in average it can be expressed as

$$k_{nn}(k) = \sum_{k'} k' P(k'|k). \tag{2.14}$$

If degrees of neighboring vertices are uncorrelated, $P(k'|k)$ is just a function of k' and $k_{nn}(k)$ is a constant. If k_{nn} increases with k then vertices with high degrees have a larger likelihood of being connected to each other. On the other hand, if k_{nn} decreases with k, high degree vertices have larger probabilities of have neighbors with low degrees [1,27,63] (See figure 2.4).

2.2 Networks Classes

In general, a network model produces graphs whith properties similar to the real system. However, the advantage of using a model is to reduce the complexity of the real world to a level that one can understand more easily. Therefore, networks are considered a powerful means of representing

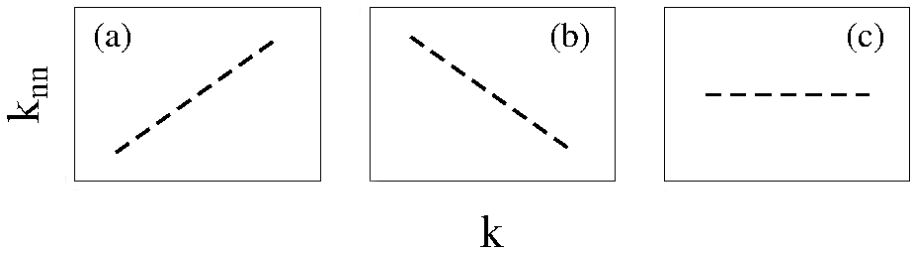

Figure 2.4: Schematic representation of the (a) assortative, (b) disasortative and (c) uncorrelated properties of the network indicated by the behavior of the average degree of the nearest neighbors, k_{nn}, for vertices with degree k.

patterns of connections between parts of systems such as Internet, power grid, food webs, social networks, etc [2,58,64].

On the one hand, technological networks as Internet are physical infrastructure networks that can be represented by static networks, *i.e.*, the nodes and edges are fixed or change very slowly over time [3]. On the other hand, networks that describe some form of social interaction between people have an intrinsic time-varying nature that should be taken into account. For instance, in a scientific collaboration network, the authors are not in contact with all their collaborators simultaneously during all the time. Indeed, real contact networks are dynamic with connections that appear and disappear with different characteristic time scales [28,56].

From the viewpoint of dynamical processes, both classes of networks - static and temporal - are important. The first one has been widely studied and it is convenient for analytical tractability whereas the second one is more realistic and constitutes a very promising approach. According to the development of complex networks over the years, we will start discussing the static networks and on the sequence the temporal ones.

2.2.1 Static Networks

The simplest prototype of a network was investigated by Erdős and Rényi, in 1959 [65]. In its original formulation, a graph is constructed starting from a set of N nodes and all edges among them have the same probability of existing.

Afterwards, in 1998, Watts and Strogatz (WS) proposed a more realistic model inspired by social networks that became known as the *small-world model* [10]. WS networks are constructed from N vertices initially arranged in one-dimensional lattice with periodic boundary conditions, each vertex has m connections with the nearest neighbors. Vertices are then visited clockwise and for each of them the clockwise edges are rewired with probability p. The rewiring process generates

connected networks and conserves the number of edges ($\langle k \rangle = m$). However, even at small p, the emergence of shortcuts among distant nodes greatly reduces the average shortest path length.

Concomitantly, Barabási and Albert [9] proposed a preferential attachment model suited to reproduce the feature of time growth of many real networks. In this model, new vertices are added to the system at every step. Each new vertice is connected to those nodes already present in the network with a probability proportional to their degrees at that time. The properties of growth and preferential attachment are suitable to model realistic networks as the Internet and the World Wide Web [2,58]. This class of networks provides an example of the emergence of graphs with a power law degree distribution [$P(k) \sim k^{-\gamma}$] and small-world properties.

In addition to their power law degree distributions, real networks are also characterized by the presence of degree correlations reflected on their conditional probabilities $P(k'|k)$ (see previous section). For uncorrelated networks, $P(k'|k)$ can be estimated as the probability that any edge points to a vertex with degree k', leading to $P_{unc}(k'|k) = k'P(k')/\langle k \rangle$ [66]. Thus, using Eq. (2.14) the average nearest-neighbor degree becomes,

$$k_{nn}^{unc}(k) = \frac{\langle k^2 \rangle}{\langle k \rangle^2}, \tag{2.15}$$

that is independent of the degree k.

Although most real networks show the presence of correlations, uncorrelated random graphs are important from a numerical point of view, since we can test the behavior of dynamical systems whose theoretical solution is available only in the absence of correlations. For this propose, Catanzaro *et al.* [27] proposed an algorithm to generate uncorrelated random networks with power law degree distributions, called uncorrelated configuration model (UCM). The steps of the algorithm are the following:

(i) In a set of N disconnected vertices, each node i is signed with a number k_i of stubs, where k_i is a random variable with distribution $P(k) \sim k^{-\gamma}$ under the restrictions $k_0 \leq k_i \leq N^{1/2}$ and $\sum_i k_i$ even. It means that no vertex can have either a degree smaller than the minimum degree k_0 or larger than the cutoff $k_c = N^{1/2}$.

(ii) The network is constructed by randomly choosing two stubs and connecting them to form edges, avoiding both multiple and self-connections.

It is possible to show that, to avoid correlations in the absence of multiples and self-connections, the random network must have a *structural cutoff* scaling at most as $k_c(N) \sim N^{1/2}$ (see discussion below). Actually, to generate a random graph with arbitrary γ and degrees in the range $k_0 \leq k < N$,

one expects that above a value k_c we find of order of one vertex [64,67],

$$N \int_{k_c}^{\infty} P(k)dk \sim 1. \tag{2.16}$$

In this case, one obtains,

$$k_c \sim N^{1/(\gamma-1)}, \tag{2.17}$$

which is the *natural cutoff* of the network [60]. However, for networks with power law degree distributions with $2 < \gamma \leq 3$, it is possible to construct an uncorrelated network, without a structural cut-off only if one permits multiple and self-connections, so that the constraint of forbidding these kind of connections introduces correlations in the network [27].

In order to shed light on this problem, we adapted some parts of Ref. [66], in which Boguñá *et al.* analyzed the degree distribution's cutoff in finite size scale-free networks. Let us define $r_{kk'}$ as

$$r_{kk'} = \frac{E_{kk'}}{m_{kk'}}, \tag{2.18}$$

where $E_{kk'}$ is the number of edges between vertices of degree k and k', and $m_{kk'} = \min(kN_k, k'N_{k'}, N_kN_{k'})$ is the maximum number of connections allowed between them, considering the restriction of not having multiple edges. If multiples edges are instead allowed $m_{kk'}$ is simply given by $m_{kk'} = \min(kN_k, k'N_{k'})$. Here, $N_k = NP(k)$ is the number of vertices of degree k. Thus, the ratio can be written as [66]

$$r_{kk'} = \frac{\langle k \rangle P(k,k')}{\min[kP(k), k'P(k'), NP(k)P(k')]}, \tag{2.19}$$

since the joint distribution is defined as the probability that a randomly chosen edge connects two vertices of degrees k and k', that yields [1]

$$P(k,k') = \frac{E_{kk'}}{\langle k \rangle N}. \tag{2.20}$$

For uncorrelated networks, the joint distribution can be factorized as

$$P_{unc}(k,k') = \frac{kk'P(k)P(k')}{\langle k \rangle^2}. \tag{2.21}$$

We can observe that if $k > N_{k'}$ and $k' > N_k$, it is not possible to connect vertices with degrees k and k' with each other without multiples edges. Then $\min[kP(k), k'P(k'), NP(k)P(k')] = NP(k)P(k')$ and the ratio $r_{kk'}$ takes the form [68]

$$r_{kk'} = \frac{kk'}{\langle k \rangle N}. \tag{2.22}$$

Independently of the type of the network, this ratio must be smaller than or equal to 1. If one considers the space $k - k'$ in which the joint probability is defined, the curve $r_{kk'} = 1$ delimiting the region $r_{kk'} < 1$, in which the pairs (k, k') taking admissible values, from the region $r_{kk'} > 1$, physically forbidden (see Fig. 2.5). The structural cutoff k_s must preserve this physical condition, so it can be defined as the value of the degree delimiting the largest square region of admissible values. That is given as the intersection of the curves $k = k'$ and $r_{kk'} = 1$. Thus, k_s is the solution of the implicit equation

$$r_{k_s k_s} = 1. \tag{2.23}$$

According Eq. (2.22), the structural cutoff takes the form

$$k_c(N) \sim (\langle k \rangle N)^{1/2}, \tag{2.24}$$

for any γ in the power law degree distribution [66]. For $\gamma > 3$, the constraint of the structural cutoff is expendable since it diverges faster than the natural cutoff. However, scale-free networks ($2 < \gamma \leq 3$) must posses a structural cutoff because the exponent of the natural cutoff is greater than $1/2$, and consequently, it diverges faster than the structural one. Then, for UCM networks, one has the cutoff k_c scaling as $\langle k_c \rangle \sim N^{1/\omega}$, where $\omega = \max(2, \gamma - 1)$ [27].

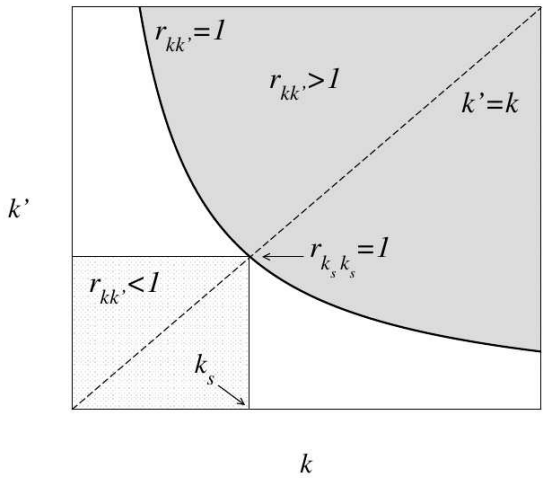

Figure 2.5: Geometrical construction of the structural cutoff k_S. Taken from Ref. [66]

In figure 2.6 we show a power law degree distribution for the UCM model [27] with different values of the degree exponent γ and check the lack of correlations. We can observe a flat behavior of $k_{nn}(k)$ [see Eqs. (2.14) and (2.15)] for all values of γ. In each realization of the degree sequence,

one obtains a random maximum degree k_{max}, with an average $\langle k_{max} \rangle = k_c$. For $\gamma > 3$, both mean and the standard deviation of k_{max} scale as $k_c \sim N^{1/\gamma-1}$ (see section 6.2 of Part II). As we can see in Fig. 2.6(b), this implies that k_{max} has large fluctuations for different network realizations [69].

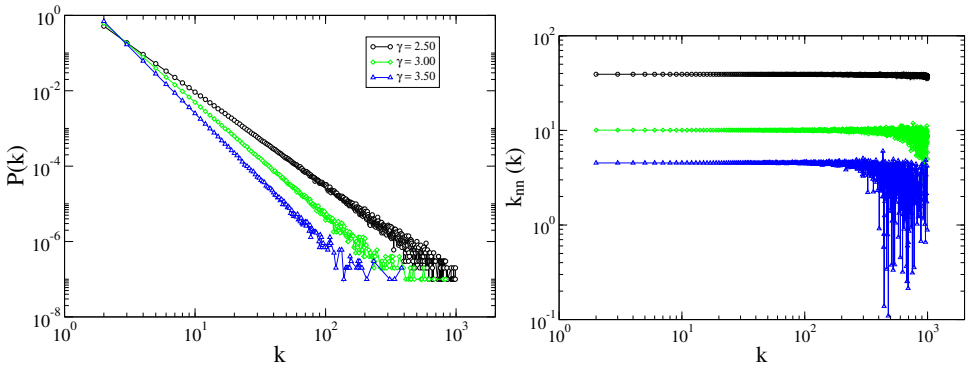

Figure 2.6: Power law degree distribution (left) and average nearest-neighbor degree of vertices of degree k (right) for the UCM network with different degree exponents γ, with $N = 10^6$ and $k_0 = 2$.

As said previously, this algorithm is very useful in order to check the accuracy of many analytical solutions of dynamical process on networks. In particular, this model is used in the Part II of this thesis, where we numerically test the behavior of epidemic models taking place on the top of complex networks and compare them with analytical approximations that are available just in the absence of degree correlations.

2.2.2 Temporal Networks

As shown in the previous section, the network structure helps us to understand the behavior of dynamical systems. However, in many cases, the edges are not continuously active. For example, in communication networks via email, edges represent sequences of instantaneous contacts [56]. In closed gatherings of individuals such as schools and conferences the agents are not simultaneously establishing interactions in the system [70,71]. Similarly to the network topology, the intrinsic time evolution of the network can also affect the system's dynamics from disease contagion to information diffusion [24,72,73].

Indeed, this mixing of time scales can induce new phenomenology on the dynamics on temporal networks, in stark contrast with what is observed in static networks. Moreover, the *bursty* nature [74–76] of the time evolution of temporal network contacts, characterized by long stretches of inactivity, interspersed by bursts of intense activity, can complicate the picture, inducing for example a noticeable dynamical slowing down in dynamical processes as varied as epidemic spreading, diffusion or synchronization [77–81].

Particularly relevant in this topic is the *activity driven* network [28]. Indeed, it represents a class of social temporal network models based on the observation that the establishment of social contacts is driven by the activity of individuals, prompting them to interact with their peers at different levels of intensity. Based on the empirical measurement of heterogeneous levels of activity denoted by a, across different datasets, activity strength has been found to be distributed according to a power law form, $F(a) \sim a^{-\gamma}$ [28].

The activity driven network model proposed by Perra *et al.* [28] is defined as follows (See figure 2.7): N nodes (individuals) in the network are endowed with an activity $a_i \in [\varepsilon, 1]$, extracted randomly from an activity distribution $F(a)$. Every time step $\Delta t = 1/N$, an agent i is uniformly chosen at random. With probability a_i, the agent becomes active and generates m links that are connected to m other agents, uniformly chosen at random. Those links last for a period of time Δt (*i.e.* are erased at the next time step). Time is updated as $t \to t + \Delta t$. The topological properties of the integrated network at time t (i.e. the network in which nodes i and j are connected if there has ever been a connection between them at any time $t' \leq t$) were studied in Ref. [82]. The main result is that the integrated degree distribution at time t, $P_t(k)$, scales in the large t limit as the activity distribution, i.e.

$$P_t(k) \sim t^{-1} F\left(\frac{k}{t} - \langle a \rangle\right), \tag{2.25}$$

considering $m = 1$.

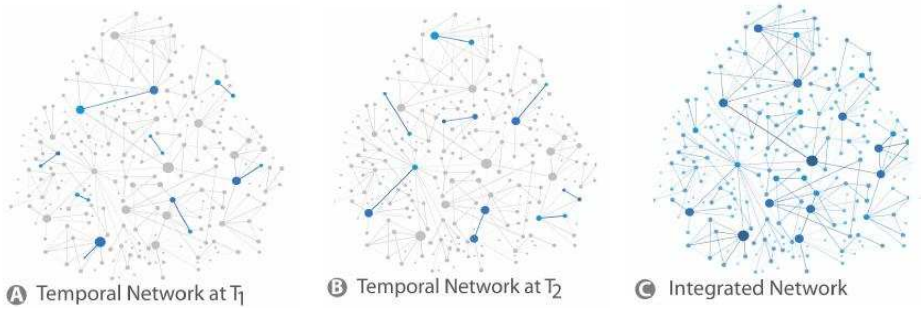

Figure 2.7: Schematic representation of the activity driven network model. We show a visualization of the resulting networks for 2 different time steps and the last visualization represents the integrated network. Figure taken from Ref. [73].

Empirical measurements report activity distributions in real temporal networks exhibiting heavy tails of the form $F(a) \sim a^{-\gamma}$ [28]. This expression thus relates in a simple way the functional form of the activity distribution and the degree distribution of the integrated network at time t, and allows to explain the power-law form of the latter observed in social networks [83].

In the third part of this thesis, we will study the random walk [84] on a activity-driven network. Even in this simple dynamical processes - although still underlying many practical realistic appli-

cations - a time-varying substrate can induce noticeable differences with respect to the behavior expected in static networks [24,29–31]. We will consider activity distributions with a power-law form. The range of values of the a is restricted to $a \in [\varepsilon, 1]$, where a minimum activity ε is set to avoid divergences. As we will see in chapter 8 - Part III, the parameter ε will play a significant role in the analysis of random walks on activity driven networks.

Part II

Epidemics Spreading on Complex Networks

Chapter 3

Phase Transitions with Absorbing States in Complex Networks

The present chapter provides a short review of the modeling and theory of non-equilibrium dynamical systems on networks. A key class of non-equilibrium process are those that exhibit absorbing states, *i.e.* states from which the dynamics cannot escape once it has fallen onto them.

A relevant feature of many systems with absorbing states is the absorbing-state phase transitions [33,34], *i.e*. non-equilibrium phase transitions between an active state, characterized by an everlasting activity in the thermodynamic limit, and an absorbing state, in which activity is absent.

The same type of transition occurs in epidemic spreading processes [5] since a fully healthy state is absorbing in the above sense, provided that immigration of infected individuals is not allowed. The susceptible-infected-susceptible (SIS) model and the contact process (CP) [35] represent the simplest epidemic models possessing an absorbing-state phase transition.

Lattice systems that exhibit such absorbing state phase transitions have universal features, determined by conservation laws and symmetries which allow to group them in a same universality class[1] [85]. The most robust class of absorbing state phase transitions is the directed percolation (DP) that was originally introduced as a model for directed random connectivity [86]. Both CP and SIS models are interacting particle systems involving self-annihilation and catalytic creation of particles that presents an absorbing-phase transition and thus belong to DP class. The SIS dynamics is indeed the most studied model to describe epidemic spreading on networks. Although the CP was initially thought as a toy model for epidemics [35], lately it has been widely used as a generic reaction-diffusion model to study phase transition with absorbing states.

[1] Once a set of models share the same symmetry properties, irrespective of the microscopic details of their dynamical rules, they belong to a single universality class and they should have the same critical exponents and scaling functions.

Thus, this chapter is devoted to review the SIS and CP models as examples to investigate absorbing phase transitions in complex networks. We firstly describe both epidemic models and, after we present distinct theoretical approaches devised for them. Finally we described the simulation techniques used to analyze both models numerically. For the SIS model, the central issue is to determine an epidemic threshold separating an absorbing, disease-free state from an active phase on heterogeneous networks [11,13–16,36–39]. While for the CP model, most of the interest is to relate the critical exponents with statistical properties of the network, in particular the degree distribution [21,22,40–43].

3.1 Epidemic Models

In the SIS epidemic model, each vertex i of the network can be in only one of two states: infected or susceptible which are represented by $\sigma_i = 1$ or $\sigma_i = 0$ respectively. Let us assume the most general case where a vertex i becomes spontaneously healthy at rate μ_i, and transmits the infection to each one of its k_i neighbors at rate λ_i. In figure 3.1, we show an example of the rates for a epidemic model. For classical SIS, one has $\mu_i = \mu$ and $\lambda_i = \lambda$ for every vertex.

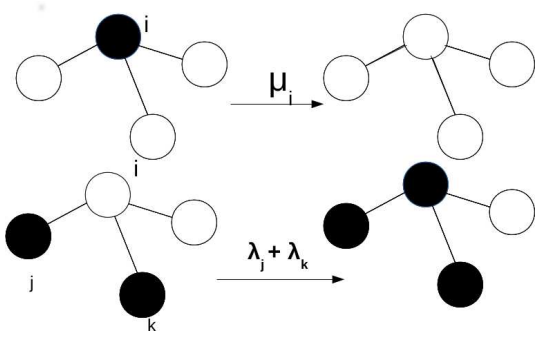

Figure 3.1: The rates in the dynamics of the SIS model for a vertex i initially infected.

As in the SIS model, vertices in the CP can be infected or susceptible, which in reaction-diffusion system's jargon are called occupied ($\sigma_i = 1$) and empty ($\sigma_i = 0$), respectively. The spontaneous cure process is exactly the same as in the SIS model: infected vertices become susceptible at rate $\mu_i = \mu$. The infection is, however, different. An infected vertex tries to transmit the infection to a randomly chosen neighbor at rate λ, implying that the transmission rate of vertex i is $\lambda_i = \lambda/k_i$, what reduces drastically the infective power of very connected vertices in comparison with the SIS dynamics.

Both SIS and CP dynamics exhibit a phase transition between a disease-free (absorbing) state and an active stationary phase where a fraction of the population is infected. These regimes are

separated by an epidemic threshold λ_c. The density of infected nodes ρ is the order parameter that describes this phase transition, as shown in Figure 3.2. For heterogeneous networks a more complex behavior can emerge as discussed in chapter 6. However, for a finite system the unique true stationary state is the absorbing state, even above the critical point, due to dynamical fluctuations. To overcome the difficulty to study the active state of finite systems some simulation strategies were proposed in the literature, as we will see in the section 3.8.

The accurate theoretical understanding of epidemic processes running on the top of complex networks rates among the hottest issues in complex network theory [11,13–22,39]. Much effort has been devoted to understand the criticality of the absorbing state phase transitions observed in CP [20–22,40,41] and SIS [11,13–16,19,39] models, mainly based on perturbative approaches (first order in ρ) around the transition point [11,13,14,18,21,39]. In the following we will present the basic mathematical approaches for the epidemic dynamics. Generally all these theories aim at understanding the properties of epidemics in the equilibrium or long term steady state, the existence of a non-zero density of infected individuals, the presence or absence of a threshold, etc. We will start with the simplest case namely the homogeneous mean-field theory, and thereafter we will review other more sophisticated mathematical approaches.

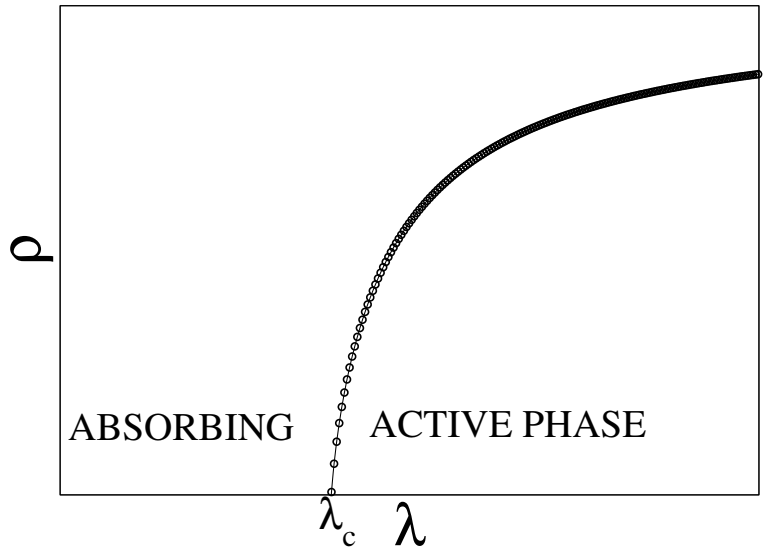

Figure 3.2: The density of infected nodes in a epidemic model as SIS or CP on regular lattices, in the thermodynamic limit.

3.2 Homogeneous mean-field theory

The prediction of disease evolution can be conceptualized within a variety of mathematical approaches. The simplest theory of epidemic spreading assumes that the population can be divided into different compartments according to the stage of the disease (for example, susceptible and infected in both SIS and CP models) and within each compartment, individuals (vertices in the complex networks' jargon) are assumed to be identical and have approximately the same number of neighbors (edges), $k \approx \langle k \rangle$ [87]. The idea is to write a time evolution equation for the number of infected individuals $I(t)$, or equivalently the corresponding density $\rho(t) = I(t)/N$, where N is the total number of individuals. For example, the equation describing the evolution of the SIS model is:

$$\frac{d\rho(t)}{dt} = -\mu\rho(t) + \lambda\langle k \rangle \rho(t)[1 - \rho(t)], \tag{3.1}$$

considering uniform infection and cure rates ($\lambda_i = \lambda$ and $\mu_i = \mu$, $\forall \;\; i = 1, 2, \cdots N$). The first term on the right-hand side of the Eq. (3.1) refers to the spontaneous healing and the second one to the infection process, that is proportional to the spreading rate $\lambda\langle k \rangle$, the density of the susceptible vertices $1 - \rho(t)$ that may become infected, and the density of infected nodes $\rho(t)$ in contact with any susceptible individual. Note that the evolution of the SIS model is completely described by Eq. (3.1), since the density of susceptible individuals $S(t)/N = 1 - \rho(t)$. The mean-field character of this equation comes from the fact that we have neglected the density correlations among different nodes. Thus, the probability that one infected vertex is connected to a susceptible one is approached as $\rho(t)[1 - \rho(t)]$.

Near the phase transition between a disease-free (absorbing) state and an active stationary phase we can assume that the number of infected nodes is small $\rho(t) \ll 1$. In this regime, we can use a linear approximation neglecting all ρ^2 terms[2]. So the Eq. (3.1) becomes[3]:

$$\frac{d\rho(t)}{dt} = -\rho(t) + \lambda\langle k \rangle \rho(t). \tag{3.2}$$

The solution is $\rho(t) \sim e^{-(1-\lambda\langle k \rangle)t}$, implying that $\overline{\rho} = 0$ is an stable fixe point for $1 - \lambda\langle k \rangle > 0$. Thus, one obtains,

$$\lambda_c = \frac{1}{\langle k \rangle}. \tag{3.3}$$

Here, λ_c is the epidemic threshold such that for any infection rate above this value the epidemic lasts forever.

[2]Indeed, this equation can be exactly integrated, but we prefered this stability analysis approach that is uses in more complex theories in the next sections

[3]From now on, we will consider $\mu = 1$, unless otherwise specified.

Similar analysis can be done for the CP model. In this case, the homogeneous mean-field equation read as

$$\frac{d\rho(t)}{dt} = -\rho(t) + \lambda\rho(t)[1 - \rho(t)], \tag{3.4}$$

since the transmission rate of each node is $\lambda/\langle k\rangle$. Performing the same linear stability analysis in the steady-state, one obtains $\lambda_c = 1$.

In this framework, one considers that the connectivity patterns among individuals are homogeneous, neglecting the highly heterogeneous structure of the contact network inherent to real systems [25]. Many biological, social and technological systems are characterized by heavy tailed distributions of the number of contacts k of an individual (the vertex degree, in the network jargon), for such systems the homogeneity hypothesis is severely violated [1,3,25]. Complex networks are, in fact, a framework where the heterogeneity of the contacts can be naturally afforded [25]. Indeed, this heterogeneity plays the main role in determining the epidemic threshold. To take it into account, other approaches have been proposed. As we shall see in the next sections, the major aim is to understand how the spreading epidemic can be strongly influenced by the topology of the networks.

3.3 Quenched Mean-field Theory

The quenched mean-field (QMF) theory [13] explicitly takes into account the actual connectivity of the network through its adjacency matrix. The central idea is to write the evolution equation for the probability $\rho_i(t)$ that a certain node i is infected. For the SIS model the dynamical equation for this probability takes the form [13]:

$$\frac{d\rho_i}{dt} = -\rho_i + \lambda(1 - \rho_i)\sum_{j=1}^{N} A_{ij}\rho_j. \tag{3.5}$$

where A_{ij} is the adjacency matrix that assumes $A_{ij} = 1$ if vertices i and j are connected and $A_{ij} = 0$, otherwise [see equation (2.1) in chapter 2]. The first term on the right-hand side considers nodes becoming healthy spontaneously while the second one considers the event that the node i is healthy and gets the infection via a neighbor node.

Performing a linear stability analysis around the trivial fixed point $\rho_i = 0$, one has

$$\frac{d\rho_i}{dt} = \sum_j L_{ij}\rho_j, \tag{3.6}$$

where the Jacobian matrix is

$$L_{ij} = -\delta_{ij} + \lambda A_{ij}, \tag{3.7}$$

δ_{ij} being the Kronecker delta symbol. The transition occurs when the fixed point loses stability or, equivalently, when the largest eigenvalue of the Jacobian matrix is $\Upsilon_m = 0$ [88]. The largest of L_{ij} is given by $\Upsilon_m = -1 + \lambda\Lambda_m$ where Λ_m is the largest eigenvalue of A_{ij}. Since A_{ij} is a real non-negative symmetric matrix, the Perron-Frobenius theorem states that one of its eigenvalues is positive and greater than, in absolute value, all other eigenvalues, and its corresponding eigenvector has positive components. So, one obtains the epidemic threshold of the SIS model in a QMF approach [13]:

$$\lambda_c^{qmf} = 1/\Lambda_m, \tag{3.8}$$

where Λ_m is the largest eigenvalue of the adjacency matrix. For the CP dynamic, the Eq. (3.5) becomes,

$$\frac{d\rho_i}{dt} = -\rho_i + \lambda(1-\rho_i)\sum_j \frac{A_{ij}\rho_j}{k_j}. \tag{3.9}$$

Performing the same linear stability analysis around the trivial fixed point, as was done for the SIS model, one obtains

$$\frac{d\rho_i}{dt} = \sum_j L_{ij}\rho_j, \tag{3.10}$$

where the Jacobian matrix is given by

$$L_{ij} = -\delta_{ij} + \frac{\lambda A_{ij}}{k_j}. \tag{3.11}$$

Once again the transition point is defined when the absorbing phase becomes unstable or, equivalently, when the largest eigenvalue of L_{ij} is null [88]. The largest of L_{ij} is given by $\Upsilon_m = -1+\lambda\Lambda_m$ where Λ_m is the largest eigenvalue of $C_{ij} = A_{ij}/k_j$. Notice that $v_i = k_i$ is an eigenvector of C_{ij} with eigenvalue $\Lambda = 1$. Now, supported by the Perron-Frobenius theorem [3], we conclude that the largest eigenvalue of C_{ij} is $\Lambda_m = 1$ resulting in the transition point $\lambda_c = 1$, as obtained in a homogeneous approximation.

Returning to the SIS model, the equation (3.8) can be complemented with the results of Chung *et. al.* [89] who calculated the largest eigenvalue of adjacency matrix of networks with a power law degree distributions as

$$\Lambda_m \simeq \begin{cases} \sqrt{k_c}, & \gamma > 5/2 \\ \frac{\langle k^2\rangle}{\langle k\rangle}, & 2 < \gamma < 5/2 \end{cases} \tag{3.12}$$

where k_c is the degree of the most connected node. Since k_c grows as a function of the network size for any γ, the central result of equation (3.12) is: Λ_m diverges for enlarging networks with power

law degree distributions even when $\langle k^2 \rangle$ remains finite [89]. Therefore, the epidemic thresholds scale as [49]

$$\lambda_c \simeq \begin{cases} 1/\sqrt{k_c}, & \gamma > 5/2 \\ \frac{\langle k \rangle}{\langle k^2 \rangle}, & 2 < \gamma < 5/2 \end{cases} \tag{3.13}$$

which vanishes for any power-law degree distribution The reasons for this difference of λ_c predicts by QMF approach, for γ larger or smaller than $5/2$ are explained in ref. [49]. In processes allowing endemic steady-states, the activation mechanisms depend on the degree of heterogeneity of the network. For $\gamma > 5/2$ the hub sustains activity and propagates it to the rest of the system while for $\gamma < 5/2$ the innermost network core collectively turns into the active state maintaining it globally. However, the behavior of the SIS model on random networks with power-law degree distribution can be much more complex than previously thought. Multiple phase transitions can arise depending on the connectivity distribution of the network. We studied this issue thoroughly and our original results are reported in the chapter 6.

3.4 Heterogeneous Mean-Field Theory

In a HMF theory, dynamical quantities, as the density of infected individuals in the SIS model, depend only of the vertex degree and do not of their specific location in the network. Actually, the HMF theory can be obtained from the QMF one performing a coarse-graining where vertices are grouped according to their degrees. To take into account the effect of the degree heterogeneity we have to consider the relative density $\rho_k(t)$ of infected nodes with a given connectivity k, *i.e.*, the probability that a node with k links is infected. Again using the SIS model as an example, the dynamical mean-field rate equation describing the system can thus be written as [44]:

$$\frac{d\rho_k(t)}{dt} = -\rho_k(t) + \lambda k[1 - \rho_k(t)] \sum_{k'} P(k'|k)\rho_{k'}(t), \tag{3.14}$$

The first term on the right-hand side considers nodes becoming healthy at unitary rate. The second term considers the event that a node with k links is healthy and gets the infection via a nearest neighbor. The probability of this event is proportional to the infection rate λ, the number of connections k and the probability that any neighbor vertex is infected $P(k'|k)\rho_{k'}$. The linearization Eq. (3.14) gives

$$\frac{d\rho_k}{dt} = \sum_k L_{kk'}\rho_{k'}, \tag{3.15}$$

where $L_{kk'} = -\delta_{kk'} + \lambda k P(k'|k)$. Therefore, the epidemic threshold is

$$\lambda_c = \frac{1}{\Lambda_m}, \tag{3.16}$$

where Λ_m is the largest value of $C_{kk'} = kP(k'|k)$.

It is difficult to find the exact solution for Λ_m for a general form of $P(k'|k)$. But it is possible to extract the value of the epidemic threshold. In the case of uncorrelated networks, $P(k'|k) = k'P(k')/\langle k\rangle$ and $C_{kk'} = k'kP(k')/\langle k\rangle$. So, it is easy to check that $v_k = k$ is an eigenvector with eigenvalue $\langle k^2\rangle/\langle k\rangle$ that, according to Perron-Frobenius theorem, is the largest. Thus, we obtain the epidemic threshold:

$$\lambda_c^{hmf} = \langle k\rangle/\langle k^2\rangle, \tag{3.17}$$

Equation (3.17) has strong implications since several real networks have a power law degree distribution $P(k) \sim k^{-\gamma}$ with exponents in the range $2 < \gamma < 3$ [25]. For these distributions, the second moment $\langle k^2\rangle$ diverges in the limit of infinite sizes implying a vanishing threshold for the SIS model or, equivalently, the epidemic prevalence for any finite infection rate. Both theories HMF and QMF predict vanishing thresholds for $\gamma < 3$ despite of different scaling for $5/2 < \gamma < 3$. However, while HMF predicts a finite threshold for networks with $\gamma > 3$, QMF still predicts a vanishing threshold [49].

For the CP model, the heterogeneous mean-field equation, analogous to Eq. (3.14), can be written as

$$\frac{d\rho_k(t)}{dt} = -\rho_k(t) + \lambda k[1-\rho_k(t)]\sum_{k'}\frac{P(k'|k)\rho_{k'}(t)}{k'}. \tag{3.18}$$

again we assume degree-uncorrelated networks, a simple linear stability analysis shows the presence of a phase transition, located at the value $\lambda_c = 1$, as found in homogeneous mean-field theory, independent of the degree distribution and degree correlations. According to simulations (see chapter 4) the transition point does not quantitatively reproduced the predictions of both approaches, HMF and QMF. However, the advantage of HMF over the QMF theory, is that we can analytically obtain the critical exponents for the dynamical model and compare with numerical results. Indeed, recent works have shown that the contact process running on the top of highly heterogeneous random networks is well-described by the heterogeneous mean-field theory [41,42]. However, some important aspects such as the threshold and strong corrections to the finite-size scaling observed in simulations are not clarified in this theory. We summarize the intense scientific discussion [21,22,41–43,90,91] about this subject in the next section.

3.5 Finite Size Scaling for CP model on heterogeneous networks

In Ref. [43], Castellano and Pastor-Satorras derived the HMF theory for the CP dynamic in the limit of infinite network size. They obtained the following scaling

$$\bar{\rho} \sim (\lambda - \lambda_c)^{\beta}, \quad \beta = \max\left[1, \frac{1}{\gamma - 2}\right]. \tag{3.19}$$

At the transition point $\lambda = \lambda_c$,

$$\rho \sim t^{-\delta}, \quad \delta = \beta. \tag{3.20}$$

Also the relaxation time scales as

$$\tau \sim (\lambda - \lambda_c)^{-\nu_{\|}}, \quad \nu_{\|} = 1. \tag{3.21}$$

These exponents are also obtained using a pair HMF approximation as we shall show in section 4.4.1.

Its predictions could not be directly checked against numerical simulations because of the presence of finite-size effects. A comparison became possible using the finite-size scaling (FSS) ansatz [92], adapted to the network topology, and they concluded that CP dynamics on networks was not described by the HMF approximation. However, it was assumed in Ref. [43] that heterogeneous networks follows the same FSS known for regular lattices [34]. Indeed, the FSS on networks is more complicated than previously assumed. The behavior of the CP on networks of finite size depends not only on the number of vertices N but also on the moments of the degree distribution [21]. This implies that, for scale-free networks, the scaling around the critical point depends explicitly on how the largest degree k_c diverges with the system size N. Such dependence introduces very strong corrections to scaling. However, if such corrections are properly taken into account, it is possible to show that the CP on heterogeneous networks agrees, with high accuracy, with the predictions of HMF theory [41].

Starting from Eq. (3.18), and considering, in addition, uncorrelated networks with $P(k|k') = kP(k)/k$, the overall density $\rho = \sum_k \rho_k P(k)$, obeys the equation [42]

$$\frac{d\rho(t)}{dt} = \rho(t) + \lambda\rho(t)\left[1 - \langle k\rangle^{-1}\sum_k kP(k)\rho_k(t)\right]. \tag{3.22}$$

A mean field theory for the FSS can be obtained using the strategy proposed by Castellano and Pastor-Satorras [21], in which the motion equation is mapped in a one-step process, in the limit of

very low densities, with transition rates

$$\begin{aligned} W(n-1,n) &= n \\ W(n+1,n) &= \lambda n\left[1-\langle k\rangle^{-1}\textstyle\sum_k kP(k)\rho_k(t)\right], \end{aligned} \tag{3.23}$$

where $W(n,m)$ represents the transitions from a state with m infected vertices to another state with n infected vertices. In the stationary state, $d\rho(t)/dt = 0$, the Eq. (3.22) read as [41]

$$\bar{\rho_k} = \frac{\lambda k\bar{\rho}/\langle k\rangle}{1+\lambda k\bar{\rho}/\langle k\rangle}. \tag{3.24}$$

Close to the criticality, when the density at long times is sufficiently small such that $\bar{\rho}k_c \ll 1$, Eq. (3.24) becomes $\bar{\rho_k} \simeq \lambda k\bar{\rho}/\langle k\rangle$. Substituting this result in Eq. (3.23), one finds that the first-order approximation for the one-step processes is

$$\begin{aligned} W(n-1,n) &= n \\ W(n+1,n) &= \lambda n(1-\lambda g n/N), \end{aligned} \tag{3.25}$$

where $g = \langle k^2\rangle/\langle k\rangle^2$.

The master equation for a standard one-step process is [93]

$$\frac{dP_n}{dt} = \sum_m W(n,m)P_m(t) - \sum_m W(m,n)P_n(t). \tag{3.26}$$

Substituting the rates (3.25), we find

$$\frac{dP_n}{dt} = (n+1)P_{n+1} + u_{n-1}P_{n-1} - (n+u_n)P_n \tag{3.27}$$

with $u_n = \lambda n(1-ng)$. Since the probability for the process not to end up in the absorbing state up to time t, named survival probability, is given by $P_s(t) = \sum_{n\geq 1} P_n(t)$, we can define the quasistationary (QS) distribution $\bar{P}_n$ as [34]

$$\bar{P}_n = \lim_{t\longrightarrow\infty} \frac{P_n(t)}{P_s(t)} \quad (n \geq 1), \tag{3.28}$$

with $\bar{P}_0 \equiv 0$ and normalized condition $\sum_{n\geq 1}\bar{P}_n = 1$ (see more details in section 3.8.1). The solutions of the equation (3.27) have already been exhaustively investigated, then we merely report the results of Ref. [41] where it was found that the critical QS distribution for large systems has the

following scaling form[4]

$$\bar{P}_n = \frac{1}{\sqrt{N/g}} f\left(\frac{n}{\sqrt{N/g}}\right), \tag{3.29}$$

where $f(x)$ is as scaling function with the following properties: $f(x) \sim \exp(-ax)$ for $x \ll 1$, where a is constant, and $f(x) \sim \exp(-x^2/2)$ for $x \gg 1$. The critical quasistationary density scale as

$$\bar{\rho} \sim (gN)^{-1/2}. \tag{3.30}$$

Similarly, the characteristic time scales as

$$\tau \sim \left(\frac{N}{g}\right)^{1/2}. \tag{3.31}$$

For a network with degree exponent γ and a cutoff scaling with the system size as $k_c \sim N^{1/\omega}$, where $\omega = \max[2, \gamma - 1]$ for UCM networks, the factor g scales for asymptotically large systems as $g \sim k_c^{3-\gamma}$ for $\gamma < 3$ and $g \sim$ const. for $\gamma > 3$. The result is a scaling law $\rho \sim N^{-\hat{\nu}}$ and $\tau \sim N^{\hat{\alpha}}$ where the exponents $\hat{\nu}$ and $\hat{\alpha}$ are given by

$$\hat{\nu} = \frac{1}{2} + \max\left(\frac{3-\gamma}{2\omega}, 0\right), \quad \hat{\alpha} = \frac{1}{2} - \max\left(\frac{\gamma-3}{2\omega}, 0\right). \tag{3.32}$$

In Ref. [42], Ferreira *et al.* investigated the CP on heterogeneous networks with power-law degree distribution by performing quasistationary simulations (see section 3.8.1), and concluded that heterogeneous mean-field theory correctly describes the critical behavior of the contact process on quenched networks. However, some important questions remained unanswered. The transition point $\lambda_c = 1$ predicted by this theory does not reflect the dependence on the degree distribution observed in simulations. Sub-leading corrections to the finite-size scaling, undetected by the one-vertex HMF theory, are quantitatively relevant for the analysis of highly heterogeneous networks ($\gamma \to 2$), for which deviations from the theoretical finite-size scaling exponents were reported [42]. The HMF theory assumes that the number of connections of a vertex is the quantity relevant to determine its state and neglects all dynamical correlations. But dynamical correlations represent an important factor in ascertaining the accuracy of the analytical results. The simplest way to explicitly consider dynamical correlations is by means of a pair-approximation [34]. In chapter 4, we will present a pair HMF approximation for the CP on heterogeneous networks that is our original contribution for this, until them, open problem. We will show that this theory yields great

[4]This was shown in Ref [41] for annealed networks, but this can also be applied for quenched large systems [42]. In annealed networks, the vertex degrees are fixed while the edges are completely rewired between successive dynamics steps implying that dynamical correlations are absent and HMF theory becomes an exact prescription [40].

improvements in relation to the one-vertex counterpart. A pair approximation approaches for the SIS model were also studied and our original results are shown in chapter 5.

3.6 Intriguing questions for the SIS model

As we saw in the previous sections, distinct theoretical approaches were devised for the SIS and CP models to determine an epidemic threshold λ_c separating an absorbing, disease-free state from an active phase [11,13,15,16,36,38,39,94]. The quenched mean-field (QMF) theory [94] explicitly includes the entire structure of the network through its adjacency matrix while the heterogeneous mean-field (HMF) theory [44,95] performs a coarse-graining of the network grouping vertices accordingly their degree. However, for the SIS model, both theories predicts different thresholds. The HMF theory predicts a vanishing threshold for the range $2 < \gamma \leq 3$ while a finite threshold is expected for $\gamma > 3$. Conversely, the QMF theory states a threshold inversely proportional to the largest eigenvalue of the adjacency matrix, implying that the threshold vanishes for any value of γ [13]. Regardless, Goltsev *et al*. [11] proposed that QMF theory predicts the threshold for an endemic phase, in which a finite fraction of the network is infected, only if the principal eigenvector of adjacency matrix is delocalized. In the case of a localized principal eigenvector, that usually happens for large random networks with $\gamma > 3$ [96], the epidemic threshold is associated to the eigenvalue of the first delocalized eigenvector. For $\gamma < 3$, there exists a consensus for SIS thresholds: both HMF and QMF are equivalent and accurate for $\gamma < 2.5$ while QMF works better for $2.5 < \gamma < 3$ [36,39].

Lee *et. al.* [15] proposed that for a range $\lambda_c^{QMF} < \lambda < \lambda_c$ with a nonzero λ_c, the hubs in a random network become infected generating epidemic activity in their neighborhoods. This activity has a characteristic lifespan $\tau(k, \lambda)$ depending on the degree k and the infection rate λ. On networks where almost all hubs are directly connected the activity can be spread among them if the lifespan $\tau(k, \lambda)$ is large enough. Then, above λ_c^{QMF}, the network is able to sustain an endemic state due to the mutual reinfection of connected hubs. However,when hubs are not directly connected, the reinfection mechanism does not work and high-degree vertices produce independent active domains. These independent domains were classified as rare-regions, in which activity can last for very long times (increasing exponentially with the domain size [97]), generating Griffiths phases (GPs) [97,98]. The sizes of these active domains increase for increasing λ leading to the overlap among them and, finally, to an endemic phase for $\lambda > \lambda_c$.

These arguments presented in Refs. [11,15] lead to the conclusion that the threshold to an endemic phase is finite in random networks with a power law degree distribution for $\gamma > 3$. Inspired in the appealing arguments of Lee *et al.* [15], Boguñá, Castellano and Pastor-Satorras (BCPS) [16]

reconsidered the problem and proposed a semi-analytical approach taking into account a long-range reinfection mechanism and found a vanishing epidemic threshold for $\gamma > 3$.

As reported by Lee *et. al.* [15], when the hubs on a network are directly connected, the activity can be spread throughout the network even in the limit $\lambda \to 0$. However, when higher degrees nodes are distant from each other these hubs are able to sustain local active domains around them and only with a nonzero λ_c, the endemic state is reached. Nevertheless, Boguñá, Castellano and Pastor-Satorras [16] (BCPS theory) revisited the problem taking into account long range dynamic correlations in a coarse-grained time scale. As explained in Ref. [16], the BCPS approach states that a directed connection between hubs is not a necessary condition for reinfected them. There is a possibility of "long-range" reinfection since the network has a small-world property. In this approach, it was concluded that the epidemic threshold vanishes for random networks with $P(k)$ decaying slower than exponentially, in particular, $P(k) \sim k^{-\gamma}$ with any γ.

To check the accuracy of the BCPS theory [16], they compared their theoretical predictions with simulations starting from a single infected vertex and a diverging epidemic lifespan was used as a criterion to determine the thresholds (Lifespan method - see section 3.8.2).

We will show in chapter 6 that this apparently competing mean-field theories: HMF, QMF and BCPS [11,13,15,16,44] can be considered, in fact, complementary, describing distinct transitions that may concomitantly emerge depending on the network structure.

3.7 Simulation of Epidemic Processes

Many of previous works [44,95] present mistaken prescriptions of how to simulate the SIS model on complex networks. To emphasize the importance to simulate the SIS dynamics correctly, we present, in Ref. [50], numerical recipes for the simulation of Markovian epidemic models on highly heterogeneous graphs. In the following sections, we summarized this work showing distinct algorithms for the SIS and CP dynamics.

3.7.1 Simulation of SIS model

The SIS dynamics in a network of size N can be simulated in a very simple way: Select a vertex at random with equal chance. If the selected vertex i is infected we turn it to susceptible with probability

$$p_i = \mu_i \zeta, \tag{3.33}$$

otherwise it becomes infected with probability

$$q_i = \sum_{j=1}^{N} \lambda_i \sigma_i A_{ij} \zeta, \tag{3.34}$$

where the sum runs over all nearest neighbors of i since A_{ij} corresponds to adjacency matrix. The time incremented by $\delta t = \zeta/N$, where the factor $1/N$ accounts the choice of a single vertex by time step. The factor ζ must, in principle, be infinitesimally small but, in practice, it should be as large as possible but assuring both $p_i, q_i \leq 1$. A good choice is

$$\zeta = \frac{1}{\max(\lambda_i + \mu_i) k_{max}}, \tag{3.35}$$

where k_{max} is maximal number of connections and $\max(\lambda_i + \mu_i)$ the maximal value of $\lambda_i + \mu_i$ of a vertex in the entire network. In the simplest case of $\lambda_i = \lambda$ and $\mu_i = \mu$ for all vertices, we have

$$p_i = \frac{\lambda n_i}{(\mu + \lambda) k_{max}}, \tag{3.36}$$

where $n_i = \sum_j A_{ij} \sigma_j$ is the number of infected nearest neighbors of the vertex i, and

$$q_i = \frac{\mu}{(\mu + \lambda) k_{max}}. \tag{3.37}$$

This algorithm is accurate and can used for any generic SIS dynamics. However, if one is interested in regions close to the threshold where the great majority of the vertices are susceptible, the algorithm is very inefficient since changes happens only inside and in the neighborhood of infected vertices. Therefore, we can use a more efficient strategy based on the previous algorithm. This strategy requires to keep and constantly update a list $\mathcal{P}$ with the positions of all infected vertices where changes will take place. The list update is simple. The position of a new infected is added at the end of the list. When a infected vertex becomes susceptible, the last entry of the list is moved to the index of the cured vertex.

The total rate that a infected vertex becomes susceptible in the whole network is

$$R = \sum_i \mu_i \sigma_i \tag{3.38}$$

Analogously, the total rate that one susceptible vertex is infected is given by

$$J = \sum_{i,j} (1 - \sigma_i) A_{ij} \lambda_j \sigma_j = \sum_j \lambda_j k_j \sigma_j - \sum_{i,j} \lambda_j \sigma_j \sigma_i A_{ij}, \tag{3.39}$$

where $\sum_i A_{ij} = k_j$ was used to perform the sum in the first term. The first term in the right-hand side $S = \sum_j \lambda_j k_j \sigma_j$ represents the total infection rate emanating from all infected vertices while the second one is that transmitted between pairs of infected vertices that does not lead to a new infection.

For uniform infection and cure rates, $\lambda_i = \lambda$ and $\mu_i = \mu$, we have $R = \mu N_i$ and $S = \lambda N_e$, where N_i is the number of infected vertices and N_e is the number of vertices emanating from them. So, the SIS dynamics can be simulated according to the algorithm proposed by Ferreira *et al.* [36] as follows: N_i and N_e are constantly updated. With probability $p = \mu N_i/(\mu N_i + \lambda N_e)$, an infected vertex is selected with equal chance and cured. With complementary probability $q = 1 - p$, an infected vertex is selected at random and accepted with probability proportional to its degree. In the infection attempt, a neighbor of the selected vertex is randomly chosen and if susceptible, it is infected. Otherwise nothing happens and simulations run to the next time step. The frustrated infection attempts reckon exactly the second term in the right hand side of Eq. 3.39. The time is incremented by $\delta t = 1/(\mu N_i + \lambda N_e)$. More technical details can be found in Cota *et. al.* [50]. In this paper we describe accurately numerical recipes for efficient simulations of the SIS model on complex networks[5].

3.7.2 Simulation of CP model

The CP dynamics can be efficiently simulated if a list of occupied vertex $\mathcal{P}$ is used analogously to the SIS algorithm. The total rate of cure is also given by Eq. (3.38). The total creation rate is

$$J = \sum_{i,j=1}^{N} (1 - \sigma_i) A_{i,j} \sigma_j \frac{\lambda_j}{k_j} = \sum_{j=1}^{N} \lambda_j \sigma_j - \sum_{i,j=1}^{N} \sigma_j \sigma_i A_{ij} \frac{\lambda_j}{k_j}, \tag{3.40}$$

where $S = \sum_i \lambda_i \sigma_i$ is again the total infection emanating from infected vertices and the second term is the rate of frustrated attempts of infections. In the case of homogeneous infection and cure rates $\lambda_i = \lambda$ and $\mu_i = \mu$, we have $S = \lambda N_i$ and $R = \mu N_i$ and the standard procedure is recovered [34]: An infected vertex i is selected with equal chance. With probability $p = R/(S + R) = \mu/(\mu + \lambda)$ it is cured. With probability $q = S/(S + R) = \lambda/(\mu + \lambda)$ one of the k_i neighbors of i is selected and, if susceptible, is infected. The time is incremented by $\delta t = 1/[N_i(\lambda + \mu)]$. Again, the frustrated infection attempts take into account the second term of Eq. (3.40). Notice that infected vertices are selected independently of their degrees and with probability n_i/k_i reach an already

[5]To simulate the continuous-time process one replaces the fixed interval dt with an exponential distribution of the waiting time. Both formulations differ at short times but share the same stationary properties and long-term dynamics [99].

infected neighbor, which is in agreement with the term $1/k_i$ in the second term of Eq. (3.40).

Although equivalent for strictly homogeneous graphs ($k_i \equiv k \; \forall \; i$), the SIS and the CP models are very different for heterogeneous substrates. The universality class of CP and SIS is the same in homogeneous lattices. Both models belong to the DP universality class [85]. Nevertheless, in complex networks, heterogeneity affects both models and, at the heterogeneous mean-field approach, they have different critical exponents (see discussion in Ref. [100]).

3.8 Simulation of dynamical process with an absorbing state

The theoretical characterization of absorbing-state phase transitions is based on mean-field approaches and field theory renormalization procedures [101]. While the former is only valid above the upper critical dimension, application of the latter in physical dimensions is hindered by large technical difficulties. For this reason, most of our knowledge about the properties of absorbing-state phase transitions is based in the computer simulation of different representative models. The numerical analysis of these computer data represents a different kind of challenge, which is mainly hampered by finite size effects. In finite systems, any realization of the dynamics is bound to reach sooner or later the absorbing state, even above the critical point, due to dynamic fluctuations. This difficulty can be overcome by applying the finite-size scaling technique [92], based on the size dependence of physical observables traditionally determined by starting with a finite initial density of active sites and averaging only over surviving runs, *i.e.*, realizations which have not yet fallen into the absorbing state [34]. Analyzing the quasistationary state defined by surviving averages, the critical point and various critical exponents can be performed by studying the decay of the survival average of different observables as a function of the system size. Averaging over surviving runs, however, is computationally extremely inefficient since surviving configurations are very rare at long times.

A much more effective alternative is provided by the quasistationary (QS) method [51,102,103], in which every time the system tries to visit an absorbing state, it jumps to an active configuration previously stored during the simulation. Recently, in the context of epidemic modeling on complex networks [104], Boguñá *et. al.* [16] proposed another strategy which considers the lifespan of spreading simulations starting from a single infected site as a tool to determine the position of the critical point. Both methods are described in the following subsections.

3.8.1 The Quasistationary Method

In this thesis, we used an efficient quasistationary method (QS) proposed by Oliveira and Dickman [51]. This method is suitable to study models that admits an active stationary state in the thermodynamic limit but which always falls into the absorbing state for a finite size system, as occurs in CP and SIS models. The QS method [41,51] is, to our knowledge, the most robust approach to overcome the difficulties intrinsic to the stationary simulations of finite systems with absorbing states. Thus, we reproduce some parts of Ref. [51] to introduce this practical simulation method.

The idea of the quasi-stationary (QS) distribution is indeed simple. Firstly, consider a Markov process X_t, in continuous time, taking values $n_t \geq 0$, with the state $n = 0$ absorbing. The distribution $P_n(t)$ denotes the probability that $X_t = n$ given some initial condition X_0. As said before, the survival probability is given by $P_s(t) = \sum_{n\geq 1} P_n(t)$. So, we define the QS distribution $\bar{P}_n$ as defined by Eq. (3.28).

For a better understanding of the method, we consider the following master equation [93]:

$$\frac{dP_n}{dt} = \sum_m W(n,m)P_m(t) - \sum_m W(m,n)P_n(t). \tag{3.41}$$

in which $W(n,m)$ and $W(m,n)$ represents the rate of transition in and out of the state n, respectively.

The purpose of the QS method is to rewrite the Eq. (3.41) such that it can represent a process X_t^* whose stationary probability distribution is the quasi-stationary distribution of X_t. In other words, we have to add in the original master equation, Eq. (3.41), another term that represents a redistribution of the probability transfered from the absorbing state to the nonabsorbing subspace. Thus, one has:

$$\frac{dP_n}{dt} = \sum_{m\neq 0}[P_m W(n,m) - P_n W(m,n)] + P_m W(0,m). \tag{3.42}$$

Each nonabsorbing state receives a share equal to its probability. The evolution of X_t^* is identical to that of X_t, for $n > 0$. Nevertheless, when $n = 0$, *i.e.*, X_t is into the absorbing space, X_t^* instead jumps to a nonabsorbing state and returns to its ordinary evolution until the time when the system is upcoming to fall into the absorbing state again (see Fig. 3.3).

In spite of the fact that Eq. (3.42) is not a master equation, it does suggest a simulation strategy for sampling the QS distribution. One has no prior knowledge of P_n but, in a simulation, one can use the history $X_s^*(0 < s \leq t)$ up to time t to estimate P_n. This can be done by saving, and constantly updating a sample of the states already visited. The update is done by periodically replacing one of these configurations by the current one. Hence, at long times, the distribution

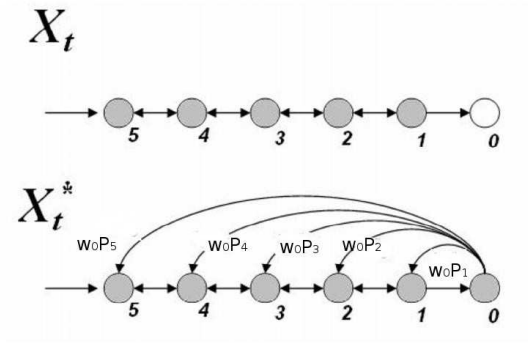

Figure 3.3: Original process X_t with an absorbing state $n = 0$ and its related process X_t^*. Figure adapted from Ref. [105].

of the process X_t^* converges to the QS distribution of the original process X_t. Essentially, the nonlinear term in Eq. (3.42) represents the memory in the simulation.

The computational demands of this approach are, in general, trivial. To implement the QS method, a list containing M configurations is stored and constantly updated. The updating is done by randomly picking up a stored configuration and replacing it by the current one with probability δtp_r. After a relaxation time t_r, the averages are computed over a time t_{av}.

The characteristic relaxation time is always short for epidemics on random networks due to the very small average shortest path [3]. The averaging time, on the other hand, must be large enough to guaranty that epidemics over the whole network was suitably averaged. It means that very long times are required for very low QS density (sub-critical phase in phase transition jargon) whereas relatively short times are sufficient for high density states. Notice that the simulation time step becomes tiny for a very supercritical system (large number of infected vertices) and a huge number of configurations are visited during a time interval $\delta t = 1$.

Both equilibrium and non-equilibrium critical phenomena are hallmarked by simultaneously diverging correlation length and correlation time which microscopically reflect divergences of the spatial and temporal fluctuations [33], respectively. Even tough a diverging correlation length has little sense on complex networks due to the small-world property [106], the diverging fluctuation concept is still applicable. We used different criteria to determine the thresholds, relied on the fluctuations or singularities of the order parameters.

The QS probability $\bar{P}_n$, defined as the probability that the system has n occupied vertices in the QS regime, is computed during the averaging time and basic QS quantities, as lifespan and density of infected vertices, are derived form $\bar{P}_n$. Indeed, we have that $\rho = \frac{1}{N}\sum_n \bar{P}_n$ and $\tau = 1/\bar{P}_1$ [51].

Thus, thresholds for finite networks can be determined using the modified susceptibility [36]

$$\chi \equiv \frac{\langle n^2 \rangle - \langle n \rangle^2}{\langle n \rangle} = \frac{N(\langle \rho^2 \rangle - \langle \rho \rangle^2)}{\langle \rho \rangle}, \tag{3.43}$$

that does exhibit a pronounced divergence at the transition point for SIS [15,36,39] and contact process [46,47] models on networks. The choice of the alternative definition, Eq. (3.43), instead of the standard susceptibility $\tilde{\chi} = N(\langle \rho^2 \rangle - \langle \rho^2 \rangle)$ [85] is due to the peculiarities of dynamical processes on complex networks. For example, as shown in section 3.5, the QS probability distribution at the transition point for the CP on heterogeneous networks has the analytically known form [41]

$$\bar{P}_n = \frac{1}{\sqrt{\Omega}} f\left(\frac{N}{\sqrt{\Omega}}\right), \tag{3.44}$$

where $\Omega = N/g$, $g = \langle k^2 \rangle / \langle k \rangle^2$ and $f(x)$ is a scaling function independent of the degree distribution. It is easy to show [100] that $\langle n^l \rangle \sim \sqrt{\Omega^l}$, leading to $\chi \sim \sqrt{\Omega}$ and $\tilde{\chi} \sim \Omega/N \sim g^{-1}$. Using the scaling properties of g [66],

$$g \sim \begin{cases} k_c^{3-\gamma} = N^{(3-\gamma)/\omega} & 2 < \gamma < 3 \\ \text{const.} & \gamma > 3 \end{cases}, \tag{3.45}$$

for the cutoff scaling as $k_c \sim N^{1/\omega}$, one concludes that, at $\lambda = \lambda_c$, $\chi \sim N^{\vartheta}$ and $\tilde{\chi} \sim N^{\vartheta'}$ where $\vartheta = \min[(\gamma - 3 + \omega)/2\omega, 1/2] > 0$ and $\vartheta' = \min[(\gamma - 3)/\omega, 0] \leq 0$. So, the susceptibility χ always diverges at the transition point while $\tilde{\chi}$ does not.

In a finite system of size N, χ shows a diverging peak at $\lambda = \lambda_p^{QS}(N)$, providing a finite size approximation of the critical point. In the thermodynamic limit, $\lambda_p^{QS}(N)$ approaches the true critical point with the scaling form [107]

$$\lambda_p^{QS}(N) = \lambda_c + A_{QS} N^{-1/\nu}, \tag{3.46}$$

as we can see for the SIS model in Figure 3.4. The network was generated with the UCM model [27], where vertex degree is selected from a power-law distribution with a lower bound $k_0 = 3$.

It is expected that the QS state does not depend on the initial condition. Figure 3.5 shows a comparison of QS simulations for the same network with different initial densities $\rho(0) = 10^{-3}$ to 0.50, randomly distributed. The results are completely independent of the initial condition.

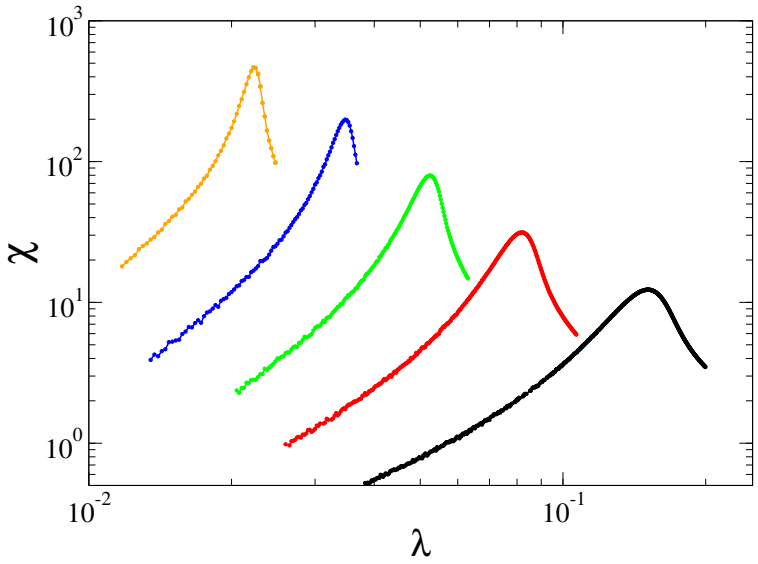

Figure 3.4: Susceptibility curves against infection rate for $N = 10^3, 10^4, 10^5, 10^6$ and 10^7 (from the right to the left) used to determine the thresholds in simulations (position of the peaks λ_p). The network parameters are $\gamma = 2.75$ and $k_0 = 3$.

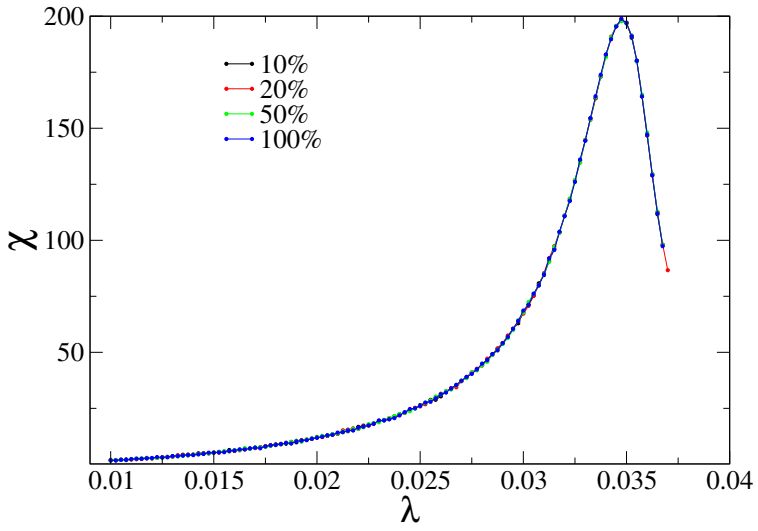

Figure 3.5: Susceptibility versus infection rate for the SIS model on a single network with different fraction of initially infected vertices, which are randomly distributed in the network. The network parameters are $\gamma = 2.75$, $k_0 = 3$ and $N = 10^6$.

3.8.2 The Lifespan Method

The lifespan (LS) method proposed by Boguñá *et. al.* [16] is based on spreading simulations starting from a single occupied site. Each realization of the dynamical process is characterized by its lifespan and its coverage C, defined as the fraction of different sites which have been occupied at least once during the realization. In the thermodynamic limit realizations can have either *finite* or

infinite, according to whether they proceed below or above the critical point. Endemic realizations have an infinite lifetime and their coverage is equal to 1. Finite realizations have instead a finite lifetime and a vanishing coverage in the limit of diverging size.

In finite systems this distinction is blurred, since any realization is bound to end, reaching the absorbing state, although this can occur over long temporal scales. In practice, a realization is assumed as active whenever its coverage reaches a predefined threshold value $C_{\rm th}$, which was generally takes equal to $C_{\rm th} = 0.5$[6]. Realizations ending before value $C = C_{\rm th}$ is reached are considered to be finite.

In the LS method the role of the order parameter is played by the probability $\mathrm{Prob}(\lambda - \lambda_c, N)$ that a run is long-term, while the role of susceptibility is played by the average lifetime of finite realizations $\langle\tau\rangle$. For small values of λ all realizations are finite and have a very short duration τ. As λ grows the average duration of finite realizations increases, but for very large λ almost all realizations are long-term, only very short realizations remaining finite. For this reason $\langle\tau\rangle$ exhibits a peak for a value $\lambda_p(N)$ depending on N and converging to λ_c in the thermodynamic limit, as

$$\lambda_p^{LS}(N) = \lambda_c + A_{LS} N^{-1/\nu_\perp}. \tag{3.47}$$

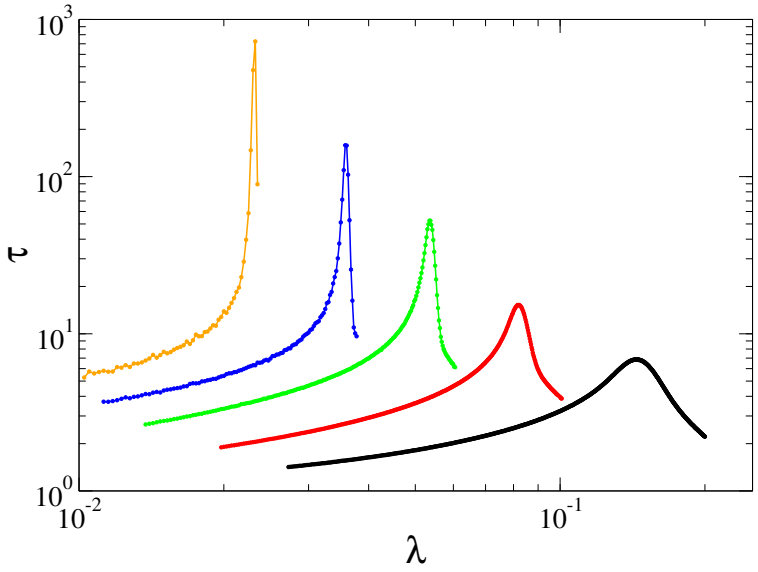

Figure 3.6: Lifespan curves versus infection rate for $N = 10^3, 10^4, 10^5, 10^6$ and 10^7 (from the right to the left) used to determine the thresholds in simulations (position of the peaks λ_p). The network parameters are the same of Fig.3.4.

We can then use the average lifespan to determine numerically the critical point, as shown in

[6]The method is robust with respect to the coverage threshold (see Refs. [16,52,108]).

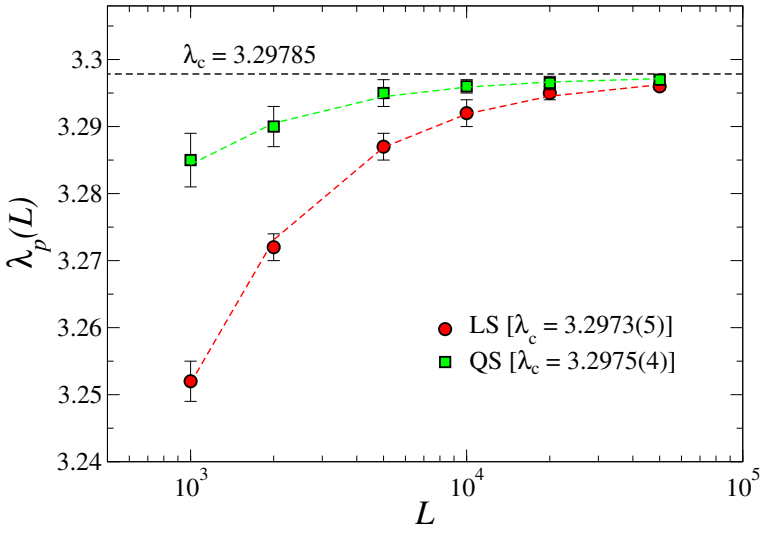

Figure 3.7: Size dependence of the $\lambda_p(L)$ estimates of the transition point for the quasi-stationary and lifespan methods. Dashed lines are non-linear regressions used to determine the critical point. The horizontal line marks the accepted best estimated value of the critical threshold [34].

Figure 3.6. In general, the method can be applied starting from any node of the network, however to minimize the fluctuations of $\tau(\lambda, N)$ close to the critical point, we start our simulations from the node with highest degree [16].

In order to show the feasibility of the LS method, I and collaborators, whose partnership was consolidated during my interuniversity exchange doctorate, reported results regarding the application of the lifespan method to the contact process in a $d = 1$ lattice of size L. In comparison with results from the quasi-stationary method, we showed that the new approach is reliable (see Fig. 3.7). This work can be found in Ref. [52].

The lifespan method is thus an alternative way to numerically studying systems with absorbing states, which complements more traditional techniques. However, this methods is not able to discern between localized and delocalized epidemic activity since lifetime and survival probabilities are used instead of densities. For example, the SIS model in heterogeneous substrates can exhibit a much more complex behavior with multiple phase transitions [109]. In this case, the applicability of LS method to determine a phase transition involving a real endemic phase has been debated [54,55,109]. This topic will be discussed in Chapter 6.

Chapter 4

Pair Approximation for the Contact Process on Complex Networks

After an intense discussion briefly summarized in section 3.5 [21,22,43,90,91], the HMF theory showed up as the best available approach to describe scaling exponents associated to the phase transition of the CP on networks [42]. However, some important questions remained unanswered. The transition point $\lambda_c = 1$ predicted by the HMF theory [43] does not reflect the dependence on the degree distribution observed in simulations [20,42,43]. Finally, sub-leading corrections to the finite-size scaling, undetected by the one-vertex HMF theory, are quantitatively relevant for the analysis of highly heterogeneous networks, for which deviations from the theoretical finite-size scaling exponents were reported [42].

Dynamical correlations is an important factor to ascertain the accuracy of the analytical results. The simplest way to explicitly consider dynamical correlations is by a pair-approximation [34] in which the dynamic of an individual is explicitly influenced by its nearest neighbors. In this chapter, we present a pair QMF and HMF approximations for the CP on heterogeneous networks. The transcendental equations given the transition points are derived. The numerical investigation of the thresholds and the comparison with quasi-stationary simulations are also presented. Finally, the critical exponents are analytically obtained and compared with simulations in pair HMF theory [46].

4.1 Pair QMF theory

To develop the pair QMF theory, let us introduce the following notation: $[A_i]$ is the probability that the vertex i is in the state A; $[A_i, B_j]$ is probability that the vertices i and j are in states

A and B, respectively; $[A_i, B_j, C_k]$ is the extension to three vertices; and so forth. The infected state is represented by 1 and the susceptible one by 0. We also introduce the variables $\rho_i = [1_i]$ and, consequently, $[0_i] = 1 - \rho_i$, $\psi_{ij} = [1_i, 1_j]$, $\omega_{ij} = [0_i, 0_j]$, $\phi_{ij} = [0_i, 1_j]$, and $\bar{\phi}_{ij} = [1_i, 0_j]$. Obviously we have that $\psi_{ij} = \psi_{ji}$, $\omega_{ij} = \omega_{ji}$, and $\phi_{ij} = \bar{\phi}_{ji}$. Independently of the dynamical rules, the following closure relations can be derived from simple probabilistic reasoning:

$$\begin{aligned} \psi_{ij} + \phi_{ij} &= \rho_j \\ \psi_{ij} + \bar{\phi}_{ij} &= \rho_i \\ \omega_{ij} + \phi_{ij} &= 1 - \rho_i \\ \omega_{ij} + \bar{\phi}_{ij} &= 1 - \rho_j. \end{aligned} \tag{4.1}$$

The dynamical equation for the probability that a vertex i is occupied in the CP model takes the form

$$\frac{d\rho_i}{dt} = -\rho_i + \lambda \sum_{j \in \mathcal{N}(i)} \frac{\phi_{ij}}{k_j}, \tag{4.2}$$

where the sum runs over all nearest-neighbors of i. The first term of Eq. (4.2) represents the spontaneous annihilation event and the second term reckons the creation in vertex i due to its nearest neighbors. This equation is exact but not analytical tractable in the present form due to the dependence on ϕ_{ij}.

The (exact) dynamical equation for ϕ_{ij} in a pair of connected vertices is

$$\frac{d\phi_{ij}}{dt} = -\phi_{ij} - \frac{\lambda\phi_{ij}}{k_j} + \psi_{ij} + \lambda \sum_{\substack{l \in \mathcal{N}(j) \\ l \neq i}} \frac{[0_i 0_j 1_l]}{k_l} - \lambda \sum_{\substack{l \in \mathcal{N}(i) \\ l \neq j}} \frac{[1_l 0_i 1_j]}{k_l}. \tag{4.3}$$

The first term represents the annihilation in vertex i, the second includes the creation in vertex i due to the edge (i, j) and the third is due to the annihilation of vertex j. These terms represent the reactions inside the pair (i, j) that create or destroy a configuration $[0_i, 1_j]$. The fourth and fifth terms represent changes due to the creation in vertices i and j, respectively, due to all neighbors of i and j except the link (i, j) itself, which is explicitly included in the second term.

Equations (4.2) and (4.3) cannot be solved due to the triplets. However, the dynamical equations for triplets will depend on quadruplets, and so forth. So, the hierarchy of clusters must be broken in some point to obtain an approximated solution. In the present work, we apply the standard

pair-approximation [33,110]

$$[A_i, B_j, C_l] \approx \frac{[A_i, B_j][B_j, C_l]}{[B_j]} \tag{4.4}$$

in equation (4.3) to obtain

$$\frac{d\phi_{ij}}{dt} = -\phi_{ij} - \frac{\lambda\phi_{ij}}{k_j} + \psi_{ij} + \lambda\sum_l \frac{\omega_{ij}\phi_{jl}(A_{jl} - \delta_{il})}{(1-\rho_j)k_l} - \lambda\sum_l \frac{\phi_{ij}\bar{\phi}_{li}(A_{il} - \delta_{lj})}{(1-\rho_i)k_l}, \tag{4.5}$$

where the adjacency matrix was used to express the vertex neighborhood. Substituting closure relations [Eqs. (4.1)] in Eq. (4.5) and performing the linearization for $\rho_i \approx 0$ and $\phi_{ij} \approx 0$ one finds

$$\frac{d\phi_{ij}}{dt} = \rho_j - \left(2 + \frac{\lambda}{k_i} + \frac{\lambda}{k_j}\right)\phi_{ij} + \frac{\lambda(\rho_j - \rho_i)}{k_i} + \lambda\sum_l \frac{\phi_{jl}A_{jl}}{k_l}. \tag{4.6}$$

The next step is to perform a quasi-static approximation for $t \to \infty$, $d\rho_i/dt \approx 0$ and $d\phi_{ij}/dt \approx 0$, to find

$$\phi_{ij} \approx \frac{2\rho_j + (\rho_j - \rho_i)\frac{\lambda}{k_i}}{2 + \frac{\lambda}{k_i} + \frac{\lambda}{k_j}}, \tag{4.7}$$

which holds only slightly above the transition point and for long times.

Finally, we plug Eq. (4.7) in Eq. (4.2) to find

$$\frac{d\rho_i}{dt} = -(1 + \lambda^2\alpha_i)\rho_i + \lambda(2k_i + \lambda)\sum_j \frac{\rho_j A_{ij}}{2k_ik_j + \lambda(k_i + k_j)} \tag{4.8}$$

where the vertex-dependent quantity α_i is defined as

$$\alpha_i = \sum_j \frac{A_{ij}}{2k_ik_j + \lambda(k_i + k_j)}.$$

Therefore, the critical point is obtained when the largest eigenvalue of the Jacobian matrix

$$L_{ij} = -(1 + \lambda^2\alpha_i)\delta_{ij} + \frac{\lambda(2k_i + \lambda)A_{ij}}{2k_ik_j + \lambda(k_i + k_j)} \tag{4.9}$$

is null. From a numerical viewpoint, it is more interesting to rewrite Eq. (4.9) as

$$L_{ij} = -(1 + \lambda^2\bar{\alpha})\delta_{ij} + C_{ij} \tag{4.10}$$

where

$$\bar{\alpha}(\lambda) = \frac{k_c}{2k_0^2 + 2\lambda k_0} \geq \alpha_i \tag{4.11}$$

and

$$C_{ij} = \lambda^2(\bar{\alpha} - \alpha_i)\delta_{ij} + \frac{\lambda(2k_i + \lambda)A_{ij}}{2k_i k_j + \lambda(k_i + k_j)}. \tag{4.12}$$

This choice of $\bar{\alpha}$ implies that C_{ij} is positive semidefinite and irreducible (the network is connected)[1] and, thus, Perron-Frobenius theorem [3] guaranties that the eigenvalue of C_{ij} is real positive and non-degenerate. Therefore, the transition point is given by the transcendent equation

$$\Lambda_m(\lambda_c) = 1 + \lambda_c^2 \bar{\alpha}(\lambda_c), \tag{4.13}$$

where Λ_m is the largest eigenvalue of C_{ij}. A general analytical expression for Λ_m is not available but, in principle, it can be obtained numerically for any kind of network (section 4.3).

To check the consistency of the theory, we consider the random regular networks with degree m. Using the property $\sum_{j=1}^{N} A_{ij} = k_i$ [3] and the Perron-Frobenius theorem one easily shows that

$$\bar{\alpha} = \frac{1}{2m + \lambda} \text{ and } \Lambda_m = \frac{\lambda(2m + \lambda)}{2m + 2\lambda} \tag{4.14}$$

resulting in the transition point

$$\lambda_c = \frac{m}{m - 1}, \tag{4.15}$$

that is the same value yield by the simple homogeneous pair-approximation [34].

4.2 Pair HMF theory

We develop the pair HMF theory where the evolution of the system is given by the average behavior of vertices with the same degree. So, we introduce the notation similar to that of the section 4.1: $[A_k]$ is the probability that a vertex of degree k is in the state A; $[A_k B_{k'}]$ is the probability that a vertex of degree k in state A is connected to a vertex of degree k' in state B; $[A_k B_{k'} C_{k''}]$ is the generalization to three vertices such that the pairs $[A_k B_{k'}]$ and $[B_{k'} C_{k''}]$ are connected through a node of degree k' and so forth. An infected state is represented by 1 and an susceptible one by 0. The pair-approximation carried out hereafter uses the following notation: $[1_k] = \rho_k$, $[0_k] = 1 - \rho_k$, $[0_k 1_{k'}] = \phi_{kk'}$, $[1_k 0_{k'}] = \bar{\phi}_{kk'}$, $[1_k 1_{k'}] = \psi_{kk'}$ and $[0_k 0_{k'}] = \omega_{kk'}$. Obviously, we have that $\psi_{kk'} = \psi_{k'k}$, $\omega_{kk'} = \omega_{k'k}$, and $\phi_{kk'} = \bar{\phi}_{k'k}$. Analogous to Eq. (4.1), the

[1] We use the power method [111] to find the eigenvalue of largest absolute magnitude, that is always positive, in the case of a matrix with all elements non-negative such as the C_{ij}.

following relations hold for any pair of vertices

$$\begin{aligned}
\psi_{kk'} + \phi_{kk'} &= \rho_{k'} \\
\psi_{kk'} + \bar{\phi}_{kk'} &= \rho_k \\
\omega_{kk'} + \phi_{kk'} &= 1 - \rho_k \\
\omega_{kk'} + \bar{\phi}_{kk'} &= 1 - \rho_{k'}.
\end{aligned} \tag{4.16}$$

For CP the master equation for the probability that a vertex with degree k is occupied takes the form

$$\frac{d\rho_k}{dt} = -\rho_k + \lambda k \sum_{k'} \frac{\phi_{kk'}}{k'} P(k'|k). \tag{4.17}$$

The first term of Eq. (4.17) represents the spontaneous annihilation and the second term reckons the creation in a vertex of degree k due to its nearest neighbors. The dynamical equation for $\phi_{kk'}$ is

$$\begin{aligned}
\frac{d\phi_{kk'}}{dt} &= -\phi_{kk'} - \lambda\frac{\phi_{kk'}}{k'} + \psi_{kk'} + \lambda(k'-1)\sum_{k''}\frac{[0_k 0_{k'} 1_{k''}]P(k''|k')}{k''} \\
&\quad -\lambda(k-1)\sum_{k''}\frac{[1_{k''} 0_k 1_{k'}]P(k''|k)}{k''}.
\end{aligned} \tag{4.18}$$

The first term represents the annihilation in the vertex of degree k', the second one includes the creation in the vertex of degree k due to the connection with the neighbor of degree k' and the third one is due to the annihilation of the vertex with degree k. These terms represent the reactions inside pairs with degrees k and k', that create or destroy a configuration $[0_k, 1_{k'}]$. The fourth and fifth terms represent changes due to creation in vertices with degree k' and k, respectively, due to all their neighbors except the link between the vertices of the pair itself, which is explicitly included in the second term.

We now approximate the triplets in Eq. (4.18) with the same pair-approximation of Eq. (4.4)

$$[A_k, B_{k'}, C_{k''}] \approx \frac{[A_k, B_{k'}][B_{k'}, C_{k''}]}{[B_{k'}]}, \tag{4.19}$$

to find

$$\begin{aligned}
\frac{d\phi_{kk'}}{dt} &= -\phi_{kk'} - \lambda\frac{\phi_{kk'}}{k'} + \psi_{kk'} + \frac{\lambda(k'-1)\omega_{kk'}}{1-\rho_{k'}}\sum_{k''}\frac{\phi_{k'k''}P(k''|k')}{k''} \\
&\quad -\frac{\lambda(k-1)\phi_{kk'}}{1-\rho_k}\sum_{k''}\frac{\phi_{kk''}P(k''|k)}{k''}.
\end{aligned} \tag{4.20}$$

Substituting Eqs. (4.16) in (4.20) and performing linearization and a quasi-static approximation, the Jacobian equivalent to Eq. (4.9) is

$$L_{kk'} = -\delta_{kk'} + \frac{\lambda k(2k'-1)P(k'|k)}{(2k'+\lambda)k'} = -\delta_{kk'} + C_{kk'}. \tag{4.21}$$

Once again assuming degree-uncorrelated networks, $P(k'|k) = k'P(k')/\langle k\rangle$, it is easy to check that $u_k = k$ is an eigenvector of $C_{kk'}$ with eigenvalue

$$\Lambda = \frac{\lambda}{\langle k\rangle}\sum_{k'}\frac{(2k'-1)P(k')k'}{(2k'+\lambda)}. \tag{4.22}$$

Since $C_{kk'} > 0$ is irreducible (all compartments have non-null chance of being connected) and $u_k > 0$, the Perron-Frobenius theorem [3] warranties that Λ is the largest eigenvalue of $C_{kk'}$. The transition point is, therefore, given by $-1 + \Lambda = 0$ that results the transcendent equation

$$\frac{\lambda_c}{\langle k\rangle}\sum_{k'}\frac{(2k'-1)k'P(k')}{(2k'+\lambda_c)} = 1, \tag{4.23}$$

that can be numerically solved for any kind of degree distribution (see section 4.3).

To check the consistency of the theory, we consider again the RRN, with $P(k) = \delta_{k,m}$. One easily shows that the transition point is

$$\lambda_c = \frac{m}{m-1}, \tag{4.24}$$

that is the same of the homogeneous and quenched pair-approximation. Simulations of CP on RRNs with $m = 6$ yield a critical point $\lambda_c = 1.2155(1)$ [47], slightly above the pair-approximation prediction $\lambda_c = 1.2$.

4.3 Threshold for arbitrary random networks

In this section, we compare the thresholds given pair-approximation theories with simulations of the CP dynamics on random networks generated by the UCM model [27], with minimum degree $k_0 = 3$ and structural cutoff $k_c = N^{1/2}$. The choice of a UCM network is suitable for comparison with the HMF theory where the simplification related to uncorrelated degrees is adopted. We also investigated networks with $k_0 = 6$ to compare with the results of Ref. [42] and to remark the improvement of the present theory. Networks of sizes up to $N = 10^7$ and degree exponents $\gamma = 2.3,\ 2.5,\ 2.7,\ 3.0$ and 3.5 were analyzed. The transition points in pair QMF [Eq. (4.13)] theory

are slightly below those in pair HMF theory [Eq. (4.23)], but they are very close (see Fig. 4.1 and Table 4.1).

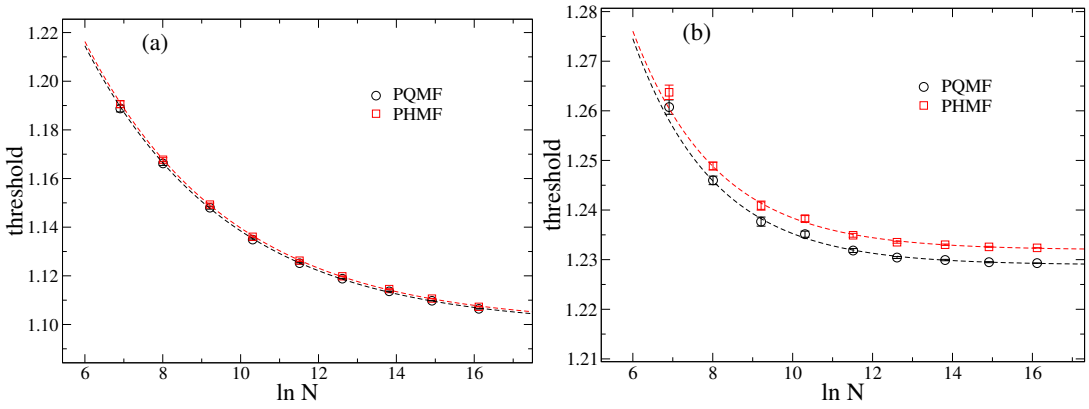

Figure 4.1: Thresholds versus network size for the CP on UCM networks with degree exponents (a) $\gamma = 2.30$ and (b) $\gamma = 3.0$ and $k_0 = 3$ obtained in both pair mean-field theories. Dashed lines are non-linear regressions used to extrapolate the infinite-size limit of the thresholds.

Therefore, from now on we will compare the simulation only with the numerical results of pair-HMF theory. The thresholds were determined for each network realization and averages done over 10 independent networks. Sample-to-sample fluctuations of the threshold positions become very small for large networks. The thresholds against network sizes for two degree exponents are shown in Fig. 4.2.

We performed simulations of CP dynamics using the standard scheme explained in section 3.7.2 and the QS simulation method [51]. The transition point for finite networks was determined using the modified susceptibility (see section 3.8.1).

Typical susceptibility versus λ curves are shown in Fig. 4.3. The peak positions shift leftwards converging to a finite threshold as network size increases. Notice that the larger the degree exponent the narrower the susceptibility curves and the faster the convergence to the asymptotic threshold. The infinite-size threshold λ_c^* is estimated in QS simulations as well as in the mean-field theories using an extrapolation

$$\lambda_c(N) = \lambda_c^* + a_1 N^{-b_1}(1 + a_2 N^{-b_2}). \tag{4.25}$$

As one can see in Fig. 4.2, the curves λ_c *vs.* N for different mean-field theories are only shifted indicating that the exponents b_i are the same. They can be obtained using a continuous approximation

$$\langle k \rangle = \int_{k_0}^{k_c} kP(k)dk \simeq \frac{\gamma - 1}{\gamma - 2} k_0 \left[1 - (k_c/k_0)^{2-\gamma}\right] \tag{4.26}$$

in Eq. (4.31) to obtain $b_1 = b_2 = (\gamma - 2)/\omega$ for $k_c \sim N^{1/\omega}$, where $\omega = \max(2, \gamma - 1)$ for UCM

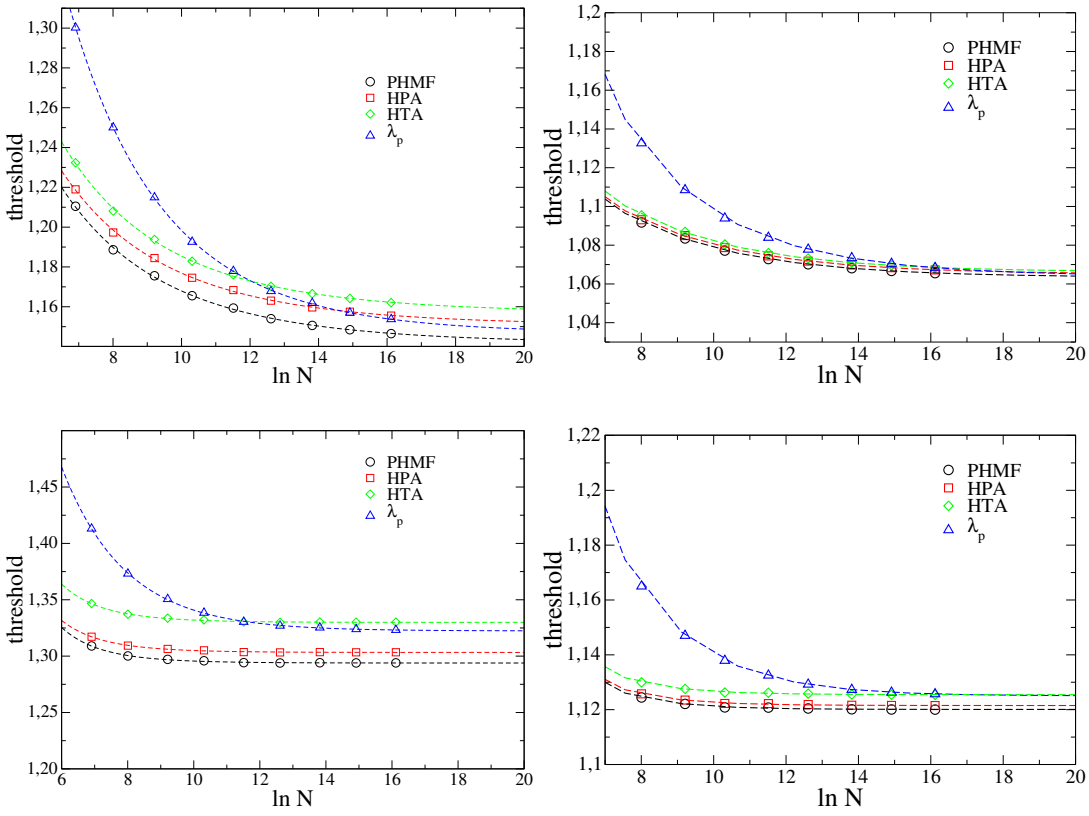

Figure 4.2: Thresholds versus network size for the CP on UCM networks with degree exponents $\gamma = 2.50$ (top) and $\gamma = 3.50$ (bottom), $k_0 = 3$ (left) and $k_0 = 6$ (right), obtained in mean-field theory and QS simulations (position of the susceptibility peak λ_p). Dashed lines are non-linear regressions used to extrapolate the infinite-size limit of the thresholds.

networks [27].

The exponents b_i in QS simulations differ from those of the mean-field theories. They can be analytically estimated using the scaling theory presented in Refs. [40,41] and revised in section 3.5, where it was showed that the QS density at the transition point scales as

$$\bar{\rho}(\lambda_c) \sim (gN)^{-1/2} \tag{4.27}$$

while above it

$$\bar{\rho} \sim (\lambda - \lambda_c)^{\beta}, \tag{4.28}$$

where $\beta = \max[1, 1/(\gamma - 2)]$ [40]. These scaling laws are confirmed in the pair HMF theory developed in section 4.4. Assuming that both scaling laws hold at λ_p one obtains

$$\lambda_p - \lambda_c \sim (gN)^{-1/2\beta}. \tag{4.29}$$

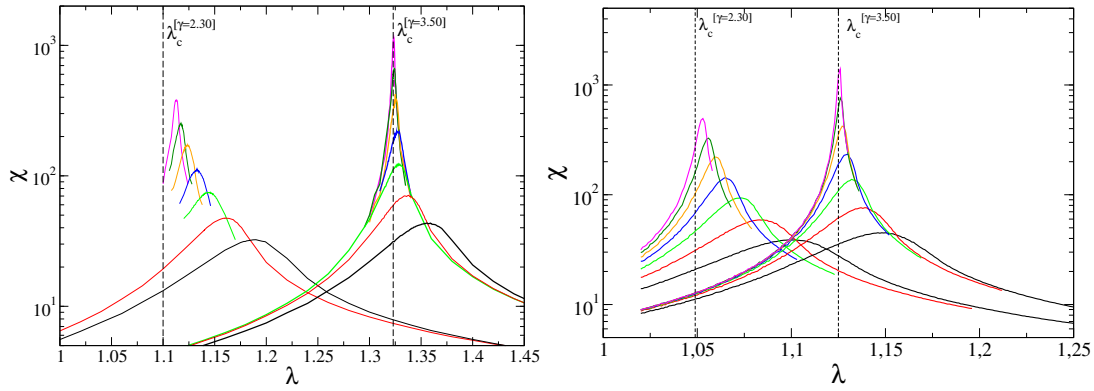

Figure 4.3: Susceptibility versus creation rate for $\gamma = 2.30$ (leftmost group) and $\gamma = 3.50$ (rightmost group), $k_0 = 3$ (left) and $k_0 = 6$ (right). The network sizes are $N = 10^4, 3 \times 10^4, 10^5, 3 \times 10^5, 10^6, 3 \times 10^7, 10^7$, increasing from the right. Dashed lines are the extrapolations of the peak position for $N \to \infty$

.

Using again the continuous approximation to compute g and neglecting higher order terms one finds

$$g = C_\gamma \times \begin{cases} \xi^{3-\gamma}\left[1 + \xi^{2-\gamma} + \cdots\right] & \gamma < 3 \\ 1 - \xi^{3-\gamma} + \cdots & \gamma > 3 \end{cases} \tag{4.30}$$

where, $\xi \equiv k_c/k_0$, $C_\gamma = |(\gamma-2)^2/(3-\gamma)(\gamma-1)|$ and a logarithmic dependence is found for $\gamma = 3$. Upon substitution of g in Eq. (4.29), the exponents $b_1 = (\gamma-2)(3+\omega-\gamma)/2\omega$ and $b_2 = (\gamma-2)/\omega$ for $\gamma < 3$ while $b_1 = 1/2$ and $b_2 = (\gamma-3)/\omega$ for $\gamma > 3$ and $k_c \sim N^{1/\omega}$are found.

We performed non-linear regressions using Eq. (4.25) with λ_c^*, a_1 and a_2 free and fixing b_i according to the theoretical corrections. Excellent fits were obtained, as can be seen in Fig. 4.2 and the numerical estimates of λ_c^* are shown in table 4.1. As expected, both PQMF and PHMF theories are very good improvements when compared to the one-vertex approximation $\lambda_c = 1$.

However it was observed, for some values of γ, a better accordance between simulations and the heuristic homogeneous pair-approximation (HPA)[2], as can seen in Fig. 4.2. It is an intriguing result since heterogeneity is expected to play some important role in dynamical correlations even for degree distributions without a heavy tail as in the case $\gamma > 3$.

The puzzle behind this apparent paradox is that cluster approximations underestimate the real threshold and the convergence is expected only in the limit of large cluster approximations. A homogeneous triplet approximation (HTA) for the CP on unclustered networks yields the thresh-

[2]In HPA the fixed vertex degree is replaced by the average degree of the network and the thresholds obtained is [20,42]

$$\lambda_c = \frac{\langle k \rangle}{\langle k \rangle - 1}. \tag{4.31}$$

γ	PQMF	PHMF	HPA	HTA	λ_p
2.30	1.097(1)	1.098(1)	1.105(1)	1.108(1)	1.1009(5)
2.50	1.1400(4)	1.1415(4)	1.1505(5)	1.1567(5)	1.1473(6)
2.70	1.1794(3)	1.1817(3)	1.1916(3)	1.2018(4)	1.1906(4)
3.00	1.2287(3)	1.2320(3)	1.2422(3)	1.2586(3)	1.2479(3)
3.50	1.2898(1)	1.2938(1)	1.3032(1)	1.3299(1)	1.3224(2)

Table 4.1: Transition points of the contact process on UCM networks with different degree exponents, minimum vertex degree $k_0 = 3$ and structural cutoff $k_c = N^{1/2}$ for both mean-field theories and QS simulations (λ_p). Number in parenthesis are uncertainties in the last digit. The values obtained for $k_0 = 6$ have smaller uncertainties than for $k_0 = 3$. Acronyms: Pair quenched mean-field (PQMF); Pair heterogeneous mean-field (PHMF); Homogeneous pair approximation (HPA); Homogeneous triplet approximation (HTA).

old [47]:

$$\lambda_c = \frac{\langle k\rangle + 2\sqrt{\langle k\rangle^2 - \langle k\rangle}}{3\langle k\rangle - 4}. \tag{4.32}$$

Comparing this approximation with simulations, figure 4.2, one sees that HTA thresholds are, as expected, higher than the HPA ones but overestimate the simulation thresholds for all investigated networks. This result shows that the homogeneous cluster approximations will converge to a threshold above the correct one and they are, in principle, not applicable to the CP dynamics on heterogeneous networks as previously done [20,42]. The proximity between HPA theory and simulations is therefore just a coincidence.

4.4 Critical exponents

In this section, the critical exponents of the CP in the pair HMF theory are derived and compared with results of QS simulations.

4.4.1 Critical exponents in the pair HMF theory for infinite networks

It is well known that cluster approximations of higher orders improve the critical point estimates but does not change the critical exponents in lattice systems [85]. As expected, the pair HMF theory for the CP yields the same scaling exponents as the one-vertex approximation [21,40,41], changing only the amplitudes and the finite-size corrections to the scaling as we will show in this section.

In a pair level, the scaling exponents associated to the absorbing state phase transition can be derived from Eqs. (4.17) and (4.18) keeping terms up to second order. Assuming again uncorrelated

networks, the dynamical equations become

$$\frac{d\rho_k}{dt} = -\rho_k + \frac{\lambda k}{\langle k\rangle}\sum_{k'}\phi_{kk'}P(k') \tag{4.33}$$

and

$$\begin{aligned}\frac{d\phi_{kk'}}{dt} &= -\phi_{kk'} - \lambda\frac{\phi_{kk'}}{k'} + \psi_{kk'} + \frac{\lambda(k'-1)}{\langle k\rangle}(1+\rho_{k'}-\rho_k-\phi_{kk'})\sum_{k''}\phi_{k'k''}P(k'') \\ &\quad -\frac{\lambda(k-1)}{\langle k\rangle}\phi_{kk'}\sum_{k''}\phi_{kk''}P(k'') + \mathcal{O}(3).\end{aligned} \tag{4.34}$$

The quasi-static approximation with $d\rho_k/dt \approx 0$ and $d\phi_{kk'}/dt \approx 0$ leads to

$$\phi_{kk'} = \frac{2k'-1}{2k'+\lambda}\rho_{k'}\left\{1 + \frac{(\lambda+1)(k'-1)}{(2k'-1)(2k'+\lambda)}\rho'_k - \left[\frac{k'-1}{2k'-1} + \frac{k'(k-1)}{k(2k'+\lambda)}\right]\rho_k\right\} + \mathcal{O}(3), \tag{4.35}$$

which is inserted in Eq. (4.33) to result

$$\frac{d\rho_k}{dt} = -\rho_k + \frac{\lambda k}{\langle k\rangle}\left[\Theta_1 - \rho_k\left(\Theta_2 - \frac{\Theta_3}{k}\right)\right] \tag{4.36}$$

and, consequently, the stationary density

$$\rho_k = \frac{\lambda k\Theta_1/\langle k\rangle}{1+\lambda k\Theta_2/\langle k\rangle - \lambda\Theta_3/\langle k\rangle}, \tag{4.37}$$

where Θ_i are given by

$$\Theta_1 = \rho - (\lambda+1)\sum_k\left[\frac{P(k)\rho_k}{(2k+\lambda)} - \frac{P(k)(k-1)\rho_k^2}{(2k+\lambda)^2}\right] = \frac{\rho}{\mathcal{A}_1(\lambda)} + a_1(\lambda)\rho^2, \tag{4.38}$$

$$\Theta_2 = \rho - (\lambda+1)\sum_k\frac{P(k)(3k+\lambda)\rho_k}{(2k+\lambda)^2} = \frac{\mathcal{A}_2(\lambda)}{\mathcal{A}_1(\lambda)}\rho + a_2(\lambda)\rho^2 + \cdots \tag{4.39}$$

and

$$\Theta_3 = \sum_k\frac{P(k)(2k-1)k\rho_k}{(2k+\lambda)^2} = \frac{\mathcal{A}_3(\lambda)}{\mathcal{A}_1(\lambda)}\rho + a_3(\lambda)\rho^2, \tag{4.40}$$

where $\rho = \sum_k P(k)\rho_k$ while A_i are constants of order 1 given by

$$\mathcal{A}_1(\lambda) = 1 + \frac{\lambda(\lambda+1)}{\langle k\rangle}\sum_k\frac{kP(k)}{2k+\lambda}, \tag{4.41}$$

$$\mathcal{A}_2(\lambda) = 1 - \frac{\lambda(\lambda+1)}{\langle k\rangle}\sum_k \frac{k^2 P(k)}{(2k+\lambda)^2} \tag{4.42}$$

and

$$\mathcal{A}_3(\lambda) = \frac{\lambda}{\langle k\rangle}\sum_k \frac{k^2(2k-1)P(k)}{(2k+\lambda)^2}. \tag{4.43}$$

The rightmost sides of Eqs. (4.38)-(4.40) were obtained using $\Theta_i < \rho$ (the proofs of these bounds are simple) and Eq. (4.37) in a self-consistent approach [1]. The constants a_i are of order $1/\langle k\rangle^2$ and their explicit forms are omitted.

Multiplying Eq. (4.36) by $P(k)$ and summing over k ($k_c \to \infty$) one finds

$$\frac{d\rho}{dt} = -\rho + \lambda\Theta_1 + \frac{\lambda\Theta_3\rho}{\langle k\rangle} - \frac{\lambda\Theta_2}{\langle k\rangle}\langle k\rho_k\rangle \tag{4.44}$$

where

$$\langle k\rho_k\rangle = (\gamma-1)k_0^{\gamma-1}\psi_1\int_{k_0}^{\infty}\frac{k^{-\gamma+2}}{1+\psi_2 k}dk = \frac{\gamma-1}{\gamma-2}\frac{\psi_1}{\psi_2}F\left(1,\gamma-2,\gamma-1,\frac{-1}{\psi_2 k_0}\right), \tag{4.45}$$

$\psi_i = \lambda\Theta_i/[\langle k\rangle - \lambda\Theta_3]$ and $F(a,b,c,x)$ is the Gauss hypergeometric function [112]. Near to the critical point, $\psi_i \ll 1$, we can use the asymptotic form of $F(a,b,c,x)$[3] to finally find

$$\frac{d\rho}{dt} = -\rho + \frac{\lambda}{\mathcal{A}_1}\rho - \tilde{\alpha}_1\rho^2 - \tilde{\alpha}_2\rho^{\gamma-1} + \cdots, \tag{4.47}$$

where $\tilde{\alpha}_i(\lambda)$, $i = 1, 2$, are positive parameters whose details are omitted for sake of conciseness.

The stationary density close to the transition point is given by

$$\tilde{\alpha}_1\bar{\rho} + \tilde{\alpha}_2\bar{\rho}^{\gamma-2} \simeq \frac{\lambda - \mathcal{A}_1}{\mathcal{A}_1}. \tag{4.48}$$

An expansion around $\lambda = \lambda_c$ yields

$$\mathcal{A}_1(\lambda) = \lambda_c + (\lambda-\lambda_c)\mathcal{A}_1'(\lambda_c) + \cdots \tag{4.49}$$

where the identity $\lambda_c = \mathcal{A}_1(\lambda_c)$ comes from Eq. (4.23). Considering only the leading term in ρ one finds

$$\bar{\rho} \sim (\lambda-\lambda_c)^{\beta}, \quad \beta = \max\left[1, \frac{1}{\gamma-2}\right]. \tag{4.50}$$

[3]

$$F(a,b,c;x) = \frac{\Gamma(b-a)\Gamma(c)}{\Gamma(b)\Gamma(c-a)}(-x)^{-a} + \frac{\Gamma(a-b)\Gamma(c)}{\Gamma(a)\Gamma(c-b)}(-x)^{-b} + \ldots \quad x \to \infty \tag{4.46}$$

At the transition point $\lambda = \lambda_c$, equation (4.47) becomes

$$\frac{d\rho}{dt} = -\tilde{\alpha}_1\rho^2 - \tilde{\alpha}_2\rho^{\gamma-1}, \tag{4.51}$$

which yields $\rho \sim t^{-\delta}$ where $\delta = \beta = \max[1, 1/(\gamma-2)]$. Finally, close to the critical point one can show that

$$\rho - \bar{\rho} \sim \exp\left[-\left(\frac{\lambda - \mathcal{A}_1}{\mathcal{A}_1}\right)t\right] \tag{4.52}$$

leading to a relaxation time scaling as

$$\tau = \frac{\mathcal{A}_1}{\lambda - \mathcal{A}_1} \sim (\lambda - \lambda_c)^{-\nu_\parallel} \tag{4.53}$$

with a γ-independent exponent $\nu_\parallel = 1$. The exponents $(\beta, \delta, \nu_\parallel)$ obtained in this section are exactly the same as the one-vertex HMF theory [43].

4.4.2 Finite-size scaling critical exponents

Finite-size scaling exponents associated to the QS state can obtained using a mapping of the CP dynamics in a one-step process [93] as proposed in Ref. [21] and summarized in section 3.5. For finite-size systems the condition $\rho k_c \ll 1$ is applicable for long times and very close to the transition point. So, we approximate Eq. (4.37) by $\rho_k \simeq \lambda k \Theta_1/\langle k\rangle$ which is inserted in Eq. (4.44) to find

$$\frac{d\rho}{dt} = -\rho + \frac{\lambda}{\mathcal{A}_1}(1 - \tilde{g}\rho)\rho. \tag{4.54}$$

Now, the factor $\tilde{g}$ is given by

$$\tilde{g} = \frac{\lambda\mathcal{A}_2}{\mathcal{A}_1}\frac{\langle k^2\rangle}{\langle k\rangle^2} - \mathcal{A}_1 a_1 - \frac{\mathcal{A}_3}{\langle k\rangle}. \tag{4.55}$$

The first term proportional to ρ in Eq. (4.54) represents an annihilation $n \to n-1$ whereas the second one a creation event $n \to n+1$. In a mean-field level Eq. (4.54) represents a one-step process (see section 3.5) defined by a transition rate $W(n, m)$ from a state with m to another with n particles given by

$$W(m, n) = n\delta_{m,n-1} + \frac{\lambda}{\mathcal{A}_1}(1 - \tilde{g}\rho)n\delta_{m,n+1}. \tag{4.56}$$

At the critical point, we have the additional simplification $\lambda_c = \mathcal{A}_1$ and the transition rate becomes equal to that of the one-step process associated to the CP dynamics in a one-vertex HMF theory [21], with the factor $g = \langle k^2\rangle/\langle k\rangle^2$ replaced by $\tilde{g}$, given by Eq. (4.55).

The factor $\tilde{g}$ has exactly the same asymptotic scaling properties as the factor g, which are given

by Eq. (3.45):

$$\rho \sim (\tilde{g}N)^{-1/2} \quad \text{and} \quad \tau \sim (N/\tilde{g})^{1/2}, \tag{4.57}$$

therefore the same FSS exponents of the one-vertex HMF are obtained in pair HMF approximation (see section 3.5). The scaling laws $\bar{\rho} \sim N^{-\nu}$ and $\tau \sim N^{\alpha}$ with $\nu = \max[(5-\gamma)/2, 1/2]$ and $\alpha = \max[(\gamma-1)/4, 1/2]$ are obtained for UCM networks with a structural cutoff $k_c \sim N^{1/2}$ [27]. Despite of the same asymptotic scaling, the sub-leading corrections in the new factor $\tilde{g}$ are not negligible as one can see in Fig. 4.4.

	$k_0 = 3$		$k_0 = 6$	
γ	S_ν	S_α	S_ν	S_α
2.3	0.50(1)	0.48(2)	0.50(1)	0.50(1)
2.5	0.51(2)	0.47(2)	0.50(1)	0.51(1)
2.7	0.51(2)	0.49(2)	0.50(1)	0.50(1)
3.0	0.51(2)	0.49(2)	0.50(1)	0.50(1)
3.5	0.51(2)	0.48(2)	0.51(1)	0.50(1)

Table 4.2: Critical exponents obtained in QS simulations of the CP on UCM networks with minimum degrees $k_0 = 3$ and $k_0 = 6$ and cutoff $k_c = N^{1/2}$. The exponents were obtained in power law regressions $\bar{\rho} \sim (\tilde{g}N)^{-S_\nu}$ and $\tau \sim (N/\tilde{g})^{S_\alpha}$.

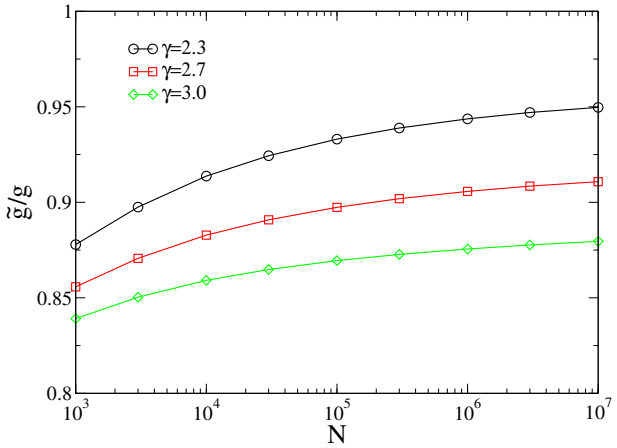

Figure 4.4: Ratios between the factor $\tilde{g}$ and g obtained in pair HMF theory, Eq. (4.55) with $\lambda = \lambda_c(N)$, and the factor $g = \langle k^2 \rangle / \langle k \rangle^2$ of the one-vertex HMF theory, for $k_0 = 3$.

Moreover, the finite-size corrections in the critical point position observed for pair HMF theory as well as in QS simulations (Fig. 4.2) suggest that we must compute the critical quantities at $\lambda_p(N)$ and not λ_c^* as done previously done [42]. Figure 4.5 shows double-logarithmic plots for the FSS of the critical QS density and characteristic time following this strategy. For the wide range of degree exponents analyzed, the exponents obtained from power law regressions $\bar{\rho} \sim (\tilde{g}N)^{-S_\nu}$ and

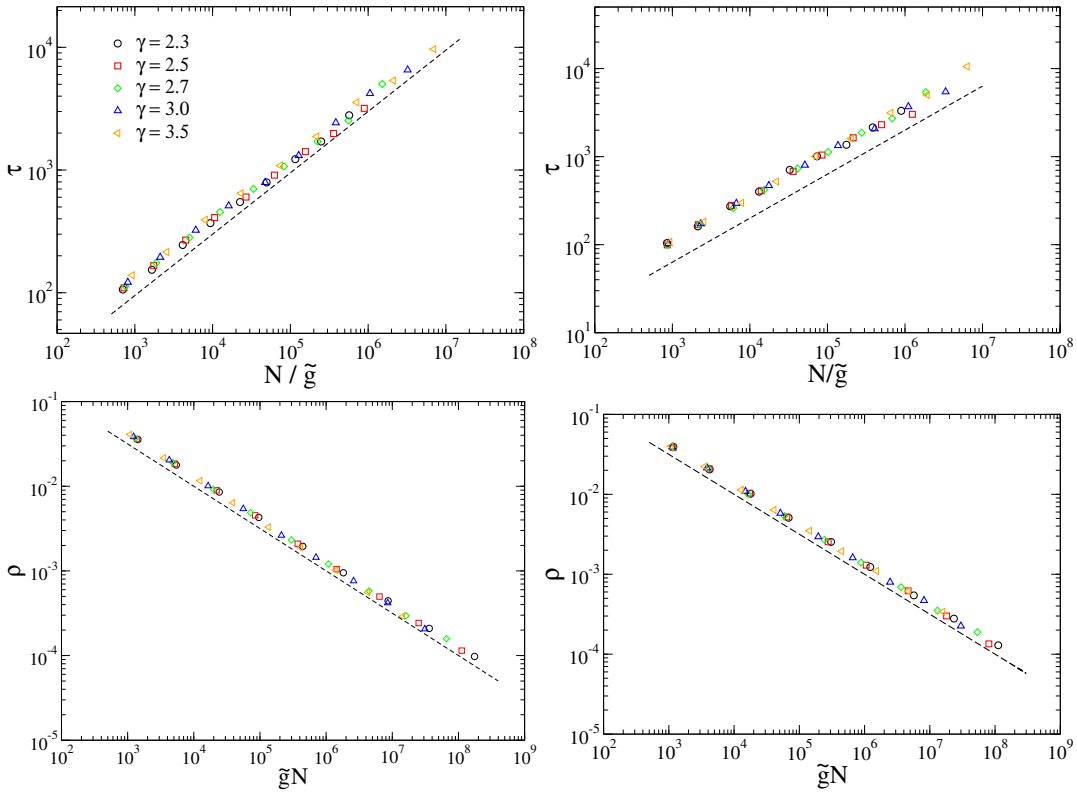

Figure 4.5: FSS of the characteristic time (top) and critical QS density (bottom); $k_0 = 3$ (left) and $k_0 = 6$ (right), for $\lambda = \lambda_p(N)$. The dashed lines have slope $\pm 1/2$ as guides to the eyes.

$\tau \sim (N/\tilde{g})^{S_\alpha}$ are in remarkable agreement with the theoretical prediction $S_\nu = S_\alpha = 1/2$, as one can verify in table 4.2. Most importantly, the scaling laws hold for the entire range of investigated sizes in contrast with the analysis for a fixed $\lambda = \lambda_p^*$ and using the old factor g, for which large deviations of the theoretical scaling laws are observed at small sizes, the more evident for more heterogeneous networks ($\gamma \leq 2.5$) [42]. Noticeably, the exponent of the characteristic time for $\gamma = 2.3$ is in great agreement with the theory if factor $\tilde{g}$ is used in contrast with a poor accordance observed for a similar degree exponent reported in Ref. [42]. It is worth stressing that the almost perfect match is found only if both factor $\tilde{g}$ and corrections in $\lambda_p(N)$ are used concomitantly. In particular, for the $k_0 = 3$ case the scaling laws obtained in simulations are not consistent with HMF if this strategy is not used. Thus, we filled a missing gap showing that the critical exponents as well the sub-leading corrections to the FSS are very accurately predicted by the pair HMF theory.

4.5 Summary and Discussion

The dynamics of the contact process on complex networks was investigated using pair mean-field theories. We compared the theoretical results with QS simulations. The pair HMF and QMF theories represent great improvements in relation the corresponding one-vertex approaches. However, for a wide range of the degree distributions, a heuristic homogeneous pair approximation [20,42] is apparently more accurate than our heterogeneous theories. To unveil this contradiction we compared simulations results with a homogeneous triplet approximations that must be more accurate that pair-approximations. We observed, however, that the HTA theory overestimates the simulation thresholds showing that higher order cluster approximations [110] converge to the wrong critical point and, therefore, that the agreement between HPA and simulations is only a coincidence.

We have also determined the critical exponents in the pair HMF approach. For the infinite size limit the exponents are the same as the one-vertex theory, as expected. However, the finite-size corrections to the scaling obtained in the pair HMF theory allowed a remarkable agreement with QS simulations for all degree exponents ($2.3 \leq \gamma \leq 3.5$) and network sizes ($10^3 \leq N \leq 10^7$) investigated, suppressing a deviation observed for low degree exponents in the one-vertex HMF theory [42].

The present theoretical approaches (pair HMF and pair QMF) can be extended to other dynamical processes taking place on complex networks, for which pair approximations have exhibited great improvement in relation to one-site mean-field theories [17,20,42,100], for example, the SIS model, which will be shown in the next chapter. Our approach permits to explicitly derive analytical expressions whereas previous pair approximations for dynamical processes in complex networks [17,37] usually needs a numerical integration of the corresponding master equations that limits the analysis to relatively small systems.

As a prospect, it would be interesting to perform numerical integration of the pair dynamical equation in a non-perturbative analysis for a comparison with the non-perturbative HMF [113] and the general pair approximation for binary states [108,114].

Chapter 5

Pair Approximation for the SIS Model on Complex Networks

Although mean-field theories are a simplified description of models, it is expected that they correctly predicts the behavior of dynamical process on networks, due to its small-world property. However, dynamical correlations are not taken into account since the states of a node and its neighbors are considered independent. As explained before, one can consider dynamical correlations by means of a pair-approximation [34]. In this chapter, we investigated the role of dynamical correlations on the dynamic of the SIS epidemic model on different substrates [39].

5.1 Pair Quenched Mean-field Theory

In this section, we develop the pair QMF theory for the SIS model. Analytical expressions are presented for the random regular networks, star and wheel graphs. We also investigated large random networks with a power law degree distribution. The thresholds obtained in pair and one-vertex QMF theories have the same scaling with the system size but the pair QMF theory is quantitatively much more accurate than the one-vertex theory when compared with simulations.

5.1.1 Development of the pair approximation

Let us use the same notation of section 4.1.

The dynamical equation for the vertex i is

$$\frac{d\rho_i}{dt} = -\rho_i + \lambda \sum_j \phi_{ij} A_{ij}, \tag{5.1}$$

where A_{ij} is the adjacency matrix. Using a one-vertex approximation where the joint probability ϕ_{ij} is factorized as $\phi_{ij} \approx (1-\rho_i)\rho_j$, one directly finds the threshold given by Eq. (3.8).

The dynamical equation for ϕ_{ij}, considering a pair of connected vertices (i,j), is given by

$$\frac{d\phi_{ij}}{dt} = -\phi_{ij} - \lambda\phi_{ij} + \psi_{ij} + \lambda \sum_{l\neq i} [0_i, 0_j, 1_l] A_{jl} - \lambda \sum_{l\neq j} [1_l, 0_i, 1_j] A_{il}. \tag{5.2}$$

Analogously to Eq. (4.3), the first three terms represents the reactions involving only the pair (i,j), that can create or destroy the configuration $[0_i, 1_j]$: spontaneous annihilation events $[0_i, 1_j] \to [0_i, 0_j]$ and $[1_i, 1_j] \to [0_i, 1_j]$ and the creation in vertex i due to j, $[0_i, 1_j] \to [1_i, 1_j]$. The third and fourth terms represent changes due to the interaction with the neighbors of i and j, respectively, excluding the link (i,j): creation events in i or j due another vertex l, represented by transitions $[1_l, 0_i, 1_j] \to [1_l, 1_i, 1_j]$ and $[0_i, 0_j, 1_l] \to [0_i, 1_j, 1_l]$, respectively, can also destroy/create a configuration $[0_i, 1_j]$.

We now approximate the triplets in Eq. (5.2) with a standard pair-approximation given by Eq. (4.4), to find

$$\frac{d\phi_{ij}}{dt} = -(1+\lambda)\phi_{ij} + \psi_{ij} + \lambda \sum_l \frac{\omega_{ij}\phi_{jl}}{1-\rho_j}(A_{jl} - \delta_{il}) - \lambda \sum_l \frac{\phi_{ij}\bar{\phi}_{li}}{1-\rho_i}(A_{il} - \delta_{lj}). \tag{5.3}$$

We now perform a linear stability analysis in (5.3) around the fixed point $\rho_i = \phi_{ij} = \psi_{ij} = 0$ to find

$$\frac{d\phi_{ij}}{dt} = -(1+\lambda)\phi_{ij} + \psi_{ij} + \lambda \sum_l \phi_{jl}(A_{jl} - \delta_{il}). \tag{5.4}$$

Performing a quasi-static approximation for $t \to \infty$, $d\rho_i/dt \approx 0$ and $d\phi_{ij}/dt \approx 0$, in Eqs. (5.1) and (5.4), respectively, one finds

$$\phi_{ij} \approx \frac{(2+\lambda)\rho_j - \lambda\rho_i}{2+2\lambda}, \tag{5.5}$$

where the relations given by Eq. (4.1) were used to eliminate other dynamical variables. Substituting Eq. (5.5) in (5.1) one finds the Jacobian matrix

$$L_{ij} = -\left(1 + \frac{\lambda^2 k_i}{2\lambda+2}\right)\delta_{ij} + \frac{\lambda(2+\lambda)}{2\lambda+2} A_{ij}. \tag{5.6}$$

As in the case of one-vertex QMF theory, the critical point is obtained when the largest eigenvalue of L_{ij} is null. Equation (5.6) is the central result of this chapter. Even though we do not present a closed expression for the threshold in an arbitrary network, we have obtained analytical solutions of transition points for simple networks. These solutions are very important to test the consistency of the results and to unveil the basic mechanisms that sustain an epidemic phase [13,49]. For the general case, the critical point can be obtained solving Eq. (5.6) numerically, what is done in section 5.1.3.

An approach similar to ours was developed in Ref. [115], where a different approximation was used to split the joint probabilities in cluster approximation: $[A_iB_jC_k] \approx [A_iB_j][C_k]$ instead of the standard pair approximation, Eq. (4.4), which has been generally accepted in the nonequilibrium statistical community as the most reliable approach [33].

5.1.2 Thresholds for Simple Networks

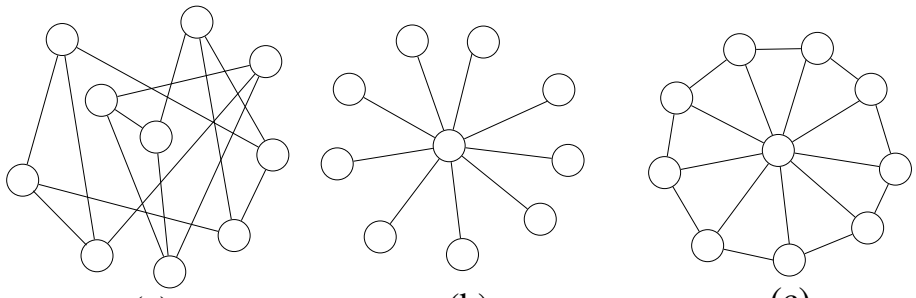

Figure 5.1: Simple graphs used to study SIS dynamics under pair QMF theory: (a) Random regular networks, (b) star and (c) wheel graphs.

Let us start the investigation of Eq. (5.6) for a simple homogeneous network, the random regular network (RRN) illustrated in Fig. 5.1(a). In this network, all N vertices have the same connectivity m, $P(k) = \delta_{km}$, while the connections are done at random, avoiding both self and multiple connections. The largest eigenvalue of L_{ij} is given by

$$\Upsilon_m = -\left[1 + \frac{\lambda^2 m}{2\lambda + 2}\right] + \frac{\lambda(2+\lambda)}{2\lambda+2} m, \tag{5.7}$$

where we used the largest eigenvalue of the A_{ij} given by $\Lambda_m = m$ [36][1]. The threshold is then

[1]We can see that $v_i = 1$ is an eigenvector of the adjacency matrix A with eigenvalue m. Applying the Perron-Frobenius theorem [3] once again, we conclude that the largest eigenvalue of A is m.

obtained as

$$\lambda_c^{pqmf} = \frac{1}{m-1}, \tag{5.8}$$

that corresponds to the threshold of a simple homogeneous pair approximation [36]. Actually, simulations of the SIS model on RRNs reported in Ref. [36] showed that the thresholds are, in fact, much closer to the homogeneous pair approximation than to the standard QMF theory, a fact captured by the pair QMF theory.

We performed simulations of the SIS model using the quasi-stationary method [41,51] described in section 3.8.1. The threshold in finite networks can be estimated using the peaks of the susceptibility χ (see equation (3.43)).

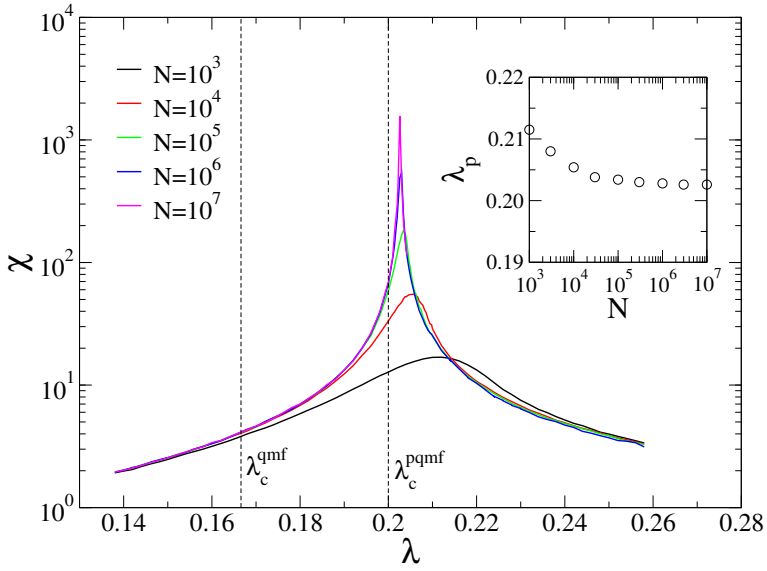

Figure 5.2: Susceptibility versus infection rate for SIS model on RRNs with fixed degree $m = 6$. Inset shows the positions of the peaks of the susceptibility against network size.

Figure 5.2 shows the susceptibility against infection rate exhibiting a sharp peak that asymptotically converges to a position $\lambda_c \simeq 0.2026$ that is only 1% above the theoretical value predicted by the pair QMF theory, $\lambda_c^{pqmf} = 0.2$. So, the pair QMF theory improves a lot the estimate of the thresholds in relation to the simple QMF theory $\lambda_c^{qmf} = 0.166$, which errs approximately 22% the peak position for $m = 6$. Moreover, the larger the vertex degree m the better the pair approximation. For $m = 3$, the peak converges to $\lambda_p = 0.5421$ that is relatively much farther from the pair QMF threshold, $\lambda_c^{pqmf} = 0.5$, than in the case $m = 6$. The better accuracy of the pair QMF theory for larger m is intuitive since the average distance among vertices decreases as the average degree increases making the mean-field premise a more credible hypothesis.

As an example of simple heterogeneous network, we consider star graph defined as a hub, $i = 0$, connected to N leaves, $i = 1, \ldots, N$, of degree $k_i = 1$, as shown in Fig. 5.1(b). This structure

plays a central role in the SIS dynamics since several studies indicate that the epidemic activity may be sustained by the sub-graph composed by the most connected vertex and its neighborhood for networks with degree exponent $\gamma > 2.5$ [36,49,116]. As we will show later, star sub-graphs are responsible by multiple activation transition on scale-free networks. The adjacency matrix of a star graph is $A_{0i} = A_{i0} = 1$ for $i = 1 \ldots N$ and $A_{ij} = 0$, otherwise. Therefore, the elements of the Jacobian L_{ij} are given by

$$L_{ii} = -1 - \frac{\lambda^2}{2\lambda + 2}[(N-1)\delta_{i0} + 1] \tag{5.9}$$

for the diagonal and

$$L_{ij} = \frac{\lambda(2+\lambda)}{(2\lambda+2)}(\delta_{0i} + \delta_{0j}) \tag{5.10}$$

for $i \neq j$. Thus, the eigenvalue equations for L_{ij} are

$$-\left(1 + \frac{\lambda^2 N}{2\lambda+2}\right) v_0 + \frac{\lambda(2+\lambda)}{2\lambda+2} \sum_{j=1}^{N} v_j = \Upsilon v_0 \tag{5.11}$$

and

$$\left[\frac{\lambda(2+\lambda)}{2\lambda+2}\right] v_0 - \left(1 + \frac{\lambda^2}{2\lambda+2}\right) v_i = \Upsilon v_i, \quad i = 1 \ldots N. \tag{5.12}$$

Isolating v_i in Eq. (5.12) and substituting in Eq. (5.11), two different eigenvalues are obtained. Taking the largest one as zero, one obtains the threshold

$$\lambda_c = \frac{\sqrt{2N-1}+1}{N-1} \simeq \sqrt{\frac{2}{N}}, \tag{5.13}$$

which is larger than the prediction of both the standard QMF theory, $\lambda_c^{qmf} = 1/\sqrt{N}$, and the pair approximation developed in Ref. [115], $\lambda_c \approx 1.37/\sqrt{N}$. Our result explains very well the pre-factor larger than 1 observed in simulations of the SIS model on star graphs [36].

Figure 5.3 shows the susceptibility against the infection rate exhibiting a rounded peak characteristic of SIS model on star graphs [36]. The inset of Fig. 5.3 compares the thresholds of the simple and the pair QMF theories with the positions of the susceptibility peaks for different network sizes. The last one is adopted as the real threshold of finite networks [36]. An excellent agreement between simulations and pair QMF results is obtained implying in a remarkable improvement in relation to the standard QMF approach. However, it is important to emphasize that the pair QMF is still an approximation and that a small discrepancy (less than 5%) is observed for the largest investigated system.

A wheel graph is defined as a regular chain of N vertices and periodic boundary and a central vertex connected to all vertices of the chain, Fig. 5.1(c). This network is interesting in the context

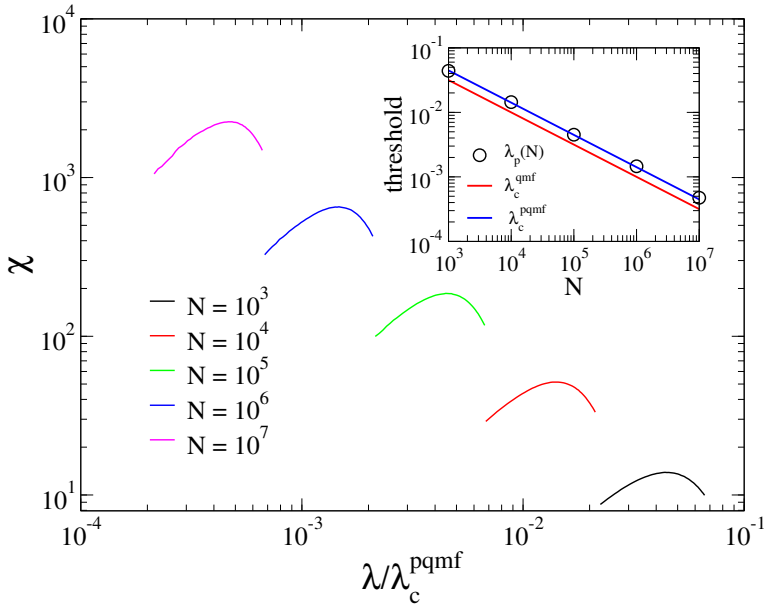

Figure 5.3: Susceptibility versus infection rate for star graphs of different sizes. Inset compares the threshold predicted by one-vertex and pair QMF theories with the position of the peaks of the susceptibility.

of epidemic spreading due to high clustering coefficient $\langle c \rangle \to 2/3$ that contrasts with the null cluster coefficient of the star graph. Following steps similar to those performed for the star graph, one finds

$$\lambda_c = \sqrt{\frac{2}{N}} - \frac{3}{N} + \mathcal{O}(N^{-3/2}). \tag{5.14}$$

This threshold is essentially the same obtained for the star graph, which was confirmed in simulations (see Fig. 5.4).

Triangles, characteristic of clustered networks, enhance dynamical correlations and, therefore, are expected to interfere in the thresholds of dynamical processes in general. So, the clustering-independence observed for wheel graphs must be a characteristic of transitions ruled by the star sub-graph centered at the most connected vertex [49].

5.1.3 Threshold for Heterogeneous Random Networks

For arbitrary random networks, the largest eigenvalue of Eq. (5.6) can be numerically determined [117]. We considered the UCM model [27] to generate networks with power-law degree distribution[2] with minimal vertex degree fixed to $k_{min} = 3$ and a structural cutoff $k_c = N^{1/2}$ in the degree distribution to investigate SIS dynamics via both Eq. (5.6) and quasi-stationary simula-

[2]To generate the degree distribution we used the improved rejection method provided in Ref. [117].

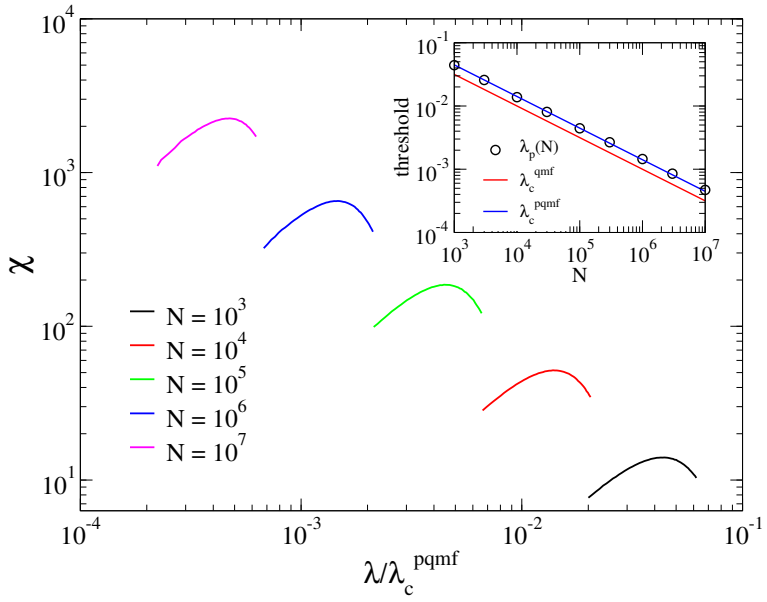

Figure 5.4: Susceptibility versus infection rate for wheel graphs of different sizes. Inset thresholds versus network size predicted by one-vertex and pair QMF theories compared to the position of the peaks of the susceptibility.

tions. It is known that fluctuations of the degree of the most connected vertex drastically change the position of the threshold for $\gamma > 3$ [13]. Therefore, we did our analysis for networks with $k_{max} \equiv \langle k_{max} \rangle$ [13,36], in order to have representative results from a single sample. Unconstrained k_{max} was investigated in chapter 6.

To implement the QS method, a list containing $M = 70$ configurations is stored and constantly updated. The updating is done by randomly picking up a stored configuration and replacing it by the current one with probability $p_r \Delta t$. We fixed $p_r \simeq 10^{-2}$ since no significant dependence on this parameter was detected for a wide range of simulation parameters. We used $t_r = 10^5$ since the relaxation time is short for epidemics on random network due its small-worl property. However, the averaging time must be large. We used averaging times from 10^5 to 10^9, being the larger the average time the smaller the infection rate, since long times are computationally unapproachable for highly infected QS states. It is important to notice that the QS method becomes expendable for a large part of our simulations since the system never visits the absorbing state for the considered simulation times.

For the range $2 < \gamma < 2.50$, the QMF and HMF theories are essentially equal [13] and both theories agree with thresholds estimated from the peaks of the susceptibility curves [36]. We investigated networks with $\gamma = 2.25$ and verified that the pair QMF is very close to QMF and, consequently, to HMF theories, being the pair QMF the one closer to the simulation results. Figure 5.5 compares the three theories with the peak of the susceptibility (top inset). One can see that

pair QMF theory fits better the thresholds for small networks (bottom inset).

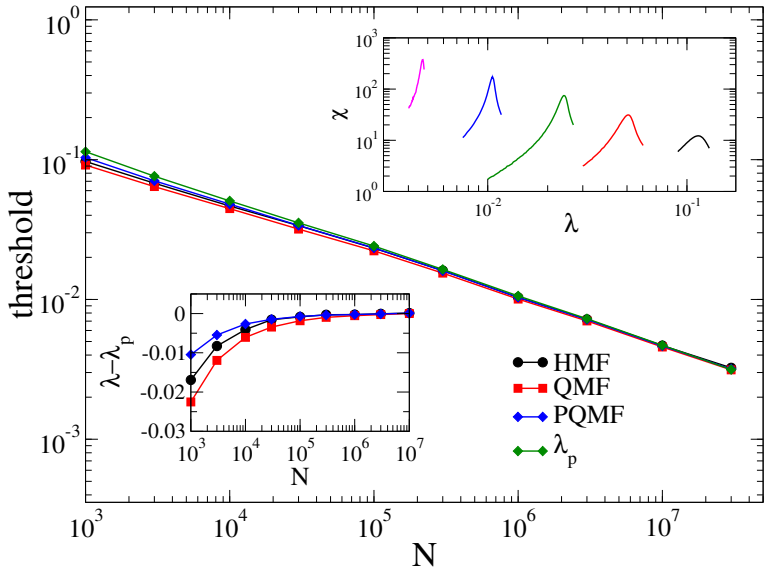

Figure 5.5: Thresholds versus network size for SIS model on UCM networks with degree exponent $\gamma = 2.25$. The top inset shows the susceptibility curves against infection rate for $N = 10^3, 10^4, 10^5, 10^6$, and 10^7 (from the right to the left) used to determine the thresholds in simulations (position of the peaks λ_p). The bottom inset shows the difference between theoretical thresholds and the peaks in the susceptibility curves.

Figure 5.6 shows the thresholds for $\gamma = 2.75$. In this case, the pair QMF consists in a great improvement in relation to the standard QMF (bottom inset of Fig. 5.6). The difference is less than 8% while standard QMF errs in approximately 30%. It was proposed that the star sub-graph composed by the most connected vertex and its neighbors is responsible by sustaining activity in random network with $\gamma > 2.5$ [49]. The threshold for the corresponding star sub-graph, $\lambda_c^{star} = \sqrt{2/k_{max}}$, is also included in Fig. 5.6. One can see that this threshold converges to the pair QMF as network increases confirming that the star sub-graph is actually the structure responsible by sustaining the epidemics activity[3]. Notice that HMF theory does not capture the scaling of threshold against network size[4].

The most drastic differences among theories appear for $\gamma > 3$, as illustrated in Fig. 5.7 where we show the threshold against size for $\gamma = 3.50$. While HMF theory predicts a finite threshold, both simple and pair QMF theories yield asymptotically vanishing thresholds. The χ *vs.* λ curves have a single sharp peak for small sizes but a secondary rounded peak at small λ emerges for very large sizes. Such doubly peaked susceptibility was interpreted as the competition between two mechanisms triggering the epidemic spreading in the network: The activity in the star sub-graph

[3]Later, we realized that the constraint of the UCM model $k \ll N^{1/2}$ forbids the emergence of outlier with $k \gg \langle k_{max} \rangle$ and this cutoff slows-down the convergence to the star sub-graph threshold.

[4]Better agreement is obtained with pair HMF theory presented in section 5.2.

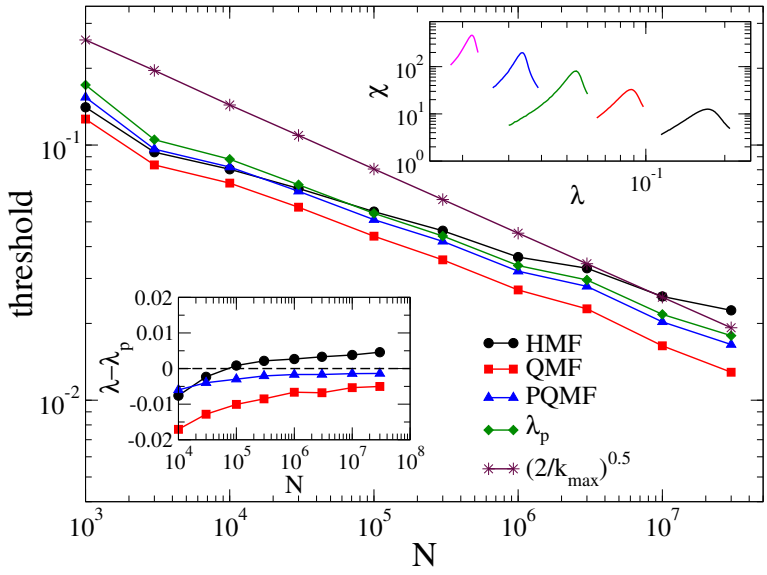

Figure 5.6: The same analysis of Fig. 5.5 for $\gamma = 2.75$.

centered at most connected vertex against that in the most densely connected component of the network [36]. These competing mechanisms are also associated to the localization/delocalization of the epidemic activity in network [11]. The peaks at small λ are well fitted by the pair QMF theory (less than 10% of difference against 40% for QMF theory). Notice that the threshold of the pair QMF theory quickly converges to that of a star sub-graph $\lambda_c^{star} = \sqrt{2/k_{max}}$. However, the peak at larger λ was not captured in this theoretical approach. In fact, the susceptibility curves can exhibit multiple peaks as the value of λ increases. Trying to find an explanation about this complex behavior of the SIS model on random networks with a power law degree distribution with $\gamma > 3$ was the main motivation for the next step of our research, which will be shown in the chapter 6.

5.2 Heterogeneous Pair Approximation

Our first motivation for develop a heterogeneous pair approximation stems from recent works have shown that the contact process running on the top of highly heterogeneous random networks is described by the heterogeneous mean-field theory (see chapter 4). Indeed, the pair HMF approach can be suited to dynamical processes on networks in general. Therefore we present in this section the pair HMF theory for the SIS model. This analytical result will be compared with simulations in the chapter 6.

We use the same notation of the section 4.2, but for the SIS model, the equation for the proba-

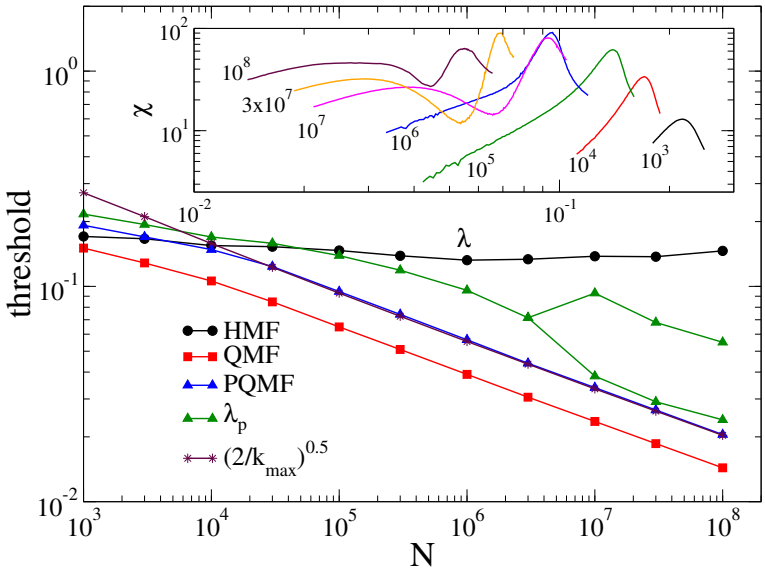

Figure 5.7: Thresholds versus network size for the SIS model on random networks with degree exponent $\gamma = 3.50$. Inset shows the susceptibility curves against infection rate for different sizes (indicated near each curve) used to determine the thresholds (peaks) in simulations.

bility that a vertex with degree k is occupied takes the form

$$\frac{d\rho_k}{dt} = -\rho_k + \lambda k \sum_{k'} \phi_{kk'} P(k'|k), \tag{5.15}$$

where the conditional probability $P(k'|k)$, which gives the probability that a vertex of degree k is connected to a vertex of degree k', weighs the connectivity between compartments of degrees k and k'. The dynamical equation for $\phi_{kk'}$ is

$$\begin{aligned}\frac{d\phi_{kk'}}{dt} &= -\phi_{kk'} - \lambda\phi_{kk'}k' + \psi_{kk'} + \lambda(k'-1)\sum_{k''}[0_k 0_{k'} 1_{k''}]P(k''|k') \\ &\quad -\lambda(k-1)\sum_{k''}[1_{k''} 0_k 1_{k'}]P(k''|k).\end{aligned} \tag{5.16}$$

The one-vertex mean-field equation [Eq. (3.14)] is obtained factoring the joint probability $\phi_{kk'} \approx (1-\rho_k)\rho_{k'}$ in Eq. (5.15). The factor $k'-1$ preceding the first summation in Eq. (5.16) is due to the k' neighbors of middle vertex except the link of the pair $[0_k 0_{k'}]$ (similarly for $k-1$ preceding the second summation).

We now approximate the triplets in Eq. (5.16) with the pair-approximation of Eq. (4.19), to find

$$\begin{aligned}\frac{d\phi_{kk'}}{dt} &= -\phi_{kk'} - \lambda\phi_{kk'} + \psi_{kk'} + \frac{\lambda(k'-1)\omega_{kk'}}{1-\rho_{k'}}\sum_{k''}\phi_{k'k''}P(k''|k') \\ &\quad -\frac{\lambda(k-1)\phi_{kk'}}{1-\rho_k}\sum_{k''}\phi_{kk''}P(k''|k). \end{aligned} \tag{5.17}$$

Substituting the relations given by Eqs. (4.16) in (5.17) and performing a linearization around the fixed point $\rho_k \approx 0$ and $\phi_{kk'} \approx 0$, one finds

$$\frac{d\phi_{kk'}}{dt} = -\left(2+\lambda\right)\phi_{kk'} + \rho_{k'} + \lambda(k'-1)\sum_{k''}\phi_{k'k''}P(k''|k'). \tag{5.18}$$

The next step is to perform a quasi-static approximation for $t \to \infty$, in which $d\rho_k/dt \approx 0$ and $d\phi_{kk'}/dt \approx 0$,

$$\phi_{kk'} = \frac{2k'-1}{2k'+\lambda}\rho_{k'}, \tag{5.19}$$

considering uncorrelated random networks. Finally, we plug Eq. (5.19) in Eq. (5.15) to produce

$$\frac{d\rho_k}{dt} = \sum_{k'} L_{kk'}\rho_{k'}, \tag{5.20}$$

where the Jacobian $L_{kk'}$ is given by

$$L_{kk'} = -\delta_{kk'} + \frac{\lambda k}{\langle k\rangle}\frac{(2k'-1)}{(2+\lambda)} \tag{5.21}$$

with $\delta_{kk'}$ being the Kronecker delta symbol.

Again, the absorbing state is unstable when the largest eigenvalue of $L_{kk'}$ is positive. Therefore, the critical point is obtained when the largest eigenvalue of the Jacobian matrix is null, thus obtaining:

$$\lambda_c = \frac{\langle k\rangle}{\langle k^2\rangle - \langle k\rangle}. \tag{5.22}$$

This threshold coincides with that of the susceptible-infected-recovered (SIR) model in a one-vertex HMF theory [1]. This results was recently proposed in Ref. [16] using heuristic arguments. They argued that, dynamical correlations, that are neglected in a one-vertex HMF theory, account for the fact that infected nodes have higher probability to be still infected. This means that, in the next step, this node can be considered immunized (recovered for a while). So, a better upper bound for the spreading of the disease is given by the HMF theory of the SIR model, that is exactly the threshold given by Eq. (5.22).

5.3 Summary and Discussion

In this chapter, we have investigated the epidemic spreading of the SIS model performing mean-field pair approximations, introducing the effects of dynamical correlations. Fistly, we proposed a theory that is an extension of the QMF theory [13,45] that includes the actual network connectivity. Analytical expressions for the epidemic thresholds are presented for some simple networks while the thresholds for the most interesting case of random networks with a power law degree distribution $P(k) \sim k^{-\gamma}$ are obtained from the numerical solution of an eigenvalue problem.

We compared our pair theory with the one-vertex QMF and HMF theories and with the peaks of susceptibility as a function of infection rate obtained in quasi-stationary simulations. We have shown that the thresholds in the pair QMF theory as a function of the network size scale as in the standard QMF theory. However, the pair QMF thresholds are quantitatively much closer to the simulation results than those of standard QMF.

Our theoretical approach represents an important advance in relation to other improvements of the QMF theory, which are that limited to small networks [37,115] whereas we were able to investigate networks as large as $N = 10^8$. Despite of the considerable improvement when compared to QMF theory, our approach is still an approximation. Certainly, a n-vertex theory with $n > 2$ should enhance the accuracy of the threshold determination. Also, the critical exponents associated to the transition of the SIS model are still an open problem in our approach.

The SIS dynamics was also investigated using a pair heterogeneous mean-field theory. The threshold of the SIS model in a pair HMF approximation coincides with that of the SIR model in a one-vertex HMF theory [1].

Finally, the present theoretical approaches can be applied to other important dynamical processes on complex networks as generalized voter models [118], sandpiles [119] as well as more sophisticated structures as multiscale and multiplex network [113,120].

Chapter 6

Multiple transitions of the SIS Model on Complex Networks

The existence/absence of finite epidemic thresholds involving an endemic phase of the susceptible-infected-susceptible (SIS) model on the top of scale-free (SF) networks with a degree distribution $P(k) \sim k^{-\gamma}$, where γ is the degree exponent, has been target of a recent and intense investigation [11,13,15,16,36,38].

As discussed in section 3.6, for $\gamma < 3$, there exists a consensus for SIS thresholds: both HMF and QMF are equivalent and accurate for $\gamma < 2.5$ while QMF works better for $2.5 < \gamma < 3$ [36,39]. However, for $\gamma > 3$ the HMF theory predicts a finite threshold and the QMF theory states that the threshold vanishes for any value of γ [13]. Moreover, the BCPS theory also points a vanishing epidemic threshold for $\gamma > 3$ [16].

As discussed in chapter 5 and firstly reported in Ref. [36], the SIS dynamics running on the top of scale-free networks with $\gamma > 3$ can exhibit more complex behavior than previously thought. Therefore, we performed extensive simulations to investigate this peculiarity for heterogeneous networks with $\gamma > 3$. We found that, in this case, the SIS dynamics can exhibit multiple transitions, with multiple thresholds, which are clearly resolved when the degree distribution presents outliers separated by large gaps. These gaps permits the formation of non directly connected domains centered on hubs with different connectivity and thus having distinct local activation thresholds. Thresholds consistent with those predicted by QMF, HMF and BCPS theories were found in our analysis. Moreover, our finds indicate that the vanishing thresholds, as those predicted by QMF [13] and BCPS theories [16], involve long-term but still localized epidemics rather than an endemic state, in which a finite fraction of the network has non-vanishing probability to be infected, in the thermodynamic limit. We propose that this localized long-term epidemics takes place in highly

connected domains involving hubs and their nearest-neighbors. Finally, our numerical results show a transition to the endemic state occurring at a finite threshold, which intriguingly is qualitatively well described by the classic and simpler HMF theory [44,95]. This chapter corresponds to our original results of the Ref [109].

6.1 Details of the simulation implementations

We implement the SIS model using the standard simulation scheme and the QS method (see sections 3.7.1 and 3.8.1) with the same parameters described in chapter 5. However, reference [16] claimed that the QS method is unreliable for networks with degree exponents $\gamma > 3$ and proposed a new simulation strategy, which is referred here as lifespan simulation method. In order to draw a comparison with the QS method, we implemented the LS method exactly as in Ref. [16] and explained in section 3.8.2.

We applied both methods to the SIS model on UCM networks with $\gamma = 3.50$, minimum degree $k_0 = 3$, and upper cutoff $k_{max} = \langle k_{max} \rangle$, to compare with the results of Ref. [16]. The constraint $k_{max} = \langle k_{max} \rangle$[1] avoids fluctuations in the most connected vertex and, consequently, in the largest eigenvalue of the adjacency matrix and is useful for comparisons with the QMF theory [36]. We remark that the constraint $k_{max} = \langle k_{max} \rangle$ is only used in this comparison.

Figures 6.1(a) and (b) show the lifespan and susceptibility versus infection rate for networks of different sizes. Two-peaks on the susceptibility versus infection rate for SIS were firstly reported in the previous chapter where we focused on the analysis of the peak at low λ and showed that it is well described by the pair QMF theory. The peak positions versus network size are compared in Fig 6.1(c). As can be clearly seen, the right susceptibility peaks are very close to the lifespan ones showing that the susceptibility method is able to capture the same transitions as the lifespan method does but going beyond as will be discussed hereafter.

It is worth do notice that, if larger values of λ are simulated, other peaks will emerge in susceptibility curves even using the cutoff $k \leq \langle k_{max} \rangle$. These multiple peaks were not reported in previous works dealing with the same network model [16,36,39]. These multiple peaks were analyzed accurately and the results will be shown in this chapter.

Moreover, a lifespan can also be obtained in the QS method as [51] (see also section 3.8.1)

$$\tau_{qs} = \frac{1}{\bar{P}(1)}. \tag{6.1}$$

[1] $\langle k_{max} \rangle$ is the analytically determined mean value of the most connected vertex k_{max} of a random degree sequence with distribution $P(k)$ without upper bounds.

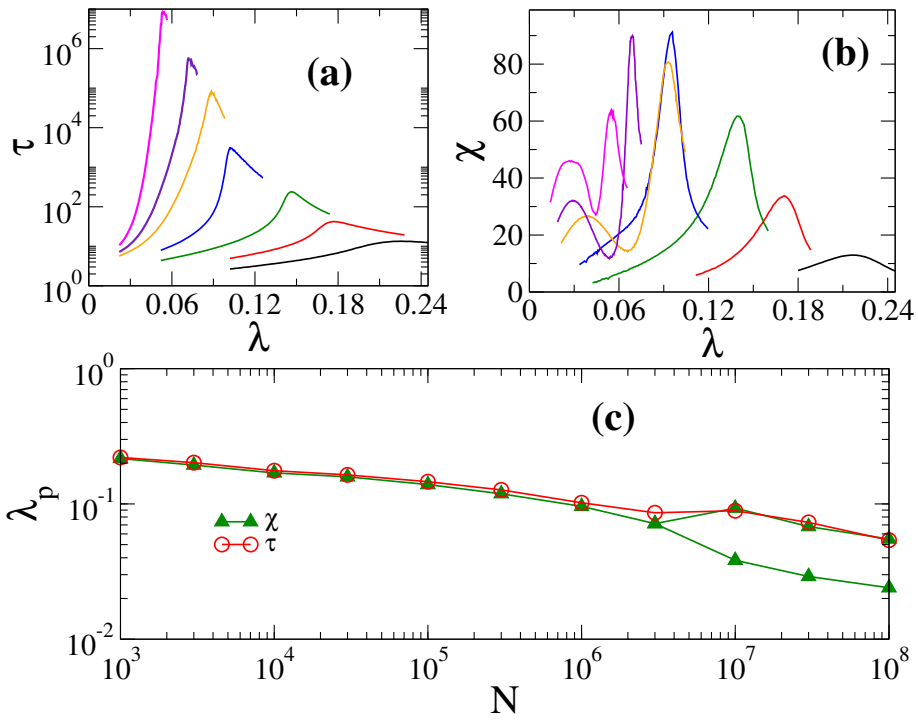

Figure 6.1: Numerical determination of the thresholds for the SIS model on UCM networks with $\gamma = 3.50$, $k_0 = 3$ and $k_{max} = \langle k_{max} \rangle$ for network sizes $N = 10^3, 10^4, 10^5, 10^6, 10^7, 3 \times 10^7$, and 10^8, increasing from the right. The same network sample for each size was used in both methods. Both (a) lifespan calculated using the method of Ref. [16] and (b) susceptibility via QS method are shown in the top panels. (c) Peak positions as functions of the network size estimated with both methods.

We have checked that the lifespans obtained in the QS and LS methods diverge at the same threshold; the basic difference is that the former is "infinite" above the threshold whereas the latter remains finite.

We believe the lifespan method is indeed an alternative way to numerically study systems with absorbing states, which complements more traditional techniques, such as the quasistationary method. However, in heterogeneous substrates, we verified that the lifespan method predicts an epidemic threshold when an activity survives for long times, but there is no guaranty that it is necessarily an endemic phase (see figures 6.7 and 6.8 for a concrete counter-example). On the other hand, the QS analysis is able to simultaneously determine transitions involving endemic as well as localized states and the one involving a diverging lifespan is resolved using Eq. (6.1). So, we conclude that the LS method must not be used alone in systems with multiple transitions since it captures the first transition with a long-term activity.

6.2 Thresholds for random networks with $\gamma > 3$

As previously explained, we have found two-peaks on the susceptibility versus infection rate for SIS model. In a previous work we focused on the analysis of the peak at low λ and showed that it is well described by the pair QMF theory but did not realize that the peak at higher λ is the one associated to a diverging lifespan (Fig. 6.1). However, depending on the network realization, the susceptibility curves can exhibit much more complex behaviors with multiple peaks for values of λ larger than those reported in Refs. [36,39]. These complex behaviors become very frequent for large networks. From now on, we scrutinize such a complex behavior to unveil its origin and implications to the epidemic activity.

Figure 6.2(a) shows a typical susceptibility curve (black) exhibiting such a complex behavior for an UCM network. The degree distribution is shown in Fig. 6.2(d). Multiple peaks are observed only if the degree distribution exhibits large gaps, in particular in the tails. These few vertices with degree $k \gg \langle k_{max} \rangle$, where k_{max} is the maximum value obtained in the generation of N random variables with distribution $P(k)$, are hereafter called outliers. Notice that these multiple peaks were not detected by the lifespan simulation method [16]. The role played by outliers is evidenced by their immunizations[2] as illustrated in Fig. 6.2. For instance, the immunization of three most connected vertices is sufficient to destroy two peaks and to enhance others. The stationary density varies abruptly close to the thresholds determined via susceptibility peaks, Figs. 6.2(b) and (c), which is an evidence of the singular behavior of the order parameter ρ.

The presence of gaps is a characteristic of large degree sequences with a power law distribution. The statistical representativity of specific properties of a finite set of networks, generated under the same conditions, in relation to the entire ensemble is a complex issue [35], but the existence of gaps can be understood with a simple non-rigorous reasoning. Using extreme value theory one can show that the most connected vertex has an average $\langle k_{max} \rangle \sim N^{1/(\gamma-1)}$ [36]. However, this mean value is not representative of the highest degree since the dispersion $\sigma_{max} = \sqrt{k_{max}^2 - \langle k_{max} \rangle^2}$ diverges as[3] $\sigma_{max} \sim N^{1/(\gamma-1)}$ for $\gamma > 3$. Outliers should behave in this same way and therefore we expect larger dispersion in outlier connectivity as network size increases.

It is interesting to observe that while the peaks at small λ can or not appear depending on the presence of outliers and the gaps, the rightmost one essentially does not change its position from a network realization to another, such that it should depend on network properties representative of the entire ensemble of networks with a specified set of parameters. Indeed, later we will see that the behavior of the rightmost peak is described by the HMF threshold which depends only on $\langle k^2 \rangle$

[2] Immunized vertices cannot be infected, which is equivalent to remove them from the network.
[3] This result can be derived using the same steps to obtain $\langle k_{max} \rangle$ in Ref. [36].

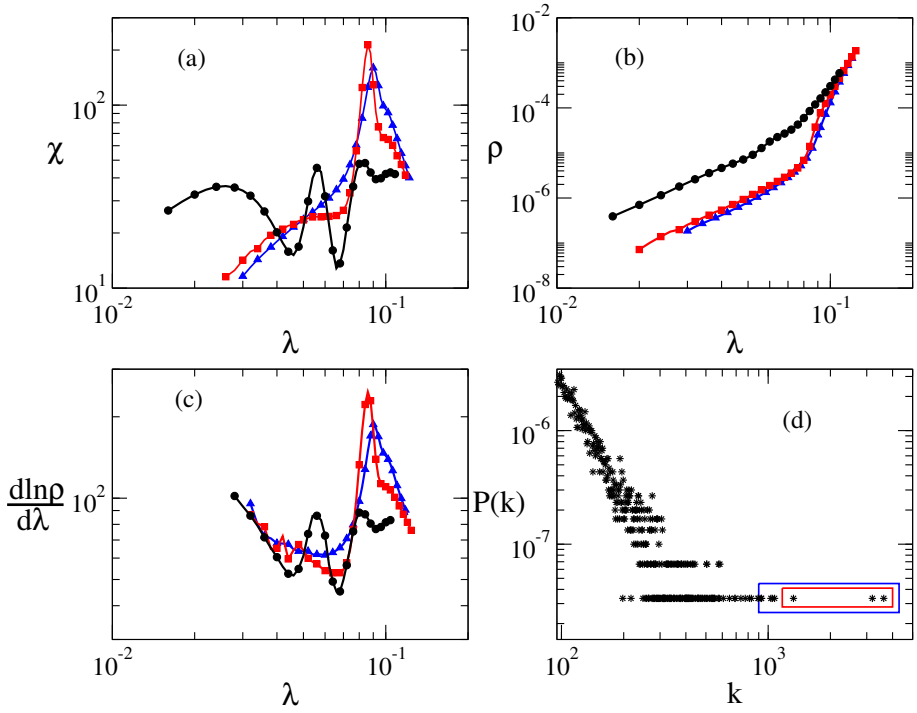

Figure 6.2: (a) Susceptibility, (b) stationary density and (c) its logarithmic derivative versus infection rate for a SF networks with 3×10^7 vertices, degree exponent $\gamma = 3.5$, minimum degree $k_0 = 3$ and k_{max} unconstrained. The degree distribution is shown in panel (d). Different immunization strategies are shown: Black circles represent no immunization; red squares represent the immunization of three largest outliers (inner box in panel (d)); blue triangles represent the immunization of eight most connected vertices (outer box in panel (d)).

and $\langle k \rangle$.

A deeper physical explanation for the multiple peaks can be extracted using another order parameter in the QS state, the participation ratio (PR), defined as

$$\Phi = \frac{1}{N} \frac{(\sum_i \rho_i)^2}{\sum_i \rho_i^2}, \tag{6.2}$$

where ρ_i is the probability that the vertex i is infected in the stationary state. The inverse of the PR is a standard measure for localization/delocalization of states in condensed matter [121] and has been applied to statistical physics problems [122] including epidemic spreading on networks [11, 14,123]. The limiting cases of totally delocalized ($\rho_i = \rho \; \forall \; i$) and localized ($\rho_i = \rho\delta_{i,0}$) states, where 0 is the vertex where localization occurs, are $\Phi = 1$ and $\Phi = 1/N$, respectively.

The PR as a function of the infection rate is shown in Fig. 6.3. The PR is an estimate of the fraction of vertices that effectively contribute to the present epidemic activity. Thus, the multiple transitions are related to the rapid delocalization process of the epidemics as λ increases, hall-

marked by the singular behavior of Φ around distinct values of λ. When the PR corresponds to a finite fraction of the network in an active phase one has an authentic endemic state, since a finite fraction of nodes has a non-vanishing probability of being infected.

The logarithmic derivative of the PR exhibits several peaks in analogy to susceptibility peaks, as shown in the inset of Fig. 6.3. Indeed, PR can be seen as a susceptibility but from an origin different of χ. The latter is a measure of stochastic fluctuations of the order parameter (density of infected vertices) whereas the former is a measure of stationary spatial fluctuations that make sense only for heterogeneous substrates.

The PR versus network size for a fixed distance to either λ_p^{ls} (the threshold marking the lifespan divergence) and λ_p^{right} (the threshold referent to the rightmost peak observed for susceptibility) are shown in Fig. 6.4(a). In the considered size range, the PR decays as a power law. Analogous results are obtained for $\bar{\rho}$ vs N curves [see Fig. 6.4(b)]. For a fixed distance to the lifespan peaks, the power-law fittings yield approximately $\Phi \sim N^{-0.8}$ and N^{-1} for $\gamma = 3.5$ and 4, respectively, $\rho \sim N^{-0.8}$ for both $\gamma = 3.5$ and 4. These decays constitute a strong evidence for epidemics localization at $\lambda \gtrsim \lambda_p^{ls}$ whereas the constant dependence on N observed for $\lambda \gtrsim \lambda_p^{right}$ surely represents an endemic phase[4].

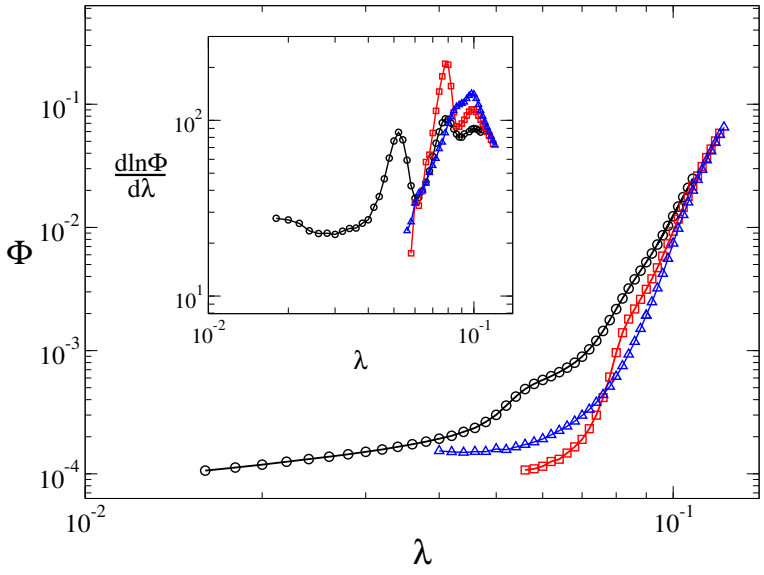

Figure 6.3: Main: PR as a function of the infection rate for the same networks and immunization strategies shown in Fig. 6.2. Symbols as in Fig. 6.2. Inset: Logarithmic derivative of the PR as a function of the infection rate.

Figure 6.5 shows the positions λ_p^{left} (the leftmost peak), λ_p^{right} and λ_p^{ls} against the network size. One can see that λ_p^{right} reaches a constant value for large N whereas the other ones neatly decays

[4]Notice that a scaling $\bar{\rho} \sim (\lambda - \lambda_p)^{\beta}$, independent of the size, is expected for an usual endemic phase transition in the thermodynamic limit [33].

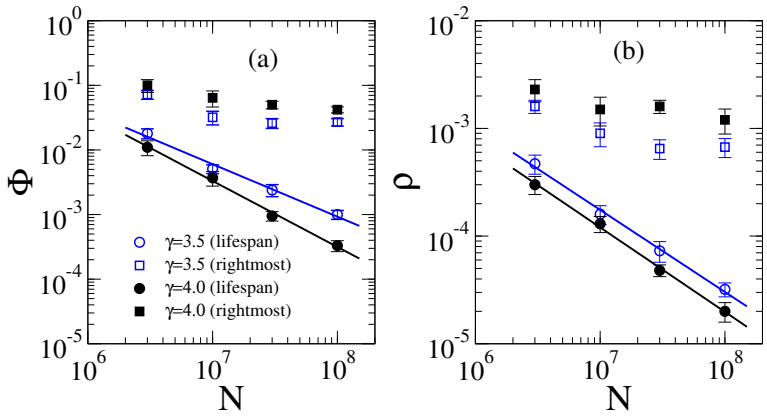

Figure 6.4: (a) PR versus system size for a fixed distance $\lambda - \lambda_p = 0.012$ to either lifespan (circles) and rightmost (squares) peaks. (b) The same analysis of panel (a) for the QS density. Lines are power-law fittings regressions. At least 10 network samples were used to perform averages for $\lambda > \lambda_p^{right}$ (top curves) and at least 20 for $\lambda_p^{ls} < \lambda < \lambda_p^{right}$ (bottom curves).

with N. In a nutshell, our results show that the case $\gamma > 3$ may concomitantly exhibit transitions predicted by three competing mean-field theories: (*i*) At $\lambda = \lambda_p^{left}$, one has a transition to an epidemics highly concentrated at the star subgraph containing the most connected vertex and its nearest neighbors. The threshold dependence on the network size is very well described by QMF theories [13,36,39]. (*ii*) At $\lambda = \lambda_p^{ls}$, a transition with a threshold described by the BCPS theory [16] is observed but, our simulations indicate that it is not endemic since PR and ρ decays with N above this threshold. Notice that the threshold λ_p^{ls} decays with N much slower than λ_p^{left}. This interval is characterized by the mutual activation of stars sub-graphs centered on the outliers by means of reinfection mechanism proposed in the BCSP theory [14]. (*iii*) For $\lambda = \lambda_p^{right}$, a transition involving an authentic endemic phase with a finite threshold is observed as formerly, and now surprisingly, predicted by the HMF theory [44]. Here, the bulk of the network acts collectively in the epidemic spreading through the whole network characterizing a real phase transition.

The co-existence of localized and endemic transitions in a same network can be explained in a double random regular network (DRRN), Fig. 6.6. These networks are formed by two random regular networks (see section 5.1.2) of sizes N_1 and $N_2 = N_1^{\alpha}$ ($\alpha < 1 \Rightarrow N_2/N_1 \to 0$ in the thermodynamical limit) and degree m_1 and m_2, respectively, connected by a single edge. The DRRN has two epidemic thresholds corresponding to the activations of single RRNs. Choosing $m_1 = 6$ and $m_2 = 4$, the thresholds determined for single RRNs are $\lambda_c^{(1)} = 0.31452$ ($m_1 = 4$, present work) and $\lambda_c^{(2)} = 0.2026$ ($m_2 = 6$ [47]). By construction, the former involves an endemic and the latter a localized phase transition since the smaller RRN constitutes itself a vanishing fraction of the whole network. Figure 6.6 shows the susceptibility plots for $\alpha = 0.5$ with peaks converging exactly to the expected thresholds of single RRNs as highlighted in Fig. 6.7(a) and (b).

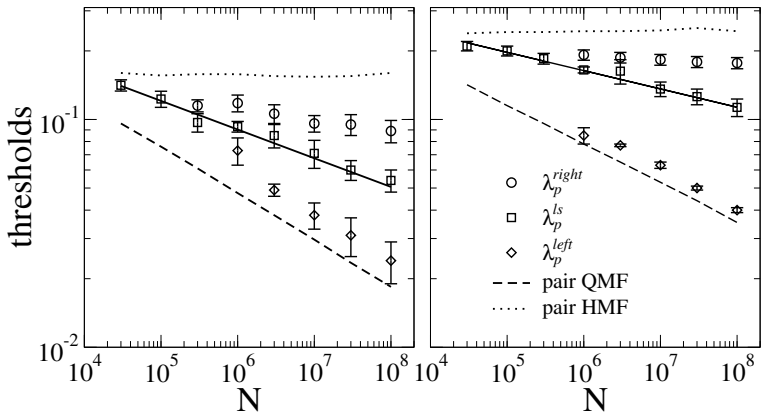

Figure 6.5: Thresholds for SIS dynamics on SF networks with degree exponents $\gamma = 3.5$ (left) and $\gamma = 4.0$ (right). Averages were done over at least 5 samples. The results predicted by pair QMF [39] and pair HMF [46] theories are shown as dashed and doted lines, respectively. Solid lines are power-law fittings. Averages were done over at least 5 samples for the statistics of the rightmost peak and at least 20 samples for lifespan and leftmost peaks.

As it is widely known, the mean-field theory for the finite-size scaling of the contact process, which in the case of strictly homogeneous networks is exactly the same as SIS model with a rescaled infection rate λ/m, predicts that the threshold approaches its asymptotic values as $\lambda_p - \lambda_c \sim S^{-1/2}$, where S is the graph size (see section 4.3). So, the endemic threshold is expected to scale as $\lambda_p - \lambda_c^{(1)} \sim N_1^{-1/2} \sim N^{-1/2}$ and the localized one as $\lambda_p - \lambda_c^{(2)} \sim N_2^{-1/2} \sim N^{-\alpha/2}$. These power-laws are confirmed in Fig. 6.7(b). The lifespan curves, obtained using as initial condition only the most connected vertex infected (the one connecting sub-graphs), have single peaks that converge to the threshold corresponding to a localized epidemic. Interestingly this threshold follows the same scaling law as the left QS peak as shown in Figs. 6.7 and 6.8(a). The central point here is that the lifespan method detected the first threshold where the absorbing state becomes globally unstable (an exponentially long-term activity). However, in this case, this threshold is not the endemic one as shown in Fig. 6.8(b).

It is worth do notice that the QS simulations around the peaks are orders of DRRN model can be generalized to produce an arbitrary number of transitions providing a clearer analogy with multiple phase transitions observed for random networks with $\gamma > 3$.

An additional property can be derived for random networks with $\gamma > 3$: outliers have negligibly low probability to be connected to each other. Due to the absence of degree correlation, the probability that a vertex of degree k is connected to an outlier of degree k_{out} is given by $P(k|k_{out}) = kP(k)/\langle k \rangle$ [41] irrespective of outlier's degree. Therefore the probability that an

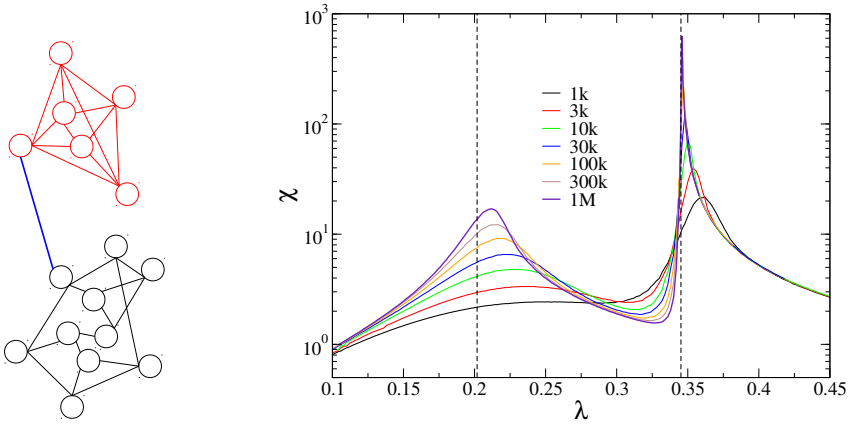

Figure 6.6: Left: Schematics of a double random regular network (DRRN). Right: Susceptibility versus infection rate for DRRNs with $m_1 = 4$, $m_2 = 6$, $\alpha = 1/2$ and different sizes. Dashed lines are thresholds predicted for DRRNs.

outlier is connected to other outlier is given by

$$P_{out} \simeq \int_{k \gtrsim \langle k_{max} \rangle} kP(k|k_{out})dk \sim \langle k_{max} \rangle^{-\gamma+2}, \tag{6.3}$$

which goes to zero for large networks permitting the emergence of non directly connected domains centered on the outliers. This result can be obtained rigorously using hidden variable theory [124]. We have now a simple physical explanation for multiple thresholds observed in SF networks with $\gamma > 3$ and its connection with the lifespan simulation method: The core containing the outliers plus its nearest neighbors form a subgraph with $N_2 \sim \sum_{k>\langle k_{max} \rangle} NP(k)k \sim N^{1/(\gamma-1)} \ll N$. This domain size diverges as network increases and is able to sustain a long-term epidemic activity, but still represents a vanishing fraction of the whole network. Above the activation of this domain but still below the endemic phase, the epidemics is eventually transmitted to any other vertex of the network due to the small-world property, but this activity dies out quickly outside this core since there the process is locally sub-critical. However, all network vertices will be infected for some period since the active central core acts as a reservoir of infectiousness to the rest of the network.

Our conjecture is confirmed in Fig. 6.9 where SIS dynamics in a large network ($N = 3 \times 10^7$ vertices) is compared with dynamics restricted to either its core of outliers (7 most connected vertices) plus their nearest neighbors ($\approx$ 13200 vertices) or to its outer shell excluding the core[5]. The multiple peaks for the core are observed approximately at the same place as those for the whole network but the outer shell exhibits a single peak around λ_p^{right}. However, the lifespan determined via QS method (see section 3.8.1) diverges at $\lambda \approx \lambda_p^{ls}$ for both core and whole network whereas the divergence coincides with λ_p^{right} for the outer shell.

[5]To restrict the epidemics to the core we immunize the shell and vice-versa.

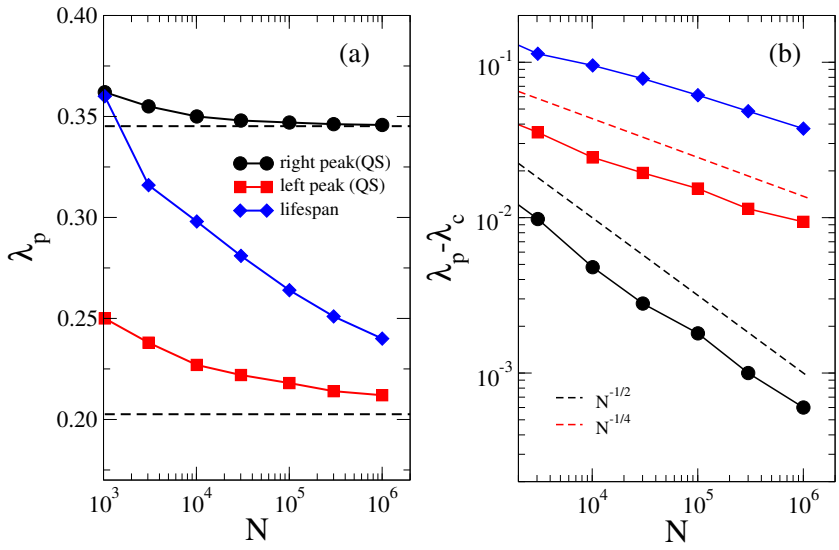

Figure 6.7: Threshold analysis for DRRN with $\alpha = 1/2$, $m_1 = 4$, and $m_2 = 6$. (a) The thresholds estimated as the peaks in the susceptibility or lifespan curves. The dashed lines are thresholds obtained on single RRNs with the respective m_i. (b) Difference between peaks and the thresholds for single RRNs with $m = 4$ (lifespan and left susceptibility peaks) or $m = 6$ (right susceptibility peak).

We also analyzed the lifespan using the QS method, Eq. (6.1), for a fixed distance to both left-most and lifespan peaks. For the investigated size range $N < 10^8$, the lifespan values are relatively short ($< 10^2$) and increase algebraically with system size in the interval $\lambda_p^{left} < \lambda < \lambda_p^{ls}$ while long and exponentially diverging lifespans, granting long-term activity for large networks [125], are obtained for $\lambda_p^{ls} < \lambda < \lambda_p^{right}$. The algebraic dependence for the former case is almost certainly a finite-size effect. We calculated the lifespan above the epidemic threshold for the SIS model on star graphs with k leaves and an algebraic growth of the lifespan with N is also obtained for $k < 2000$ which coincides with the range size of typical star subgraphs obtained for UCM networks investigated here. However, a crossover to an exponential growth is obtained for larger star graphs ($k > 10^4$) showing that this structure is itself able to sustain alone a long-term epidemic activity. So, if one could simulate the SIS model on much larger UCM networks ($N > 10^{12}$) the threshold λ_p^{left} would define a transition to a localized but long-term epidemics and the lifespan method would detect the transition given the QMF theory which certainly involves localized phases.

Outliers play a central role even not being able to produce alone a genuine endemic phase where the whole network has a non-vanishing probability to be infected. To highlight such a role, we introduce a hard cutoff in the degree distribution as $k_{max} = k_0 N^{0.75/(\gamma-1)}$, which suppresses the emergence of outliers as shown in Fig. 6.10(a). This choice is because random networks without a rigid upper bound have a highly fluctuating natural cutoff with an average value $\langle k_{max} \rangle \simeq k_0 N^{1/(\gamma-1)}$ [66]. Fig. 6.10(b) compares the QS density for rigid and natural cutoffs. The

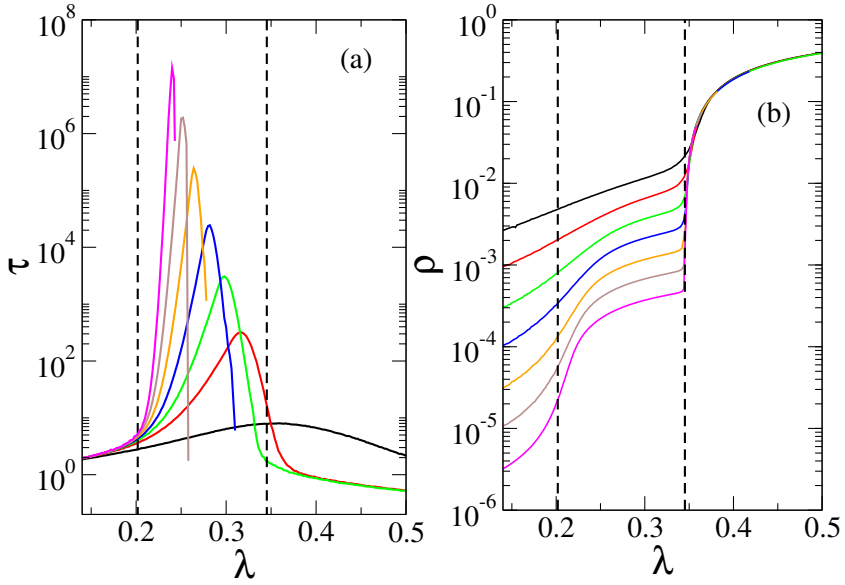

Figure 6.8: (a)The lifespan according Ref. [16] and (b) the QS density of infected vertices versus infection rate for SIS model on DRRNs with $\alpha = 1/2$, $m_1 = 4$, $m_2 = 6$, $N_1 = 10^3$, 3×10^3, 10^4, 3×10^4, 10^5, 3×10^5, and 10^6 (increasing to left/bottom in (a)/(b)). Dashed vertical lines indicate the activation thresholds in each sub-graph.

infectiousness for $\lambda < \lambda_c^{endemic}$ is highly reduced in the absence of outliers. The susceptibility no longer exhibits multiple peaks for a hard cutoff, as can be seen in Fig. 6.11(a), confirming the existence of a single transition. Also, the thresholds for hard cutoff networks are quite close to λ_p^{right} obtained with the natural cutoff, as shown in Fig. 6.11(b). Such an observation is in agreement with the HMF theory where the thresholds for $\gamma > 3$ are asymptotically independent of how k_c diverges [44,46].

6.3 Summary and Discussion

In summary, we extensively simulated the dynamics of the SIS epidemic model on complex networks with power law degree distributions with exponents $\gamma > 3$. For such networks conflicting theories discussing the existence or not of a finite epidemic threshold for the endemic phase have recently been proposed [11,13,15,16]. We show that the SIS dynamics can indeed exhibit several transitions associated to different epidemiological scenarios. Our simulations support a picture where the threshold obtained recently in the BCPS mean-field theory [16] represents a transition to localized epidemics and that the transition to an authentic endemic state, in which a finite fraction of network is infected, possibly occurs at a finite threshold as formerly and now surprisingly foreseen by the HMF theory [44,95]. The multiple transitions are associated to large gaps in the degree

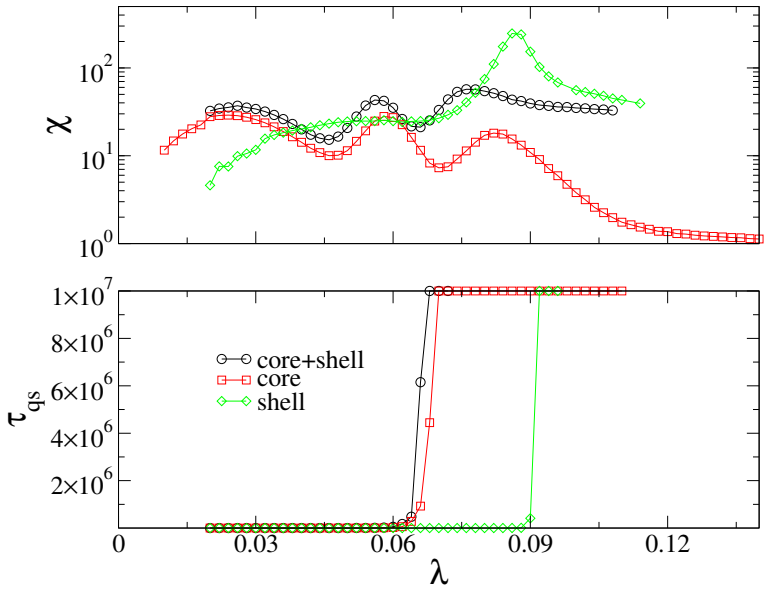

Figure 6.9: Susceptibility (top) and QS lifespan (bottom) versus infection rate for SIS dynamics on a network with $N = 3 \times 10^7$, $k_0 = 3$ and degree exponent $\gamma = 3.50$ restricted to different domains. The lifespan is considered infinite if greater than the averaging time $t_{av} = 10^7$.

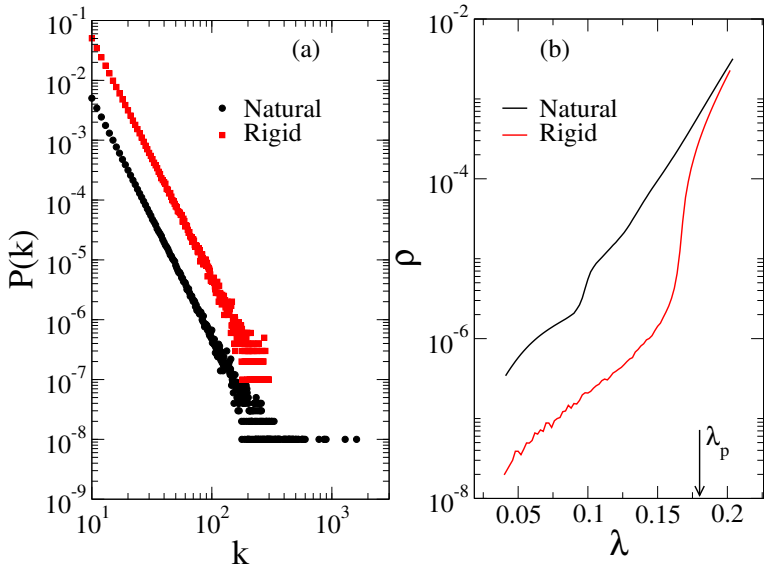

Figure 6.10: (a) The tail of the degree distributions for networks with $\gamma = 4$, $k_0 = 3$, and $N = 10^8$ vertices and either rigid or natural cutoff. The curve for rigid cutoff was shifted to enhance visibility. (b) QS density versus infection rate for a network degree exponent $\gamma = 4.0$ using different cutoffs.

distribution with a few outliers, which permits the formation of non-directly connected domains of activity centered on these outliers. If the number of hubs is large, as in the case of SF networks with $\gamma < 3$, every vertex of the network is "near" to some hub and the activation of hubs implies in the activation of the whole network, as previously reported in [13, 19]. Our finds are consistent with

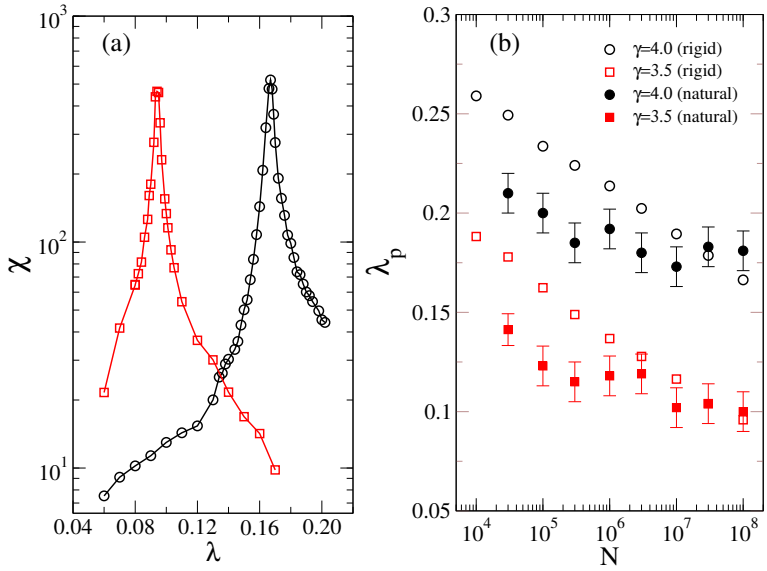

Figure 6.11: (a) Susceptibility curves for networks with rigid cutoff, $k_0 = 3$, $N = 10^8$ vertices and different degree exponents (symbols are the same used in panel (b)). (b) Threshold versus system size for rigid and natural cutoffs. The averages were done over at least 6 samples for rigid cutoff but error bars for rigid cutoff are smaller than symbols. Averages for natural cutoffs are the same as in Fig 6.5.

the conjecture proposed by Lee *et al*. [15] since the lifespans of independent domains involving outliers grow exponentially fast with the domain sizes implying that long-term epidemic activity is possible even in non-endemic phase. Our finds also do not rule out the QMF analysis of Goltsev *et. al* [11]. The intermediary transitions can be associated to distinct localized eigenvectors that are centered on the outliers while the endemic threshold involves a delocalized eigenvector with a finite eigenvalue.

Our results are in consonance with a recent line of investigation, in which the topological disorder in networks with heterogeneous degree distribution may produce rare regions and Griffiths phases (GP) leading to anomalous behaviors in the subcritical phase [14,15,126,127]. Such anomaly is characterized by localized activity that survives for long times, even though the network is macroscopically absorbing. Very recently, the possibility of rare regions effects from pure topological disorder in the SIS dynamics on unweighted SF networks as well as multiple transitions were suggested in Ref. [96]. Our results may, thus, be a fingerprint of GPs. However, more detailed analyses are demanded for a conclusive relation. Also, very recently, multiple phase transitions were found in percolation problems on SF networks with high clustering [128] and on networks of networks [129]. In both cases transitions were hallmarked by multiple singular points in the order parameter in analogy with our results for epidemics.

Our final overview is that apparently competing mean-field theories [11,13,15,16,44,95] can be

considered, in fact, complementary, describing distinct transitions that may concomitantly emerge depending on the network structure. In particular, the transitions involving localized phases, as possibly the one predicted by the BCPS theory [16], are not necessarily negligible since they become long-term and an epidemic outbreak may eventually visit a finite fraction of the network. This peculiar result is unthinkable for other substrates rather than complex networks sharing the small-world and scale-free properties. Actually, it is well known that some computer viruses can survive for long periods (years) in a very low density (below 10^{-4}) [8], exemplifying the importance of metastable non-endemic states.

Part III

Random Walks on Temporal Networks

Chapter 7

Random Walks on Activity Driven Temporal Networks

The random walk [84] is one of the simplest dynamical processes, although still underlying many realistic applications such as diffusion, searching, community detection and spreading dynamics. In the last years, empirical evidence pointing out the heterogeneous patterns of connections of many real systems has motivated a large amount of scientific work focusing on the properties of random walks in networks characterized by heavy-tailed degree distributions [12,130–134]. These studies provided a deeper understanding of diffusion processes on technological and social networks. However, such dynamic process can take a different, more complex turn when one considers the intrinsic time-varying, *temporal* nature of many real networks [56].

Even considering this simple process, the random walk, a time-varying substrate can induce very noticeable differences with respect to the behavior expected in static networks [24,29–32]. Particularly relevant in this sense is the analysis of the random walk behavior in *activity driven* networks [28], described in section 2.2.2.

In the Ref. [24], Perra *et al.* performed an analytical study of the random walk in this class of networks focusing on steady state, long time properties. These authors pointed out the striking differences imposed by a time-varying topology, with respect to a static one. In this chapter,we present a brief review of the main results presented in Ref. [24] since it is the starting point for our original study about slow dynamics and aging in random walks on temporal networks, that will be discussed in the chapter 8.

7.1 Defining the model

The random walk process on time-varying network was defined as follows [24,29,30]: at each time step, the instantaneous network with N disconnected nodes is generated and the walker diffuses for a time Δt. The walker in a vertex i can jump to a vertex j if they are connected in the time interval Δt. In the general case, the diffusion between i and j can occur either if the vertex i is active and fires a link to the vertex j or if the node i receives a link from the active vertex j. At the next time $t + \Delta t$, all the edges are deleted and the process starts over again (see figure 7.1).

Note that the concurrent dynamics of the random walker and the network takes place with the same time scale, which introduces a feature not observed in the equivalent process in static networks: the walkers can get trapped temporally in isolated nodes. This means that the diffusive dynamic of the walkers depends on the local connectivity of each node.

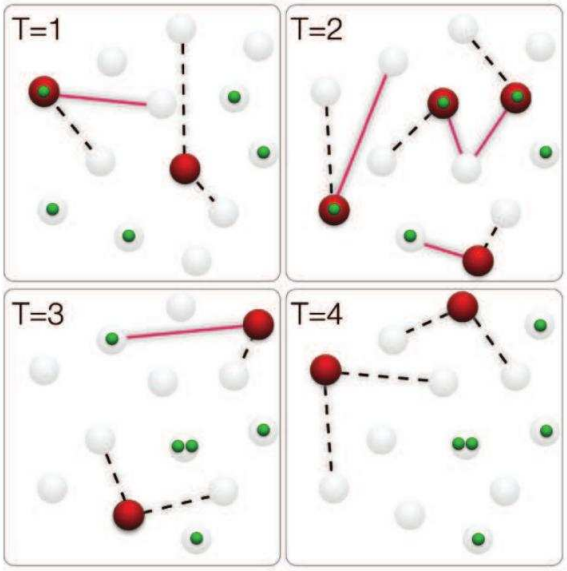

Figure 7.1: Random walk process on activity driven networks. Nodes active are shown in red and walkers in green. The edges connecting nodes are shown in dashed lines and solid red lines represent links used by walkers to jump from one vertex to another. Figure taken from Ref. [24].

7.2 Heterogeneous mean-field formalism

The probability $P(i, t)$ that a random walker is in node i at time t obeys the following equation:

$$\frac{dP(i,t)}{dt} = -a_i P(i,t) + a_i \frac{m}{N} - m\langle a\rangle P(i,t) + \frac{1}{N}\sum_j a_j P(j,t). \tag{7.1}$$

The first two terms of the right-hand side of the above equation are contributions due to the activity of a node i. When i is active, the walker can jump from it to any node with probability per unit time a_i and also, the node i can receive a walker originating from any other node with the same probability. Since the node i fires m links in each time step, it has m/N instantaneous neighbors. The final two terms represent the contribution when the node i is inactive but even so the walker can jump from (to) it due to the activity of the other nodes in the network. In this case, the probability to jump from it is proportional to the average connectivity of the network $m\langle a\rangle$, while the probability to jump to the vertex i originating from a node j is proportional to a_j/N.

We can define the probability $P(a,t)$ that the walker is in a given vertex of activity a as

$$P(a,t) = \frac{1}{NF(a)}\sum_{i\in a} P(i,t), \tag{7.2}$$

where $i \in a$ means all the vertices with activity a, according to the power law activity distribution $F(a) \sim a^{-\gamma}$. This quantity is normalized to

$$\sum_a NF(a)P(a,t) = 1. \tag{7.3}$$

So, from the Eq. (7.1), we can can obtain,

$$\frac{dP(a,t)}{dt} = -aP(a,t) + a\frac{m}{N} - m\langle a\rangle P(a,t) + \sum_{a'} a'F(a')P(a',t). \tag{7.4}$$

If there are W walkers in the network, the number of walkers in a given vertex of class a will be $W(a,t) = WP(a,t)$. So we can write

$$\frac{dW(a,t)}{dt} = -aW(a,t) + am\bar{W} - m\langle a\rangle W(a,t) + \sum_{a'} a'F(a')W(a',t), \tag{7.5}$$

where the average density of walkers per vertex is $\bar{W} = W/N$, and the proper normalization is give by

$$\sum_a F(a)W(a,t) = \frac{W}{N} = \bar{W}. \tag{7.6}$$

In the stationary state, $\lim_{t\to\infty} W(a,t) = W_\infty(a)$, the Eq. (7.5) turns into,

$$(a + m\langle a\rangle)W_\infty(a) = am\bar{W} + \sum_{a'} a'F(a')W_\infty(a'). \tag{7.7}$$

The quantity $\phi = \sum_{a'} a'F(a')W_\infty(a')$ is a constant in the steady state, so the quasistationary solution of Eq. (7.5) is

$$W_\infty(a) = \frac{am\bar{W} + \phi}{a + m\langle a\rangle}. \tag{7.8}$$

Considering the continuous a limit, the equation for ϕ becomes:

$$\phi = \int_\varepsilon^1 aF(a)\left[\frac{am\bar{W} + \phi}{a + m\langle a\rangle}\right] da. \tag{7.9}$$

That can be evaluated self-consistently. By considering power-law activity distributions, $F(a) \sim a^{-\gamma}$, the explicit solution for ϕ can be written in terms of hypergeometric functions and can be numerically computed.

7.3 Numerical Analysis

Besides the analytical treatment, Perra *et al.* [24] have also performed simulations of the random walk exploring an activity driven network with have-tailed distribution. They showed that the simulations results are in great agreement with analytical solution (see figure 7.2). In a static network, the probability of a walker to be in a vertex of degree k, in a stationary state, is a linear function of the degree $W_\infty(k) \sim k$. Nevertheless, in temporal networks, the probability of finding a walker in a node with activity a saturates at large values of a. Due to the properties of the instantaneous network, the nodes with high activity have a limited capacity of hosting walkers since they have on average just $k \sim m$ connections at each time step.

Other quantity of particular relevance in random walks on networks is the mean first passage time (MFPT), *i.e.*, the average time needed for a walker to arrive at node i starting from any other node in the network [135]. For instance, the MFPT is an important quantity to measure on searching processes on networks since it provides the number n of steps needed to find a specific target [132].

As done in Ref. [24], one can define $p(i,n)$ as the probability that the walker reaches the target node i for the first time at $t = n\Delta t$. Each node is able to connect directly to any other node a priori, then $p(i,n)$ is given by

$$p(i,n) = \xi_i(1-\xi_i)^{n-1}, \tag{7.10}$$

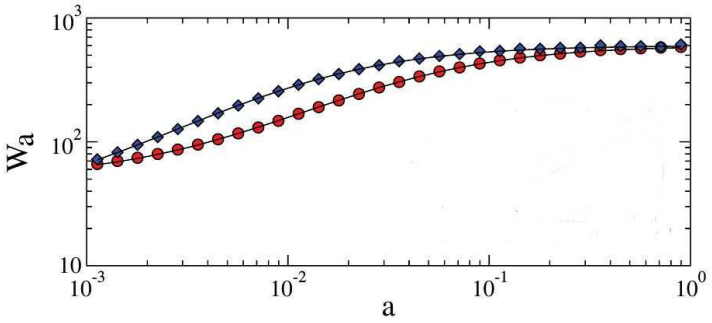

Figure 7.2: Stationary density $W_\infty(a)$ of a random walker in activity-driven network with activity distribution $F(a) \sim a^{-\gamma}$, for $\gamma = 2.0$ (circles) and $\gamma = 2.8$ (diamonds). Solid lines represent the analytical prediction of Eq. (7.8). For a network with $N = 10^5$ vertices, $W = 10^2$ walkers, $m = 6$ and $\varepsilon = 10^{-3}$. Figure taken from Ref. [24].

where ξ_i is the probability that the random walker jumps to the node i in a time interval Δt. From Eq. (7.1), we have that this probability is given by:

$$\xi_i = \frac{\Delta t}{N}\left[ma_i + \sum_j a_j W_\infty(j)\right]. \tag{7.11}$$

So, the MFPT can be estimated as

$$T_i^{MFPT} = \sum_{n=0}^{\infty} \Delta t n p(i,n) = \frac{\Delta t}{\xi_i} = \frac{N}{ma_i + \sum_j a_j W_\infty(j)}. \tag{7.12}$$

In contrast with static networks where ξ_i is equivalent to the stationary state of the random walker, in time-varying networks, the MFPT of a node i is inversely proportional to its activity plus a constant contribution from all the other nodes. The main cause of this difference is the fact that the walker can be trapped in a node with low activity for a long time. Monte Carlo simulations confirms these analytical results a shown in Fig. 7.3

In their work, Perra *et al.* [24] showed that the dynamics of time-varying networks significantly alters the standard picture achieved for the random walk process in static networks. Motivated by this appealing study, we will extended this analysis by considering the time evolution of the dynamics towards the steady state. Our original contribution about this topic will be presented in the next chapter.

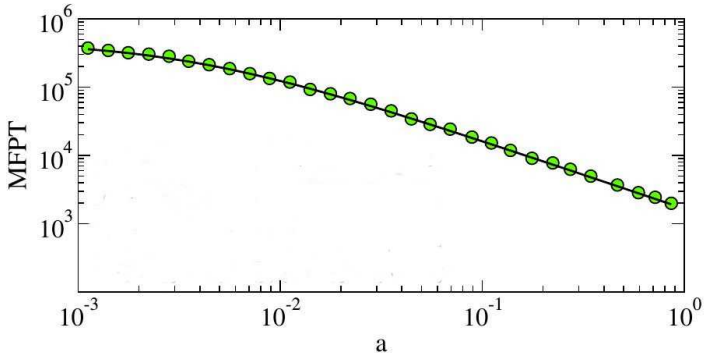

Figure 7.3: MFPT of a random walker as a function of the activity a in activity-driven network. Full line corresponds to the theoretical prediction of Eq.(7.12). For a network with $N = 10^4$ vertices, $m = 6$ and $\varepsilon = 10^{-3}$. Figure taken from Ref. [24].

Chapter 8

Slow Dynamics and Aging in Random Walks on Temporal Networks

As shown in the previous chapter, the random walks process in temporal networks reveal remarkable differences with time-varying topologies in comparison with static networks. Now, in this chapter, we extend this study, using a combination of analytic arguments and numerical simulations, to show that random walks on activity driven networks exhibit a slow relaxation to their steady state. The time scale of the relaxation is inversely proportional to a parameter ε, measuring the smallest activity in the network. In the limit $\varepsilon \to 0$, we found evidence of *aging* behavior[1] in the random walk relaxation [136], characterized by a breaking of time translation invariances for time scales smaller than ε^{-1}. By means of a mapping to Bouchaud's trap model [137,138] we show that, for $\gamma < 1$, random walks on activity driven networks exhibit simple aging, characterized by a unique relevant time scale. On the other hand, the case $\gamma > 1$ corresponds to a more complex picture, with several competing characteristic time scales.

In fact, aging behavior has been firstly observed in glassy systems. Special attention has been devoted to the dynamics of a glassy system inside its configurational space [139,140]. The idea is represent the dynamic of the system by a complex energy landscape with many local minima corresponding to metastable states that limits the ability of the system to equilibrate [141]. In this perspective, the energy landscape can be partitioned into basins of attraction of local minima (traps), and the dynamics of the system is separated into harmonic vibrations inside these traps and jumps between minima. Besides glassy systems, this approach has provided new insights about a broad range of issues such as protein folding [142], clusters [143], biomolecular isomerization processes [144], etc.

[1] Aging occurs when the dynamic relaxation of the system depends on its history.

The success of these studies has recently led to a large body of work focusing on the topology of the network in which the nodes are defined as minima and the possibility to jump between them is considered by links. This picture has stimulated the study of various models of dynamical evolution between traps on complex networks [145–150]. In particular, Baronchelli *et.al.* [148] studied the dynamics of a system in a complex energy landscape by means of a random walk in a heterogeneous, but static, network. Here, we go further considering a time-varying topology.

8.1 Random walks on activity driven networks

The dynamics of a random walk on activity driven networks is defined similarly as described in section 7.1: A walker arriving at a node i at time t remains on it until an edge is created joining i and other node j at a subsequent time $t' > t$. The walker then jumps instantaneously to node j and waits there until an edge departing from it is created. In order to simplify calculations, here we will focus on *activated random walks*: a walker can leave node i only when i becomes active and creates an edge pointing at another node [24]. Once the walker has arrived to node i, it must wait there until i creates a new connection. Since i creates new edges with constant probability a_i per unit time, the walker will remain trapped in i for a number of time steps n given by the exponential distribution, $\psi_i(n) = \frac{a_i}{N}\left(1 - \frac{a_1}{N}\right)^{n-1}$, independently of the time of the last activation of i. In the limit of large N we can take the continuous time limit and define a *waiting time* $\tau = n/N$, which is given by a local waiting time distribution

$$\psi_{a_i}(\tau) = a_i e^{-a_i \tau}. \tag{8.1}$$

That is, the dynamics of hopping from one node to another follows in time a Poisson process with a rate a_i that depends on node i.

The dynamics of activated random walks under this restriction is particularly easy to implement in continuous time: Considering that the walker arrives at vertex i with activity a_i at time t, it hops to a randomly selected node j and time is updated as $t \to t + \tau$, where τ is a random variable extracted from the distribution Eq. (8.1). This continuous time implementation has the additional benefit of not restricting the maximum possible value of the activity a, which can be now considered as a probability rate. With this definition, a directed random walk on an activity driven network can be directly mapped on a continuous time random walk on a fully connected network in which each node has a different distribution of waiting times $\psi_i(\tau)$ [84].

8.1.1 Steady state solution

The time evolution of the activated random walk on activity driven networks is given by

$$\frac{dP(i,t)}{dt} = -a_i P(i,t) + \frac{1}{N}\sum_j a_j P(j,t), \tag{8.2}$$

where a_j/N is the probability per unit time that the walker jumps from node j to node i, and a_i is the probability per unit time that the walker at i leaves this node. We can also obtain an effective equation for the probability $P(a,t)$ that the walker is in a node of activity a at time t by performing a coarse-graining of Eq. (8.2), in which we define

$$P(a,t) = \sum_{i\in\mathcal{V}(a)} P(i,t) \tag{8.3}$$

where $\mathcal{V}(a)$ is the set of nodes with activity a, with an average size $N_a = NF(a)$[2]. In performing this coarse-graining, vertices with the same activity are treated as equivalent, reasonably assuming that all dynamical properties of a node depend exclusively of its activity. Applying this definition on Eq. (8.2), and rearranging the summation over j, we obtain

$$\frac{dP(a,t)}{dt} = -aP(a,t) + F(a)\sum_{a'} a' P(a',t), \tag{8.4}$$

that can also be obtained by Eq. (7.4), if one considers just actived random walks. From Eq. (8.4) it is straightforward to obtain the steady state solution $\lim_{t\to\infty} P(a,t) \equiv P_\infty(a)$ by imposing $\frac{dP(a,t)}{dt} = 0$. The stationary solution is

$$P_\infty(a) = \frac{F(a)}{a}\sum_{a'} a' P_\infty(a') \equiv \frac{1}{\langle a^{-1}\rangle}\frac{F(a)}{a}, \tag{8.5}$$

where in the last term we have applied the normalization condition $\sum_a P_\infty(a) = 1$, thus recovering the result obtained in Ref. [24].

8.2 Slow relaxation dynamics

Eq. (8.5) yields information about the occupation probability of nodes with activity a at long times, and its accuracy has been checked numerically [24]. From it, however, it is hard to extract

[2]Note that the definition of Eq. (8.3) is different from the Eq. (7.2). The former represents the probability that the walker is in a given vertex of activity a while the latter represent a normalized probability.

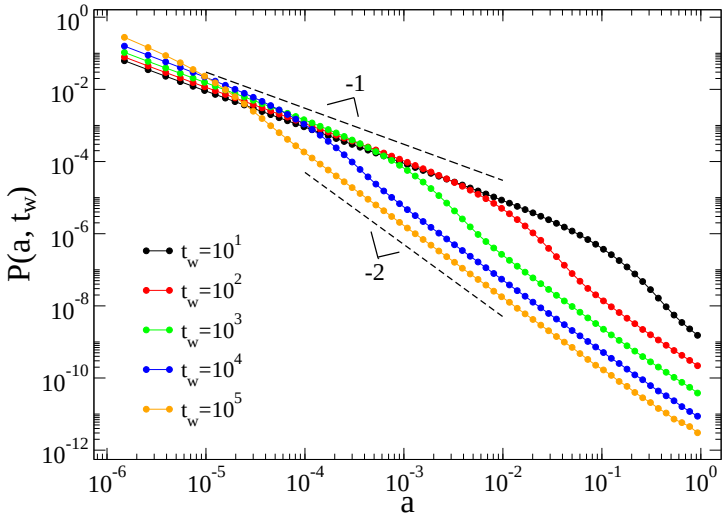

Figure 8.1: Evolution towards equilibrium of the occupation probability $P(a, t_w)$, measured after a time t_w, in activity driven networks with activity distribution $F(a) \sim a^{-\gamma}$, with $\gamma = 1$ and minimum activity $\varepsilon = 10^{-6}$. For small t_w, the occupation probability is proportional to the activity distribution, $P(a, t_w \to 0) \sim F(a) \sim a^{-1}$; for large t_w, it saturates to the steady state form $P(a, t_w \to \infty) = P_\infty(a) \sim F(a)/a \sim a^{-2}$. Network size $N = 5 \times 10^6$.

information about the time evolution of the process, and in particular, about the time scales of the relaxation to the steady state. We explore this issue by means of numerical simulations. Thus, in Fig. 8.1 we plot the occupation probability $P(a, t_w)$ of nodes of activity a, measured after letting the walker evolve for a time t_w. As Fig. 8.1 shows, the occupation probability exhibits a very slow relaxation from a state $P(a, t_w \to 0) \sim F(a)$ at short times to the equilibrium state, $P_\infty(a) \sim F(a)/a$, at long times [see Eq. (8.5)]. As a function of a, for fixed t_w, this relaxation exhibits a crossover between both scaling regimes at a crossover activity $a_c(t_w)$ which is a decreasing function of t_w.

We can understand the origin of this crossover by the following argument [148]: The average time τ_a to exit from a node with activity a is

$$\tau_a = \int_0^\infty \tau \psi_a(\tau) d\tau = \frac{1}{a}. \tag{8.6}$$

A walker initially at a node of activity a, is expected to remain there for any time smaller than τ_a. Since the smallest activity in the network is ε, for $t_w > \varepsilon^{-1}$ the walker has had the chance to explore (and scape from) all nodes in the network, and therefore we expect to find it in the steady state. For any arbitrary time $t_w < \varepsilon^{-1}$, one can thus consider that all nodes with activity a such that

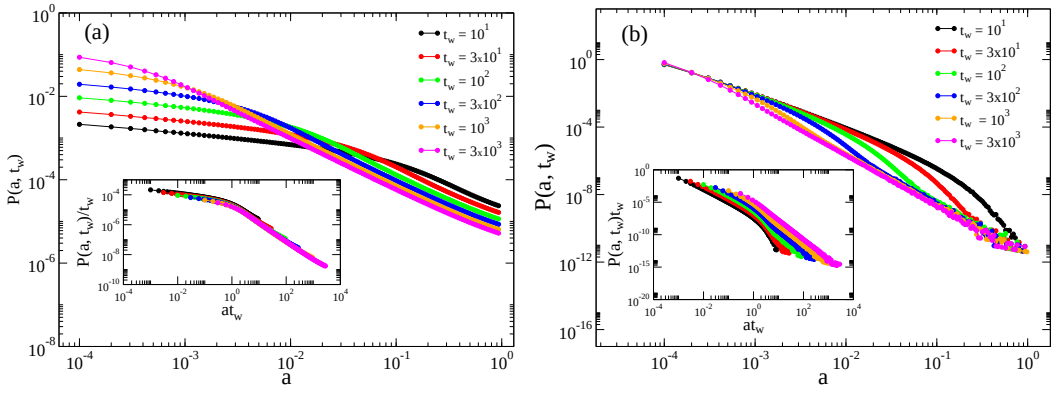

Figure 8.2: Occupation probability $P(a, t_w)$ as a function of the activity a at different times t_w. Data refer to activity-driven networks with $N = 5 \times 10^6$, $\varepsilon = 10^{-4}$, and (a) $\gamma = 0.25$, (b) $\gamma = 2.00$. Insets: Data collapse according to the scaling form Eq. (8.7).

$\tau_a < t_w$ (large a) will have had time to relax and reach the steady state, while nodes with activity fulfilling $\tau_a > t_w$ (small a) will not have relaxed. We thus see that the crossover activity fulfills $\tau_{a_c} \sim t_w$ or, from Eq. (8.6), $a_c(t_w) \sim t_w^{-1}$. The previous argument suggests therefore the following scaling form for the whole occupation probability:

$$P(a, t_w) = t_w \, \mathcal{P}(a \, t_w), \tag{8.7}$$

where $\mathcal{P}(z)$ is a scaling function satisfying

$$\mathcal{P}(z) \sim \begin{cases} z^{-\gamma} & \text{for } z \ll 1 \\ z^{-\gamma-1} & \text{for } z \gg 1 \end{cases} \tag{8.8}$$

This scaling regime is expected to hold for times $t_w < \varepsilon^{-1}$, i.e. before the full relaxation to the steady state.

In Fig. 8.2 we check the scaling form in Eq. (8.7) for activated random walks in activity driven networks with power-law activity distribution. For values of $\gamma < 1$, Fig. 8.2(a), we observe that the scaling form of the occupation probability is perfectly fulfilled for all times $t_w < \varepsilon^{-1}$. Surprisingly, however, the scaling form fares quite badly for $\gamma > 1$, performing increasingly worst for larger values of γ.

8.3 Mapping to Bouchaud's trap model and aging behavior

The radical difference in the behavior of the random walk for γ larger and smaller than 1 can be understood in terms of a mapping to the well-known Bouchaud's trap model [137,138] for glassy behavior (see also [148,151]). The trap model is defined in terms of a phase space consisting of N *traps*, each one with a depth E_i, $i = 1, \ldots, N$, extracted randomly from the probability distribution $\rho(E)$. The dynamics of the model proceeds by a succession of jumps between the traps, ruled by the temperature of the system, T. At this temperature, the system remains in a trap of depth E a random time τ distributed according to a Poisson process with rate $\tau_E^{-1} = \exp(-E/T)/\tau_0$, where τ_0 is a microscopic time scale that can be arbitrarily set equal to 1. After this time, the system jumps to a randomly chosen trap. Since all traps are equivalent, the probability that the system lands on a trap of depth E after a jump is $\rho(E)$. The average time spent in any trap is thus

$$\langle \tau \rangle = \int \rho(E) \tau_E \, dE. \tag{8.9}$$

The trap model exhibits a phase transition between a high temperature phase, where τ is finite, to a low temperature, glassy state characterized by very slow relaxation dynamics and aging behavior [136], when $\langle \tau \rangle$ diverges. This transition takes place at a finite temperature T_0 for a depth probability distribution of the form $\rho(E) = \exp(-E/T_0)$ [137,138], in this case the distribution of trapping times takes the form

$$P(\tau) \sim \tau^{-1-T/T_0} \tag{8.10}$$

For $T < T_0$, the exponent in the power-law in Eq. (8.10) is smaller than 2 and thus leads to an infinite average trapping time.

Activated random walkers can be exactly mapped to the trap model by equalizing the respective jumping rates, that is

$$a = \tau_E^{-1} = \exp(-E/T), \tag{8.11}$$

from where we obtain the equivalence between depth and activity

$$E = -T \ln(a), \tag{8.12}$$

with a range of variation $E \in [0, T \ln(\varepsilon^{-1})]$. The relation between the activity distribution and the depth distribution is given by $\rho(E)\, dE = F(a)\, da$, leading to

$$\rho(E) = \frac{e^{-E/T}}{T} F\left(e^{-E/T}\right). \tag{8.13}$$

Assuming now an activity with a power-law distribution as

$$F(a) = \frac{1-\gamma}{1-\varepsilon^{1-\gamma}}\, a^{-\gamma}, \tag{8.14}$$

we obtain,

$$\rho(E) \sim \frac{1}{T} \exp\left[-(1-\gamma)E/T\right]. \tag{8.15}$$

Let us consider separately the different possible values of γ.

8.3.1 Case $\gamma < 1$

From Eq. (8.15), the mapping to the trap model makes perfect sense for $\gamma < 1$. In this case, $\rho(E)$ is a decreasing function of the depth E, corresponding to the presence of many shallow traps and a few deep ones. Deep traps represent rare long trapping events that eventually dominate the dynamics below the glass transition and induce a very slow relaxation and aging behavior [137, 138]. In this case, however, temperature plays no role in the equivalent dynamics of the activated random walkers, as it can be absorbed in a change of variables $\bar{E} = E/T$, with a range of variation $\bar{E} \in [0, \ln(\varepsilon^{-1})]$. From the point of view of the mapping to the trap model, the activated random walker is a system in a fully glass state, corresponding to a infinite glass transition temperature. This can easily be seen by looking at the average trapping time distribution, i.e.

$$\psi(\tau) = \sum_a F(a) a e^{-a\tau} \simeq \frac{1-\gamma}{1-\varepsilon^{1-\gamma}} \int_\varepsilon^\infty a^{1-\gamma} e^{-a\tau} da \simeq \tau^{-2+\gamma} e^{-\varepsilon\tau}, \tag{8.16}$$

where we have made an expansion for $\tau < \varepsilon^{-1}$. The exponent in Eq. (8.16) is always smaller than 2, indicative of an infinite glass transition temperature [138]. The average trapping time is thus modulated by the exponential factor, diverging when $\varepsilon \to 0$, i.e. when the upper cut-off of the associated energy tends to infinity.

This analogy allows to explore in the random walk problem other features of the glassy dynamics of the trap model, in particular aging effects [136]. Aging effects are here usually measured by looking at the two-time correlation function $C(t; t_w)$, between the states of the system at times t_w and $t + t_w$. It is defined as the average probability that the system in a given trap at time t_w has not performed a jump at time $t + t_w$. This correlation function for trap model obeys the scaling relation

$$C(t; t_w) = \mathcal{C}\left(\frac{t}{t_w}\right), \tag{8.17}$$

corresponding to the so-called "simple" aging [137,138]. This scaling can be simply deduced for

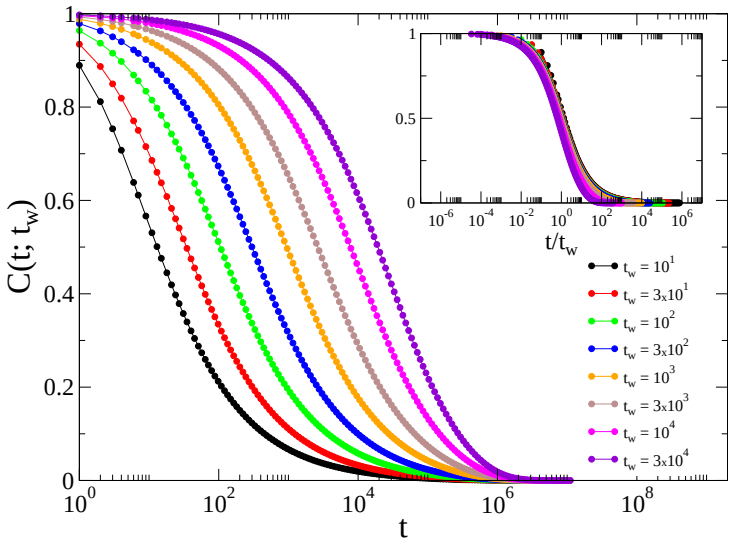

Figure 8.3: Two-time correlation function for random walks on activity driven networks with a power-law activity distribution. Data refers to $N = 5 \times 10^6$, $\gamma = 0.50$ and $\varepsilon = 10^{-6}$. Inset: Scaling plot corresponding to the form in Eq. (8.17).

the random walk on activity driven networks. Since the jumping dynamics is Poissonian in every node, the probability of not leaving a node with activity a in a time interval t is e^{-at}. We thus can write

$$C(t;t_w) = \int_\varepsilon^1 P(a,t_w)e^{-at}da = \int_\varepsilon^1 t_w \mathcal{P}(at_w)e^{-at}da = \int_{t_w\varepsilon}^{t_w} \mathcal{P}(z)e^{-zt/t_w}dz, \tag{8.18}$$

where we have used the scaling relation Eq. (8.7) for $P(a,t_w)$ and performed a change of variable. For large z, the upper limit of the integral can be safely set equal to infinity, due to the exponential cut-off. In the limit of small z, we have $\mathcal{P}(z) \sim z^{-\gamma}$, and its integral also converges for $t_w\varepsilon$ small. Thus, in the double limit $1 \ll t_w \ll \varepsilon^{-1}$, we have

$$C(t;t_w) \simeq \int_0^\infty \mathcal{P}(z)e^{-zt/t_w}\, dz, \tag{8.19}$$

recovering the scaling relation for the correlation Eq. (8.17), which is expected to hold for waiting times $t_w \ll \varepsilon^{-1}$. In Fig. 8.3 we show that, for $\gamma < 1$, the scaling of the correlations is very well fulfilled in the random walk process.

Additional information on the aging properties of the system can be gathered by looking at the average escape time $t_{\rm esc}(t_w)$ that a walker at a given node at time t_w requires to escape from it [148]. In Fig. 8.4(inset) we plot the curves of the escape time as a function of t_w, for different values of

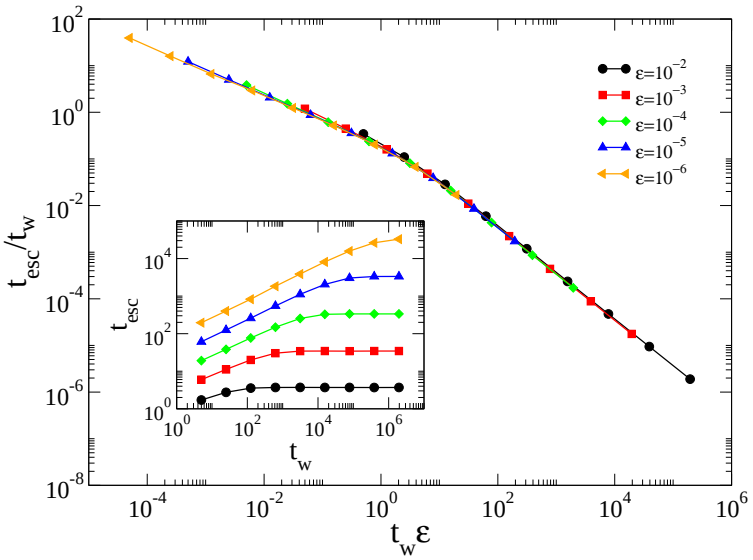

Figure 8.4: Scaling plot of the average scape time according to Eq. (8.21) for $\gamma = 0.50$. Inset: raw data. Data corresponds to a network size $N = 10^5$.

ε. As we can see, the escape time is a increasing function of t_w for small values of t_w, indicating another of the typical features of aging systems, namely, a breaking of scale invariance translation. Due to its Poissonian nature, the average time to leave a node with activity a is $\tau_a = 1/a$. Therefore, we can write $t_{\rm esc}(t_w) = \int da\ P(a, t_w)/a$. Applying the scaling relation Eq. (8.7) and performing a change of variables, we have

$$t_{\rm esc}(t_w) = t_w \int_{\varepsilon t_w}^{t_w} \frac{\mathcal{P}(z)}{z}\, dz. \tag{8.20}$$

For large t_w, the upper limit of the integral is not singular, and we can set it to infinity. We are therefore led to the scaling form

$$t_{\rm esc}(t_w) \simeq t_w \mathcal{F}(t_w\ \varepsilon), \tag{8.21}$$

which is valid for $t_w \ll \varepsilon^{-1}$.

We check this theoretical predictions by means of a data collapse analysis, plotting $t_{\rm esc}(t_w)/t_w$ as a function of $t_w\varepsilon$. In Fig. 8.4(main) we plot the result, showing an excellent agreement with the prediction.

8.3.2 Case $\gamma > 1$

For the case $\gamma > 1$, Eq. (8.15) indicates that the mapping to the trap model is not physical. For this range of γ values, the density of traps *increases* with depth, meaning that very deep traps are

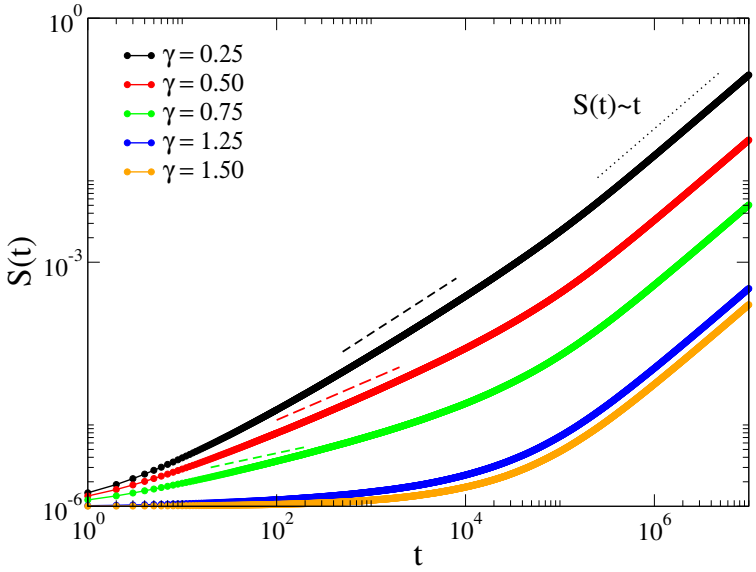

Figure 8.5: Coverage as a function of time. For $\gamma < 1$, dashed lines represent the predicted behavior $\sim t^{1-\gamma}$ from Eq. (8.25). We use $N = 10^6$ and $\varepsilon = 10^{-5}$.

much more probable than shallow ones. Long time trapping is thus not a rare event, but the norm of the system. This implies a qualitatively different, much slower dynamics than that for $\gamma < 1$. This effect can be simply seen by looking at the coverage $S(t)$ of the random walk as a function of time, defined as the average fraction of different nodes that a walker has visited up to time t, see Fig. 8.5. For very large $t > \varepsilon^{-1}$, the system has reached the steady state, and the walker jumps from any node at an average increment time $\Delta t = \langle \tau \rangle$, with the average trapping time $\langle \tau \rangle$ defined as

$$\langle \tau \rangle = \int_{\varepsilon}^{1} F(a)\tau_a \, da = \langle a^{-1} \rangle = \frac{1-\gamma}{\gamma} \frac{\varepsilon^{-\gamma} - 1}{1 - \varepsilon^{1-\gamma}}, \tag{8.22}$$

where we have used Eqs. (8.22) and (8.14). In this limit of large t, and since the walker jumps to randomly chosen new nodes, we expect

$$S(t) \sim \frac{t}{\langle a^{-1} \rangle}, \quad t \gg \varepsilon^{-1}. \tag{8.23}$$

For $\gamma < 1$ and short times, we observe a power law increase of the coverage, $S(t) \sim t^{\alpha}$. In the case $\gamma > 1$, on the other hand, the initial growth is extremely slow, numerically slower than logarithmic, in the region $t < \varepsilon^{-1}$, where the dynamics is dominated by an exceedingly large number of deep traps. After this very slow regime, the linear, steady state behavior is recovered. We can explain the exponent of the initial growth of $S(t)$ for $\gamma < 1$ by the following argument: At any time $t \ll \varepsilon^{-1}$, the random walker will have explored in average nodes with activity restricted to $a > t^{-1}$, since it will not have had time to escape deeper traps. In this case, the average inverse activity of those

explored nodes will depend on time as

$$\langle a^{-1}\rangle_t \sim \int_{t^{-1}}^{1} \frac{F(a)}{a}\, da \sim t^{\gamma}. \tag{8.24}$$

We therefore estimate a coverage

$$S(t) \sim \frac{t}{\langle a^{-1}\rangle_t} \sim t^{1-\gamma}, \tag{8.25}$$

with an exponent $\alpha = 1 - \gamma$ which is a decreasing function of γ, in agreement with the results in Fig. 8.5.

The anomalous density of deep traps for $\gamma > 1$ has a strong effect in the scaling of the occupation probability. In Fig. 8.2(b) we have plotted the function $P(a, t_w)$ for $\gamma = 2.0$. From the rescaled plot, it is evident that a simple scaling behavior such as the one represented in Eq. (8.7) is doomed to fail. In particular, as we can observe, the occupation probability for small values of a is apparently independent of t_w. This fact is in stark contrast with the behavior for $\gamma < 1$, Fig. 8.2(a), in which the value of $P(a, t_w)$ for small a increases for increasing t_w, as expected from Eq. (8.7). This phenomenology is again due to the anomalous abundance of deep traps in the region $\gamma > 1$: thus, while at t_w the walker has had the opportunity to explore and escape from nodes with activity $a > t_w^{-1}$, the fraction of such nodes is very small for large values of γ. Indeed, denoting by $\phi(t_w)$ the fraction of such nodes, we have

$$\phi(t_w) = \int_{t_w^{-1}}^{1} F(a)da = \frac{1 - t_w^{\gamma-1}}{1 - \varepsilon^{1-\gamma}}. \tag{8.26}$$

Denoting by $\phi^{>}(t_w)$ (resp. $\phi^{<}(t_w)$) the fraction corresponding to $\gamma > 1$ (resp. $\gamma < 1$), we have, in the limit of small ε,

$$\phi^{>}(t_w) \sim (t_w\varepsilon)^{\gamma-1}, \quad \phi^{<}(t_w) \sim 1 - t_w^{\gamma-1}. \tag{8.27}$$

I.e. the fraction of visited nodes up to time t_w grows much faster for $\gamma < 1$ than in the opposite case.

While the scaling relation Eq. (8.7) is invalid for $\gamma > 1$, we can still understand the functional form of the occupation probability by means of the following argument: Let us consider a walker at time t_w. Initially, the walker starts at a randomly chosen node with activity a_0. With probability $e^{a_0 t_w}$, the walker does not move from its initial position, and therefore it contributes to the initial activity a_0. With the complementary probability $1 - e^{a_0 t_w}$, the walker has performed one or more jumps. Assuming that after its first jump it already reaches the steady state $F(a)/[a\langle a^{-a}\rangle]$, we have

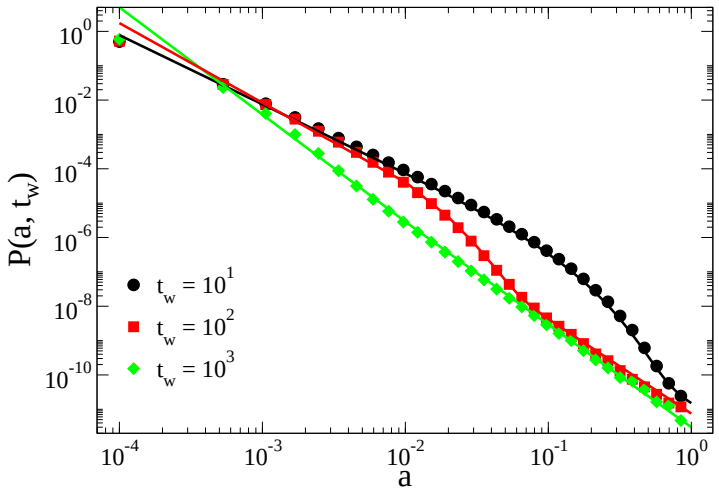

Figure 8.6: Evolution of the occupation probability $P(a,t)$. Data refer to activity-driven network with $N = 5\times10^6$, $\varepsilon = 10^{-4}$, $\gamma = 2.00$, and different waiting times t_w. Solid lines are the theoretical prediction in Eq. (8.28).

the average occupation probability

$$P(a,t_w) = F(a)e^{-at_w} + \frac{F(a)}{a\langle a^{-1}\rangle}\left[1 - \int_\varepsilon^1 e^{-a_0 t_w} F(a_0)\right].$$

For the activity distribution given by Eq. (8.14), we have

$$P(a,t_w) \;=\; F(a)e^{-at_w} + \frac{F(a)}{a\langle a^{-1}\rangle}\left[1 - \frac{1-\gamma}{1-\varepsilon^{1-\gamma}} t^{-1+\gamma}\Gamma(1-\gamma, t_w\varepsilon)\right], \qquad (8.28)$$

where in the integral we have extended the upper limit up to infinity, and $\Gamma(a,z)$ is the incomplete Gamma function [152]. In Fig. 8.6 we plot the numerical data for $\gamma = 2$, compared with the theoretical prediction in Eq. (8.28). As we can see, except for very small values of the activity a, the fit of the theoretical prediction with the numerical results is excellent. The mixing of time scales in Eq. (8.28), namely a^{-1} and ε^{-1}, allows to understand the failure of the simple scaling ansatz performed to derive Eq. (8.7).

Finally, let us consider the average escape time $t_{esc}(t_w)$ for $\gamma > 1$. The lack of simple scaling evidenced in Eq. (8.28) indicates that the simple collapse predicted in Eq. (8.21) cannot be correct, see Fig. 8.7(inset). We can recover however some form of scaling law for this quantity. Considering a fixed value of ε, the plateau at large t_w is given by the escape time at the stationary state, t^{ss}_{esc}, which is independent of t_w and, from Eq. (8.5), given by $t^{ss}_{esc} = \int P_\infty(a)/a\; da = \langle a^{-2}\rangle/\langle a^{-1}\rangle \sim$

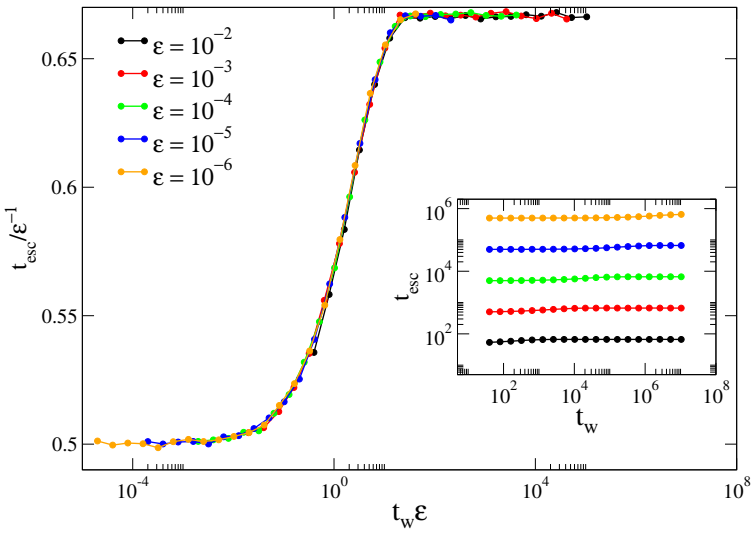

Figure 8.7: Scaling plot of the average scape time according to Eq. (8.29) for $\gamma = 2.00$. Inset: raw data. Data corresponds to a network size $N = 10^5$.

ε^{-1}, for all γ. On the other hand, for small t_w, t_{esc} is dominated by the deepest traps, and it starts only to increase when the walker has had time to explore a finite fraction of the network, that is, when time is larger than the average trapping time $\langle\tau\rangle$, which, from Eq. (8.22) is proportional to ε^{-1} for $\gamma > 1$. This reasoning suggest a scaling behavior for the escape time of the form

$$t_{esc}(t_w) = \varepsilon^{-1}\mathcal{G}(t_w\varepsilon). \tag{8.29}$$

This scaling form in checked in Fig. 8.7(main), where we can see that it is quite well satisfied. Incidentally, this scaling form can also be cast in the form valid for $\gamma < 1$, Eq. (8.21), by simply defining $\mathcal{F}(z) \equiv \mathcal{G}(z)/z$.

8.4 Summary and Discussion

In this work, we have investigated the temporal relaxation of the simplest dynamical process, namely the random walk, on the class of activity driven temporal networks. We have focused in particular in the case of activated random walks, in which a walker can only leave a node when the latter becomes active. By means of a combination of analytic calculations and numerical experiments, we have shown that, for networks with a power law distribution of activity, the random walk experiences a very slow relaxation towards its steady state. The speed of this relaxation is mainly controlled by the parameter ε, bounding the smallest activity of any node. In the limit of small

$\varepsilon \to 0$, the dynamics exhibits aging behavior, characterized additionally by a breaking of time translation symmetry. The aging properties of the random walk are studied by examining different quantities usually applied to characterize aging in glassy systems. Crucially, the aging properties of the random walk depend on the exponent γ in the activity distribution. For $\gamma < 1$, the random walk exhibits a relaxation compatible with "simple" aging, with a unique characteristic time scale given by the average escape time from the least active node, ε^{-1}. In this regime, simple scaling forms for the two-time correlation function and the average escape time can be worked out, starting from a scaling ansatz for the occupation probability $P(a, t_w)$. For $\gamma > 1$, on the other hand, the picture is more complex, with a scaling ruled by several characteristic time scales. This different behavior according to γ can be understood by means of a mapping to Bouchaud's trap model: The case $\gamma > 1$ corresponds in this case to an unphysical representation of the trap model, in which there is a majority of deep traps that induce an extraordinary slow relaxation dynamics.

The results obtained here indicate that, apart from the slowing down already reported in dynamical systems on temporal networks, more complex effects, such as aging, can also be observed. In the present case, in which the temporal network substrate is the activity driven model, aging emerges as the result of the mixing of Poisson activation processes with widely different time scales. We remark that this mixing, which we have made evident in a power-law activity distribution (the empirically observed one), can arise for any functional form $F(a)$ leading to a diverging average trapping time, as given by $\langle \tau \rangle = \int F(a)/a$. Obviously, a more complex phenomenology is to be expected in real temporal networks with non Poissonian, bursty activation rates.

Another interesting point is considering the same model not in a network, but in a one dimensional lattice. Here we suspect that the correlations induced by the multiple visits of the walks to a given site lead to qualitative changes. Because of the limited number of accessible sites, one might expect interesting properties such as dynamical localization, which means that one could have a mixing of slowing down effects, and in particular, to observe rare region effects, which would be due to clusters of adjacent sites all of them with small values of a. Indeed the one-dimensional trap model has been the focus of renewed attention recently due to its many applications ranging from the properties of one-dimensional disordered conductors to understand the dynamics of DNA "denaturation bubbles" under torsion [153–157].

Part IV

Concluding Remarks

Chapter 9

Conclusions and Perspectives

In this thesis we investigated dynamical processes on networks. Our results showed that the topological features and the intrinsic time-varying of the networked substrates have strong influence on the dynamics running on top of it.

Firstly, we reviewed some useful concepts of complex network theory and important network models, concentrating specially on the UCM and activity driven models. The first one has been used as a substrate for epidemics dynamics (II) and the latter has been used to investigate slow dynamics on temporal networks (III).

We reviewed the SIS and CP models, that represent good prototypes of non-equilibrium dynamical systems with absorbing-state phase transitions. They are the most studied models to describe reaction-diffusion processes and epidemic dynamics. These processes have been widely studied by means of the quenched and heterogeneous mean-field theories. While the former explicitly takes into account the actual connectivity of the network through its adjacency matrix, the latter takes into account the heterogeneity of the degree distribution of networks. We presented an enhancement of both approaches by means of a pair approximation. Our analytical results were compared with numerical findings showing great improvements in relation to the standard QMF and HMF theories.

For the CP model, the main interest is to relate the critical exponents associated to the absorbing state phase transition with statistical properties of the network, in our case, the power law degree distribution $P(k) \sim k^{-\gamma}$. Within this framework, we showed that for the infinite size limit, the critical exponents found in the pair HMF theory are the same as the one-vertex approach. However, the finite-size corrections to the scaling obtained in the pair HMF approximation allowed a remarkable agreement with QS simulations for all degree exponents γ investigated, suppressing a deviation observed for low degree exponents in the one-vertex HMF theory. Besides, the thresholds

obtained in the pair QMF and HMF theories are more accurate than the one-vertex approximations, which predict a transition point independent of the degree distribution and degree correlations.

For the SIS model, the main attention is devoted to determine an epidemic threshold separating an absorbing state from an active phase on heterogeneous networks with a power law degree distribution. In this context, we firstly investigated the epidemic spreading of the SIS model performing both heterogeneous and quenched mean-field pair approximations. We found that the pair QMF thresholds are quantitatively much closer to the simulations results than those of standard QMF. The thresholds obtained in a pair HMF theory coincides with the transition point of the SIR model in a one-vertex approximation.

For $\gamma < 3$ exists a consensus for the SIS thresholds and HMF and QMF are equivalent and state that the threshold vanishes. However, for $\gamma > 3$, the HMF approach predicts a finite threshold while QMF does not. This topic was widely investigated and discussed in the last few years. To shed light on this issue, we performed extensive simulations and found that the SIS dynamics can exhibit, concomitantly, multiples transitions in individual networks presenting large gaps in the degree distribution and the obtained multiple epidemic thresholds are well described by different mean-field theories. Our numeric results indicate that the transitions involving vanishing thresholds which a size increases involve localized states, in which a vanishing fraction of the network effectively contribute to epidemic activity, whereas an endemic state, with a finite density of infected vertices, occurs at a finite threshold. The multiple transitions are related to the activations of distinct sub-domains of the network, which are not directly connected.

We also focused on the impact of the temporal nature of networks on dynamical processes. The random walk is the one of the simplest diffusion processes but even in this case, an intrinsic time-varying property of the substrate can induce very noticeable differences with respect to the behavior expected in static networks. We investigated the random walk dynamic on activity driven temporal network by means analytical arguments and numerical simulations. We showed that random walks exhibit a slow relaxation to their steady state, compatible with aging effects. The mapping to Bouchaud's trap model showed that, depending on the exponent γ of the activity distribution $F(a) \sim a^{-\gamma}$, the random walk can exhibit a simple aging, for $\gamma < 1$, or a more complex slow relaxation, for $\gamma > 1$.

All these findings prompt for further studies. The theoretical approaches pair HMF and pair QMF can be extended to other dynamical processes taking place on networks. More detailed studies should be made to analyze the SIS dynamics on heterogeneous networks. A meticulous investigation are required for a conclusive relation between the anomalous behavior of the SIS epidemic model in the subcritical phase and the emergence of Griffiths phase due to heterogeneity of the network. Moreover, the random walk can be useful to explore different substrates, as a one

dimensional lattice, to investigate slowing down effects. Finally, several researches are open to explore the influence of the time-varying of the proper network on other dynamical processes.

Bibliography

[1] Alain Barrat, Marc Barthélemy, and Alessandro Vespignani. *Dynamical Processes on Complex Networks*. Cambridge University Press, Cambridge, 2008.

[2] G. Caldarelli. *Scale-Free Networks: Complex Webs in Nature and Technology*. Oxford University Press, Oxford, 2007.

[3] Mark Newman. *Networks: An Introduction*. Oxford University Press, Inc., New York, NY, USA, 2010.

[4] Guido Caldarelli and Alessandro Vespignani (Editors). *Large Scale Structure and Dynamics of Complex Networks: from information technology to finance and natural science*. World Scientific Publishing, Oxford, 2007.

[5] O. Diekmann and J.A.P Heesterbeek. *Mathematical epidemiology of infectious diseases: model building, analysis and interpretation*. John Wiley & Sons, New York, 2000.

[6] R. M. Anderson and R. M. May. *Infectious diseases in humans*. Oxford University Press, Oxford, 1992.

[7] M. Jackson. *Social and Economic Networks*. Princeton University Press, Princeton, 2010.

[8] R. Pastor-Satorras and A. Vespignani. *Evolution and structure of the Internet: A statistical physics approach*. Cambridge University Press, Cambridge, 2004.

[9] A. L. Barabàsi and R. Albert. Emergence of scaling in random networks. *Science*, 286:509–512, 1999.

[10] D. J. Watts and S. H. Strogatz. Collective dynamics of 'small-world' networks. *Nature*, 393:440–442, 1998.

[11] A. V. Goltsev, S. N. Dorogovtsev, J. G. Oliveira, and J. F. F. Mendes. Localization and spreading of diseases in complex networks. *Phys. Rev. Lett.*, 109:128702, 2012.

[12] Balázs Kozma, Matthew B. Hastings, and G. Korniss. Diffusion processes on power-law small-world networks. *Phys. Rev. Lett.*, 95:018701, 2005.

[13] Claudio Castellano and Romualdo Pastor-Satorras. Thresholds for epidemic spreading in networks. *Phys. Rev. Lett.*, 105:218701, 2010.

[14] Géza Ódor. Spectral analysis and slow spreading dynamics on complex networks. *Phys. Rev. E*, 88(3):032109, 2013.

[15] Hyun Keun Lee, Pyoung-Seop Shim, and Jae Dong Noh. Epidemic threshold of the susceptible-infected-susceptible model on complex networks. *Phys. Rev. E*, 87:062812, 2013.

[16] Marian Boguñá, Claudio Castellano, and Romualdo Pastor-Satorras. Nature of the epidemic threshold for the susceptible-infected-susceptible dynamics in networks. *Phys. Rev. Lett.*, 111:068701, 2013.

[17] E. Pugliese and C. Castellano. Heterogeneous pair approximation for voter models on networks. *Europhys. Lett.*, 88(5):58004, 2009.

[18] S. Gómez, A. Arenas, J. Borge-Holthoefer, S. Meloni, and Y. Moreno. Discrete-time markov chain approach to contact-based disease spreading in complex networks. *Eur. Lett.*, 89:38009, 2010.

[19] Sergio Gómez, Jesús Gómez-Gardeñes, Yamir Moreno, and Alex Arenas. Nonperturbative heterogeneous mean-field approach to epidemic spreading in complex networks. *Phys. Rev. E*, 84:036105, 2011.

[20] Róbert Juhász, Géza Ódor, Claudio Castellano, and Miguel A. Muñoz. Rare-region effects in the contact process on networks. *Phys. Rev. E*, 85:066125, 2012.

[21] Claudio Castellano and Romualdo Pastor-Satorras. Routes to thermodynamic limit on scale-free networks. *Phys. Rev. Lett.*, 100:148701, 2008.

[22] Hyunsuk Hong, Meesoon Ha, and Hyunggyu Park. Finite-size scaling in complex networks. *Phys. Rev. Lett.*, 98:258701, 2007.

[23] A. Vespignani. Modelling dynamical processes in complex socio-technical systems. *Nat Phys*, 8:32, 2012.

[24] Nicola Perra, Andrea Baronchelli, Delia Mocanu, Bruno Gonçalves, Romualdo Pastor-Satorras, and Alessandro Vespignani. Random walks and search in time-varying networks. *Phys. Rev. Lett.*, 109(23):238701, 2012.

[25] Réka Albert and Albert-László Barabási. Statistical mechanics of complex networks. *Rev. Mod. Phys.*, 74:47–97, 2002.

[26] S. N. Dorogovtsev, A. V. Goltsev, and J. F. F. Mendes. Critical phenomena in complex networks. *Rev. Mod. Phys.*, 80:1275–1335, 2008.

[27] M. Catanzaro, M. Boguñá, and R. Pastor-Satorras. Generation of uncorrelated random scale-free networks. *Phys. Rev. E*, 71:027103, 2005.

[28] N. Perra, B. Gonçalves, R. Pastor-Satorras, and A. Vespignani. Activity driven modeling of time varying networks. *Scientific Reports*, 2:srep00469, 2012.

[29] Till Hoffmann, Mason A. Porter, and Renaud Lambiotte. Generalized master equations for non-poisson dynamics on networks. *Phys. Rev. E*, 86(4):046102, 2012.

[30] Bruno Ribeiro, Nicola Perra, and Andrea Baronchelli. Quantifying the effect of temporal resolution on time-varying networks. *Scientific Reports*, 3:3006, 2013.

[31] Michele Starnini, Andrea Baronchelli, Alain Barrat, and Romualdo Pastor-Satorras. Random walks on temporal networks. *Phys. Rev. E*, 85:056115, 2012.

[32] Leo Speidel, Renaud Lambiotte, Kazuyuki Aihara, and Naoki Masuda. Steady state and mean recurrence time for random walks on stochastic temporal networks. *Phys. Rev. E*, 91:012806, 2015.

[33] Malte Henkel, Haye Hinrichsen, Sven Lübeck, and Michel Pleimling. *Non-equilibrium phase transitions*, volume 1. Springer, Dordrecht, Netherlands, 2008.

[34] J. Marro and R. Dickman. *Nonequilibrium phase transitions in lattice models*. Cambridge University Press, Cambridge, 1999.

[35] T. E. Harris. Contact interactions on a lattice. *Ann. Prob.*, 2:969–988, 1974.

[36] Silvio C. Ferreira, Claudio Castellano, and Romualdo Pastor-Satorras. Epidemic thresholds of the susceptible-infected-susceptible model on networks: A comparison of numerical and theoretical results. *Phys. Rev. E*, 86:041125, 2012.

[37] James P. Gleeson. High-accuracy approximation of binary-state dynamics on networks. *Phys. Rev. Lett.*, 107:068701, 2011.

[38] E. Cator and P. Van Mieghem. Second-order mean-field susceptible-infected-susceptible epidemic threshold. *Phys. Rev. E*, 85:056111, 2012.

[39] Angélica S. Mata and Silvio C. Ferreira. Pair quenched mean-field theory for the susceptible-infected-susceptible model on complex networks. *Eur. Lett.*, 103(4):48003, 2013.

[40] M. Boguñá, C. Castellano, and R. Pastor-Satorras. Langevin approach for the dynamics of the contact process on annealed scale-free networks. *Phys. Rev. E*, 79:036110, 2009.

[41] Silvio C. Ferreira, Ronan S. Ferreira, and R. Pastor-Satorras. Quasistationary analysis of the contact process on annealed scale-free networks. *Phys. Rev. E*, 83:066113, 2011.

[42] Silvio C. Ferreira, Ronan S. Ferreira, Claudio Castellano, and Romualdo Pastor-Satorras. Quasistationary simulations of the contact process on quenched networks. *Phys. Rev. E*, 84:066102, 2011.

[43] C. Castellano and R. Pastor-Satorras. Non-mean-field behavior of the contact process on scale-free networks. *Phys. Rev. Lett.*, 96:038701, 2006.

[44] Romualdo Pastor-Satorras and Alessandro Vespignani. Epidemic spreading in scale-free networks. *Phys. Rev. Lett.*, 86:3200–3203, 2001.

[45] Y. Wang, D. Chakrabarti, C. Wang, and C. Faloutsos. Epidemic spreading in real networks: An eigenvalue viewpoint. In *22nd International Symposium on Reliable Distributed Systems (SRDS'03)*, pages 25–34, Los Alamitos, CA, USA, 2003. IEEE Computer Society.

[46] Angélica S Mata, Ronan S Ferreira, and Silvio C Ferreira. Heterogeneous pair-approximation for the contact process on complex networks. *N. J. Phys.*, 16:053006, 2014.

[47] Ronan S Ferreira and Silvio C Ferreira. Critical behavior of the contact process on small-world networks. *Eur. Phys. J. B*, 86(11):1–7, 2013.

[48] Marián Boguñá and Romualdo Pastor-Satorras. Epidemic spreading in correlated complex networks. *Phys. Rev. E*, 66:047104, 2002.

[49] C. Castellano and R. Pastor-Satorras. Competing activation mechanisms in epidemics on networks. *Sci. Rep.*, 2:371, 2012.

[50] Wesley F. C. Cota, Angélica S. Mata, and Silvio C. Ferreira. Numerical recipes for efficient simulations of the markovian epidemic models on large complex networks. *in preparation*.

[51] Marcelo Martins de Oliveira and Ronald Dickman. How to simulate the quasistationary state. *Phys. Rev. E*, 71:016129, 2005.

[52] Angélica S. Mata, Marian Bogu ná, Claudio Castellano, and Romualdo Pastor-Satorras. The lifespan method as a tool to study criticality in absorbing-state phase transitions. *Preprint arXiv:1411.5835*, 2014.

[53] P. Van Mieghem, J. Omic, and R. Kooij. Virus spread in networks. *IEEE ACM T. Network.*, 17:1 –14, 2009.

[54] Hyun Keun Lee, Pyoung-Seop Shim, and Jae Dong Noh. Comment on "nature of the epidemic threshold for the susceptible-infected-susceptible dynamics in networks". *Preprint*, page ArXiv:1309.5367, 2013.

[55] Marian Boguñá, Claudio Castellano, and Romualdo Pastor-Satorras. Reply to lee et al. comment on" nature of the epidemic threshold for the susceptible-infected-susceptible dynamics in networks". *preprint arXiv:1403.7913*, 2014.

[56] Petter Holme and Jari Saramäki. Temporal networks. *Physics Reports*, 519:97–125, 2012.

[57] Angélica S. Mata and Romualdo Pastor-Satorras. Slow relaxation dynamics and aging in random walks on activity driven temporal networks. *Preprint arXiv:1411.4601*, 2014.

[58] S. N. Dorogovtsev and J. F. F. Mendes. *Evolution of networks: From biological nets to the Internet and WWW*. Oxford University Press, Oxford, 2003.

[59] S. N. Dorogovtsev and J. F. F. Mendes. *Complex Systems and Inter-disciplinary Science (The shortest path to complex networks)*. World Scientific, 2005.

[60] S. N. Dorogovtsev and J. F. F. Mendes. Evolution of networks. *Advances in Physics*, 51:1079–1187, 2002.

[61] M. E. J. Newman. Assortative mixing in networks. *Phys. Rev. Lett.*, 89:208701, 2002.

[62] S. N. Dorogovtsev. *Lectures on complex networks*. Oxford Master Series in Physics. Oxford University Press, Oxford, 2010.

[63] R. Pastor-Satorras, A. Vazquez, and A. Vespignani. Dynamical and correlation properties of the internet. *Phys. Rev. Lett*, 87:258701, 2001.

[64] M. E. K. Newman. *Handbook of Graphs and Networks: From the Genome to the Internet*. Wiley-VCH, Berlin, 2003.

[65] P. Erdős and A. Rényi. On random graphs. *Publicationes Mathematicae Debrecen*, 6:290–297, 1959.

[66] M. Boguñá, R. Pastor-Satorras, and A. Vespignani. Cut-offs and finite size effects in scale-free networks. *Eur. Phys. J. B*, 38:205–210, 2004.

[67] Michael Molloy and Bruce Reed. A critical point for random graphs with a given degree sequence. *Random Structures and Algorithms*, 6:161–180, 1995.

[68] Marián Boguñá and Romualdo Pastor-Satorras. Class of correlated random networks with hidden variables. *Phys. Rev. E*, 68:036112, 2003.

[69] Dong-Hee Kim and Adilson E. Motter. Ensemble averageability in network spectra. *Phys. Rev. Lett.*, 98:248701, 2007.

[70] José Iribarren and Esteban Moro. Impact of Human Activity Patterns on the Dynamics of Information Diffusion. *Phy. Rev. Lett.*, 103(3):038702, 2009.

[71] Michele Starnini, Andrea Baronchelli, and Romualdo Pastor-Satorras. Modeling human dynamics of face-to-face interaction networks. *Phys. Rev. Lett.*, 110:168701, 2013.

[72] Chaoming Song, Dashun Wang, and Albert-Laszlo Barabasi. Joint scaling theory of human dynamics and network science. arXiv:1209.1411v1, 2012.

[73] Suyu Liu, Nicola Perra, Márton Karsai, and Alessandro Vespignani. Controlling contagion processes in activity driven networks. *Phys. Rev. Lett.*, 112:118702, 2014.

[74] Joao Gama Oliveira and Albert-Laszlo Barabasi. Human dynamics: Darwin and einstein correspondence patterns. *Nature*, 437(7063):1251–1251, 2005.

[75] J.-P. Onnela, J. Saramäki, J. Hyvönen, G. Szabó, D. Lazer, K. Kaski, J. Kertész, and A.-L. Barabási. Structure and tie strengths in mobile communication networks. *Proceedings of the National Academy of Sciences*, 104(18):7332–7336, 2007.

[76] Ciro Cattuto, Wouter Van den Broeck, Alain Barrat, Vittoria Colizza, Jean-François Pinton, and Alessandro Vespignani. Dynamics of person-to-person interactions from distributed rfid sensor networks. *PLoS ONE*, 5:e11596, 2010.

[77] Alexei Vazquez, Balázs Rácz, András Lukács, and Albert-László Barabási. Impact of non-poissonian activity patterns on spreading processes. *Phys. Rev. Lett.*, 98:158702, 2007.

[78] Hang-Hyun Jo, Juan I. Perotti, Kimmo Kaski, and János Kertész. Analytically solvable model of spreading dynamics with non-poissonian processes. *Phys. Rev. X*, 4:011041, 2014.

[79] M. Kivela, R. Kumar Pan, K. Kaski, J. Kertesz, Jari Saramaki, and M. Karsai. Multiscale analysis of spreading in a large communication network. *J. Stat. Mech.*, page P03005, 2012.

[80] Juliette Stehle, Nicolas Voirin, Alain Barrat, Ciro Cattuto, Vittoria Colizza, Lorenzo Isella, Corinne Regis, Jean-François Pinton, Nagham Khanafer, Wouter Van den Broeck, and Philippe Vanhems. Simulation of an seir infectious disease model on the dynamic contact network of conference attendees. *BMC Medicine*, 9(87), 2011.

[81] N. Fujiwara, J. Kurths, and A. D'ıaz-Guilera. Synchronization in networks of mobile oscillators. *Phy. Rev. E*, 83(2):025101, 2011.

[82] Michele Starnini and Romualdo Pastor-Satorras. Topological properties of a time-integrated activity-driven network. *Phys. Rev. E*, 87(6):062807, 2013.

[83] M. E. J. Newman. The structure of scientific collaboration networks. *Proc. Natl. Acad. Sci. USA*, 98:404–409, 2001.

[84] George H. Weiss. *Aspects and Applications of the Random Walk*. North-Holland Publishing Co., Amsterdam, 1994.

[85] M. Henkel, H. Hinrichsen, and S. Lübeck. *Non-equilibrium phase transition: Absorbing Phase Transitions*. Springer Verlag, Netherlands, 2008.

[86] S. R. Broadbent and J. M. Hammersley. ercolation processes: I. crystals and mazes. *Proc. Camb. Phil. Soc.*, 53:629, 1957.

[87] Norman T. J. Bailey. *The mathematical theory of infectious diseases and its applications*. Charles Griffin Company Limited, London, 1975.

[88] R. C. Hilborn. *Chaos and Nonlinear Dynamics: An Introduction for Scientists and Engineers*. Oxford University Press, 2000.

[89] F. Chung, L. Lu, and V. Vu. Spectra of random graphs with given expected degrees. *Proc. Natl. Acad. Sci. USA*, 100:6313–6318, 2003.

[90] Claudio Castellano and Romualdo Pastor-Satorras. Castellano and pastor-satorras reply:. *Phys. Rev. Lett.*, 98:029802, 2007.

[91] Meesoon Ha, Hyunsuk Hong, and Hyunggyu Park. Comment on "non-mean-field behavior of the contact process on scale-free networks". *Phys. Rev. Lett.*, 98:029801, 2007.

[92] J. L. Cardy, editor. *Finite Size Scaling*, volume 2 of *Current Physics-Sources and Comments*, Amsterdam, 1988. North Holland.

[93] N.G. Van Kampen. *Stochastic Processes in Physics and Chemistry*. Elsevier, 2007.

[94] Deepayan Chakrabarti, Yang Wang, Chenxi Wang, Jurij Leskovec, and Christos Faloutsos. Epidemic thresholds in real networks. *ACM Trans. Inf. Syst. Secur.*, 10:1–26, 2008.

[95] Romualdo Pastor-Satorras and Alessandro Vespignani. Epidemic dynamics and endemic states in complex networks. *Phys. Rev. E*, 63:066117, 2001.

[96] Géza Ódor. Localization transition, lifschitz tails, and rare-region effects in network models. *Phys. Rev. E*, 90:032110, 2014.

[97] André J. Noest. New universality for spatially disordered cellular automata and directed percolation. *Phys. Rev. Lett.*, 57:90–93, 1986.

[98] Thomas Vojta, Adam Farquhar, and Jason Mast. Infinite-randomness critical point in the two-dimensional disordered contact process. *Phys. Rev. E*, 79:011111, 2009.

[99] Daniel T Gillespie. A general method for numerically simulating the stochastic time evolution of coupled chemical reactions. *Jour. of Comput. Phys*, 22(4):403 – 434, 1976.

[100] Renan S. Sander, Silvio C. Ferreira, and Romualdo Pastor-Satorras. Phase transitions with infinitely many absorbing states in complex networks. *Phys. Rev. E*, 87(2):022820, 2013.

[101] U. C. Täuber. *Critical Dynamics*. Cambridge University Press, Cambridge, 2014.

[102] Ronald Dickman. Critical exponents for the restricted sandpile. *Phys. Rev. E*, 73(3):036131, 2006.

[103] Ronald Dickman and Ronaldo Vidigal. Quasi-stationary distributions for stochastic processes with an absorbing state. *Jour. of Phys. A: Mathematical and General*, 35(5):1147, 2002.

[104] Romualdo Pastor-Satorras, Claudio Castellano, Piet Van Mieghem, and Alessandro Vespignani. Epidemic processes in complex networks. *Preprint arXiv:1408.2701*, 2014.

[105] Marcelo de Oliveira. *Tese de Doutorado: Simulações de Sistemas com Estados Absorventes: Método e Aplicação*. UFMG, 2007.

[106] Duncan J Watts and Steven H Strogatz. Collective dynamics of 'small-world' networks. *Nature*, 393(6684):440–442, 1998.

[107] Kurt Binder and Dieter Heermann. *Monte Carlo simulation in statistical physics: an introduction*. Springer, 2010.

[108] Marian Boguñá, Claudio Castellano, and Romualdo Pastor-Satorras. Supplementary information: Nature of the epidemic threshold for the susceptible-infected-susceptible dynamics in networks. *Phys. Rev. Lett.*, 111:068701, 2013.

[109] Angélica S. Mata and Silvio C. Ferreira. Multiple transitions of the susceptible-infected-susceptible epidemic model on complex networks. *Phys. Rev. E*, 91:012816, 2015.

[110] D. ben Avraham and J. Köhler. Mean-field (*n*,*m*)-cluster approximation for lattice models. *Phys. Rev. A*, 45:8358–8370, 1992.

[111] F. R. Gantmacher. *The Theory of Matrices*, volume II. Chelsea Publishing Company, New York, 1959.

[112] I.S. Gradshteyn, I.M. Ryzhik, A. Jeffrey, and D. Zwillinger. *Table of Integrals, Series, And Products*. Academic Press, 7th edition, 2007.

[113] S. Gómez, A. Díaz-Guilera, J. Gómez-Gardeñes, C. J. Pérez-Vicente, Y. Moreno, and A. Arenas. Diffusion dynamics on multiplex networks. *Phys. Rev. Lett.*, 110:028701, 2013.

[114] James P. Gleeson. Binary-state dynamics on complex networks: Pair approximation and beyond. *Phys. Rev. X*, 3:021004, 2013.

[115] Piet Van Mieghem and Eric Cator. Epidemics in networks with nodal self-infection and the epidemic threshold. *Phys. Rev. E*, 86:016116, 2012.

[116] E. Cator and P. Van Mieghem. Susceptible-infected-susceptible epidemics on the complete graph and the star graph: Exact analysis. *Phys. Rev. E*, 87:012811, 2013.

[117] W.H. Press, S.A. Teukolsky, W.T. Vetterling, and B.P. Flannery. *Numerical Recipes 3rd Edition: The Art of Scientific Computing*. Cambridge University Press, 2007.

[118] Paolo Moretti, Suyu Liu, Claudio Castellano, and Romualdo Pastor-Satorras. Mean-field analysis of the q-voter model on networks. *J. Stat. Phys.*, 151(1-2):113–130, 2013.

[119] K.-I. Goh, D.-S. Lee, B. Kahng, and D. Kim. Sandpile on scale-free networks. *Phys. Rev. Lett.*, 91:148701, 2003.

[120] Peter J. Mucha, Thomas Richardson, Kevin Macon, Mason A. Porter, and Jukka-Pekka Onnela. Community structure in time-dependent, multiscale, and multiplex networks. *Science*, 328(5980):876–878, 2010.

[121] R. J. Bell and P. Dean. Atomic vibrations in vitreous silica. *Discuss. Faraday Soc.*, 50:55–61, 1970.

[122] Vasiliki Plerou, Parameswaran Gopikrishnan, Bernd Rosenow, Luís A. Nunes Amaral, and H. Eugene Stanley. Universal and nonuniversal properties of cross correlations in financial time series. *Phys. Rev. Lett.*, 83:1471–1474, 1999.

[123] Marc Barthélemy, Alain Barrat, Romualdo Pastor-Satorras, and Alessandro Vespignani. Velocity and hierarchical spread of epidemic outbreaks in scale-free networks. *Phys. Rev. Lett.*, 92:178701, 2004.

[124] M. Ángeles Serrano, Dmitri Krioukov, and Marián Boguñá. Percolation in self-similar networks. *Phys. Rev. Lett.*, 106:048701, 2011.

[125] A. Ganesh, L. Massoulié, and D. Towsley. The effect of network topology on the spread of epidemics. In *IEEE INFOCOM*, pages 1455–1466, 2005.

[126] Miguel A. Muñoz, Róbert Juhász, Claudio Castellano, and Géza Ódor. Griffiths phases on complex networks. *Phys. Rev. Lett.*, 105:128701, 2010.

[127] C. Buono, F. Vazquez, P. A. Macri, and L. A. Braunstein. Slow epidemic extinction in populations with heterogeneous infection rates. *Phys. Rev. E*, 88:022813, 2013.

[128] Pol Colomer-de Simon and Marian Boguna. Double percolation phase transition in clustered complex networks. *arXiv preprint arXiv:1401.8176*, 2014.

[129] Ginestra Bianconi and Sergey N Dorogovtsev. Multiple percolation transitions in a configuration model of network of networks. *arXiv preprint arXiv:1402.0218*, 2014.

[130] Reuven Cohen, Keren Erez, Daniel ben Avraham, and Shlomo Havlin. Resilience of the internet to random breakdowns. *Phys. Rev. Lett.*, 85(21):4626–4628, 2000.

[131] Lazaros K. Gallos. Random walk and trapping processes on scale-free networks. *Phys. Rev. E*, 70:046116, 2004.

[132] Jae Dong Noh and Heiko Rieger. Random walks on complex networks. *Phys. Rev. Lett.*, 92:118701, 2004.

[133] A. N. Samukhin, S. N. Dorogovtsev, and J. F. F. Mendes. Laplacian spectra of, and random walks on, complex networks: Are scale-free architectures really important? *Phys. Rev. E*, 77:036115, 2008.

[134] Andrea Baronchelli, Michele Catanzaro, and Romualdo Pastor-Satorras. Random walks on complex trees. *Phys. Rev. E*, 78:011114, 2008.

[135] S. Redner. *A Guide to First Passage Processes*. Cambridge University Press, Cambridge, 2001.

[136] M. Henkel and M. Pleimling. *Non-equilibrium phase transition: Ageing and Dynamical Scaling far from Equilibrium*. Springer Verlag, Netherlands, 2010.

[137] J. P. Bouchaud. Weak ergodicity breaking and aging in disordered systems. *J. Phys. I France*, 2(9):1705–1713, 1992.

[138] Cécile Monthus and Jean-Philippe Bouchaud. Models of traps and glass phenomenology. *Jour. of Phys. A: Mathematical and General*, 29(14):3847, 1996.

[139] Michele Starnini, Andrea Baronchelli, and Romualdo Pastor-Satorras. Metastable states as a key to the dynamics of supercooled liquids. *Phys. Rev. Lett.*, 84:2168, 2000.

[140] M. Kivela, R. Kumar Pan, K. Kaski, J. Kertesz, Jari Saramaki, and M. Karsai. Relaxation in glassforming liquids and amorphous solids. *Jour. of Appl. Phys.*, 88:3113–3157, 2000.

[141] Shai Carmi, Shlomo Havlin1, Chaoming Song, Kun Wang, and Hernan A Makse. Energy landscape network approach to the glass transition. *J. Phys. A: Math. Theor*, 42:105101, 2009.

[142] José Nelson Onuich, Zaida Luthey-Schulten, and Peter G. Wolynes. Theoretical of protein folding:the energy landscape perspective. *Annu. Rev. Phys. Chem.*, 48:545–600, 1997.

[143] D. J. Wales, M. A. Miller, and T. R. Walsh. Archetypal energy landscapes. *Nature*, 394:758–760, 1998.

[144] D. J. Wales, J. P. K. Doye, M. A. Miller, P. N. Mortenson, and T. R. Walsh. Energy landscapes: From clusters to biomolecules. *Advances in Chemical Physics*, 115:1–111, 2000.

[145] Claire Massen and Jonathan Doye. Identifying communities within energy landscapes. *Phys. Rev. E*, 71:046101, 2005.

[146] Hamid Seyed-allaei, Hamed Seyed-allaei, and Mohammad Ejtehadi. Energy-landscape networks of spin glasses. *Phys. Rev. E*, 77:031105, 2008.

[147] Jonathan Doye. Network topology of a potential energy landscape: A static scale-free network. *Phys. Rev. Lett.*, 88:238701, 2002.

[148] Andrea Baronchelli, Alain Barrat, and Romualdo Pastor-Satorras. Glass transition and random walks on complex energy landscapes. *Phys. Rev. E*, 80(2):020102, 2009.

[149] David Gfeller, David de Lachapelle, Paolo De Los Rios, Guido Caldarelli, and Francesco Rao. Uncovering the topology of configuration space networks. *Phys. Rev. E*, 76:026113, 2007.

[150] Paolo Moretti, Andrea Baronchelli, Alain Barrat, and Romualdo Pastor-Satorras. Complex networks and glassy dynamics: walks in the energy landscape. *Jour of Stat. Mech.: Theory and Experiment*, 2011:P03032, 2011.

[151] Paolo Moretti, Andrea Baronchelli, Alain Barrat, and Romualdo Pastor-Satorras. Complex networks and glassy dynamics: walks in the energy landscape. *Jour. of Statis. Mech.: Theory and Experiment*, 2011:P03032, 2011.

[152] M. Abramowitz and I. A. Stegun. *Handbook of mathematical functions.* Dover, New York, 1972.

[153] E. M. Bertin and J.-P. Bouchaud. Linear and nonlinear response in the aging regime of the one-dimensional trap model. *Phy. Rev E*, 67(4):065105, 2003.

[154] E. M. Bertin and J.-P. Bouchaud. Subdiffusion and localization in the one-dimensional trap model. *Phys Rev E*, 67(20):026128, 2003.

[155] Bernd Rinn, Philipp Maass, and Jean-Philippe Bouchaud. Hopping in the glass configuration space: Subaging and generalized scaling laws. *Phys. Rev. B*, 64:104417, 2001.

[156] L.R. Fontes, M. Isopi, and C.M. Newman. Random walks with strongly inhomogeneous rates and singular diffusion: convergence, localization and aging in one dimension. *Ann. Prob.*, 30:579–604, 2002.

[157] Terence Hwa, Enzo Marinari, Kim Sneppen, and Lei-han Tang. Localization of denaturation bubbles in random dna sequences. *Proceedings of the National Academy of Sciences*, 100(8):4411–4416, 2003.